Laser Doppler Anemometry Measurements of a Confined Turbulent Water Jet with a Uniform Background Flow

by

Cheng-Hsing Hsu

Dissertation submitted to the Faculty of the
Virginia Polytechnic Institute and State University
in partial fulfillment of the requirements for the degree of
Doctor of Philosophy
in
Aerospace and Ocean Engineering

APPROVED:

D. A. Walker, Chairman

J. A. Schetz, Department Head

R. L. Simpson

B. Grossman

W. F. Ng

June, 1989

Blacksburg, Virginia

Laser Doppler Anemometry Measurements of a Confined Turbulent Water Jet with a Uniform Background Flow

by

Cheng-Hsing Hsu

D. A. Walker, Chairman

Aerospace and Ocean Engineering

(ABSTRACT)

An axisymmetric, turbulent water jet with several very slow, coflowing external streams was measured with a frequency-shifted laser Doppler anemometer. The objective was to approximate a jet submerged in an ambient fluid of infinite domain by using a confined jet in a uniform coflow. The coflow prevents flow reversal outside the jet, but if the coflow velocity is not small compared to the jet velocity, the jet will no longer be self-preserving. Thus, the objective is reached in the limit as the coflow approaches zero, but in the absence of reverse flow. In the present study, a jet with several slow coflows was examined to investigate this behavior, the data was extrapolated to the limit ($U_s/U_j = 0$) to obtain the free jet results and reduce uncertainty in earlier data.

The Reynolds number based on the jet diameter and exit velocity was 32100. Conservation of momentum of the jet was demonstrated up to the measurement limit of x/d = 100. Its distribution suggests that the near field axial pressure variation has significant effects on the momentum flux. The results also indicate that

momentum flux measurements require accurate data to the edge of the jet. The similarity of mean and rms velocity profiles suggest the existence of a region of self-preservation.

The entrainment rate, centerline velocity decay rate and spreading rate of the jet were determined and compared to previous measurements with and without a coflowing stream. The variation of these jet parameters with respect to the velocity ratios was obtained. The limiting values of the jet parameters were determined by extrapolation to zero velocity ratio.

This study indicates that a slow coflowing stream is an ideal way to eliminate the recirculating zone present outside jets without coflows. By reducing the coflow to a negligible velocity with constant Craya-Curtet number, researchers can greatly reduce the wide experimental variation in jet entrainment and spreading rates found in different facilities. The results also indicated that a confined jet with a very slow coflow without recirculation can asymptotically approach the conditions of a free jet. An estimate of the variation of the duct size versus the velocity ratio is obtained. It suggests that it is not possible to reduce the velocity ratio to an arbitrarily small value without backflow because the duct would become impractically large.

Acknowledgements

The development and completion of this study could only have occurred through the help and cooperation of many individuals. I would like to extend my thanks to all those who helped. It has been my pleasure to see all these contributions come together as a working whole.

In particular, I would like to thank my major professor, D. A. Walker, for his help as an advisor, a co-worker, and as a good friend. His contribution to this work and to my education is quite significant and very much appreciated.

Also to be noted are professors J. A. Schetz, R. L. Simpson, B. Grossman W. F. Ng and M. D. Walker (at State University of New York, SUNY Stony Brook) for their ideas and suggestions concerning the experimental work as well as the completion of this dissertation.

Special credit is due to , , and for their dedicated work as the co-workers and friends in putting the tunnel together. Their encourgements and helps in all aspects of the experiment have been a major contribution.

During various stages of the experiment, the help of was significant in operation of the experiment. His assistance and the contribution of his time has been very valuable.

The excellent job of editing the script has been done by my wife, . Her encouragement, patience and prayers along with the support of my friends in the Body of Jesus Christ, has been a constant source of strength. Of course, to the one who answered these prayers I can acknowledge everything.

Table of Contents

List of Illustrations

Nomenclature

B_u	Centerline excess mean velocity decay rate
d	Jet exit diameter
E	Entrainment coefficient
f	Doppler frequency
f_s	Shifted frequency
I_n	n'th integral of the shape function
k	Similarity shape function
L	Width of the square duct
N_{water}	Refraction index of water
N_{air}	Refraction index of air
P	Mean static pressure
$\dot{Q}$	Volumetric flow rate inside the jet
$\dot{Q}_\infty$	Total volumetric flow rate in the infinite domain
$\dot{Q}_j$	Volumetric flow rate at the jet exit

$\dot{Q}_w$	Total volumetric flow rate in the duct
r	Radial coordinate
$R_{1/2}$	Half width
R_e	Distance between the jet centerline and the edge of the jet
R_w	Distance from jet centerline to the wall
U	Jet velocity in axial direction
U_{M0}	Momentum velocity at centerline of the jet
U_{Mj}	Momentum velocity at exit of the jet
U_c	Centerline mean velocity of the jet
U_j	Jet exit velocity
U_0	Centerline excess mean velocity of the jet
U_s	Velocity of coflowing stream
u	Instantaneous velocity measured by LDA
u_{fs}	Resulting shifted velocity from frequency shifting
u_r	Radial velocity
u_x	Axial velocity
u'	Axial fluctuation velocity
x	Axial coordinate
y	Vertical coordinate
z	Transverse coordinate
ρ	Fluid density
η	Rescaled transverse coordinate
λ	Wavelegth of the laser bean

θ	Angle between two incident laser beams

Chapter 1 Introduction

1.1 Outline

In this chapter we give a brief description of the overall study including a review of previous research on related topics and the goal of this research. The problems and inconsistencies of previous investigations are also described.

The second chapter introduces the mathematics and physics of axisymmetric confined jets. The dimensions and definitions of variables describing the confined jet problem are presented. The equations are addressed and the framework of analysis are prepared.

The third chapter contains the descriptions of the flow facility. We also describe the concepts involved in designing and building the tunnel. The calibration pro-

cedure of the flow parameters are described and the value of the operating parameters used during the testing are summarized.

The measurement techniques, such as laser Doppler anemometer, traverse equipment (Linear-Variable-Displacement-Transformer, LVDT), optical arrangement, instrumentation developments, seeding and data reduction processes, are included in the fourth chapter. The circuit design concepts are briefly discussed and explained. The calibration of the instruments is presented. Calibration uncertainty is also discussed in the fourth chapter.

The fifth chapter presents and explains the results obtained. Uncertainty analysis of the measurements is discussed. The uncertainty of the extrapolated flow parameters of the free jet is estimated. The advantages and drawbacks of laser Doppler anemometry and the hot-wire anemometry in jet measurements are briefly discussed. The discussion of our results and a comparison with those of previous investigations are also included in this chapter. The final conclusions and suggestions for future research are given in the sixth chapter.

1.2 Bibliography Review

Boundary-free turbulent shear flows, especially turbulent jet flows, have been studied theoretically and through experiments many times during the past few decades. However, to date differences still persist between measurements made

at similar or different facilities and between experimental and theoretical results. Particularly, the flow outside the jet has been ignored as the source of the inconsistencies involving entrainment (Ricou and Spalding, 1961), the centerline velocity decay rate, the spreading rate of the jet and the self-preserving structure (Curtet and Ricou, 1964; Antonia and Bilger, 1973). Many measurements even fail to satisfy the integral momentum equation (Kotsovinos, 1978). Recent studies (Baker, 1980; Seif, 1981; Chevray, 1977; Khwaja, 1980, Capp 1983, Walker; 1984) suggest that conservation of momentum is a key factor to evaluate the quality of the flow and measurements.

Different experimental techniques and instruments have been used to make measurements of turbulent jets in different facilities. A thorough review of these data was given by Rodi (1975). Most frequently referenced measurements were on round jets submerged in what is taken to be a "still" fluid. This is usually referred to as a free jet. Included in this category were works by Corrsin (1943), Hinze and Van der Hegge Zijnen (1949), Corrsin and Uberoi (1950,1951), Corrsin and Kistler (1954), and Wygnanski and Fiedler (1969). The latter is the most comprehensive investigation to date. Pitot tube or a constant temperature hot-wire anemometer were used in these measurements. Frequency-shifted laser Doppler Anemometer (LDA) has been used recently to study jets (Baker,1974; Barnett and Giel, 1975; Reed, 1977; Lau, et al., 1979; Capp, 1983). The measurements of these researchers were made in air. The difficulties of using LDA on jets in air are mainly due to "seeding bias." i.e. how can particles be added to both flows in concentrations which do not affect the outcome? For details refer

to McLaughlin and Tiederman (1973) and Barnett and Giel (1975). Frequency-shifted LDA is advantageous in reversing and highly turbulent flow fields but less effective than a hot-wire anemometer in flow fields with low turbulence intensity. Moving fringes in the probe volume can identify flow direction. Broadening problem makes LDA less effective in low turbulence intensity flow (Durst, Melling and Whitelaw, 1976).

Axisymmetric jets with coflowing streams, also called confined jets or ducted jets, have also been studied extensively by numerous investigators, including Forstall and Shapiro (1950), Tani and Kabashi (1951), Kabashi (1952), Curtet (1958), Maczynski (1962), Alpinieri (1964), Curtet and Ricou (1964), Barchilon and Curtet (1964), Razinsky and Brighton (1971), Antonia and Bilger (1973), Antonia et al. (1975), Morris (1976), Fink (1977), Shaughnessy and Morton (1977), Walker (1984), and Komori and Ueda (1985). In three of these, the measurements were taken with low ratios of coflowing stream velocity to jet exit velocity, i.e. $U_s / U_j = 0.0066$ (Walker, 1984), $U_s / U_j = 0.0093$ (Komori and Ueda , 1985), $U_s / U_j = 0.022$ (Shaughnessy and Morton, 1977). All other measurements were taken with $U_s / U_j > 0.1$. With high velocity ratios the jet flows only a short distance downstream before it becomes a small perturbation on the uniform stream. Such a flow behaves quite differently from jet flows. For example, there is no turbulent energy production. This explains why these flows grow so slowly as indicated by spreading rates and entrainment.

Many measurements were also affected by recirculation zones or back flow currents outside the jet. These recirculation regions were driven by the entrainment of the jet. (The amount of external fluid entrained by the jet had to come from somewhere) Previously, the limited dimensions of a large testing facility were thought to have negligible effects on the flow. A surprising observation given by Barchilon and Curtet (1964) indicated that oscillation of the jet might occur due to these large, energetic eddies blowing the jet around along its entire length. This jet flapping would be expected to contribute greatly to the spreading and entrainment rates of the jet. Only a few people have carefully considered the flow conditions outside the jet. Taylor (1958) studied flow induced in infinite and semi-infinite domains. Schneider (1981) used asymptotic expansions to analytically study the flow induced by the jet. Craya and Curtet (1955) and Curtet (1958) analyzed and measured the recirculation due to confined jets. The similitude parameter, m, or Craya-Curtet number, C_t, (Craya and Curtet, 1955) was used to characterize whether the back flow currents occur or not. Analysis done by Barchilon and Curtet (1964) indicated that recirculation totally vanishes when C_t is bigger than 0.976. Experimentally, the critical value of C_t was found to be within 0.73 to 0.81. The values were from Rajaratnam (1983), p 268; and Curtet (1958), respectively. For C_t less than the critical value, recirculation occurs. The pressure distribution outside the jet flow was also not considered by most of the investigators. Hill (1965) calculated the wall pressure distribution on a confined jet by using empirical data taken on a free jet. Razinsky and Brighton (1971) measured the velocity profiles and wall pressure distribution. Kotsovinos

(1978) corrected the negative flowing entrained fluid by including extra terms in the momentum balance equation.

The dimensionless entrainment rate (the slope of the ratio of the volumetric rate in the jet to the jet exit volumetric rate versus the ratio of axial distance to nozzle diameter) may also be related to jet flapping. Measurements of this parameter vary from 0.22 to 0.404 (Ricou and Spalding, 1961). Wall effects, jet vibration, flow patterns outside the jets and the accuracy of velocity measurement at the edge of the jets may be the causes of such a large range of entrainment rates. For a jet in a coflowing stream the entrainment rate is calculated by integrating the mean excess velocity profile defined in chapter 2. Measurements of jets in coflowing streams to date, except Walker (1984) and Komori and Ueda (1985), all gave values of entrainment rate consistently near zero. These surprising results indicated, as mentioned earlier, that jets with stronger coflowing streams grew much more slowly than either the turbulent free jet or turbulent wake flow. Therefore, neither turbulent free jet nor turbulent wake theories can be used to estimate the entrainment rate of jets submerged in stronger coflowing stream. For this reason the study of confined jets is much more complex than other free boundary flows. However, it is believed that if the coflowing stream can be made small enough (without recirculation occuring), one can asymptotically approach the conditions of free jets (Walker, 1984). The measurements of the confined jet with very slow coflowing stream can be used to verify the self-preservation concept, which means the jet flow can be described by single length and velocity scales. Under the condition of the self-preservation, flow variables, like mean

velocity profiles and turbulent fluctuation velocity distributions, could be rescaled at different locations to collapse to a single profile. Also, the measured results can give the quantitative information closely related to that of the free jets.

The centerline velocity decay rate (the slope of the ratio of jet exit velocity to the centerline excess velocity versus the ratio of axial distance to nozzle diameter) is an important parameter used to describe the growth of the jet flow. The value varies from 5.0 to 7.5 (Townsend, 1976; Wygnanski and Fiedler, 1969; Capp, 1983; List, 1982; Rodi, 1974; Seif, 1981) for free jets measured in different flow facilities. Higher values indicate slower decay of the centerline velocity. However, the decay of the centerline velocity will not be linear if the jet is in a strong coflowing stream (Antonia and Bilger, 1973).

The spreading rate of the jet (the slope of the half width versus axial distance) varies from 0.075 to 0.11 (Albertson et al., 1950; Becker et al., 1967; Corrsin, 1943; Corrsin and Uberoi, 1950; Forstall and Gaylord, 1955; Hinze and Van der Hegge Zijnen, 1949; Keagy and Weller, 1949; Kizer, 1963; Rosenweig et al., 1961; Ruden, 1933; Sunavala et al., 1957; Uberoi and Garby, 1967; Wilson and Danckwerts, 1964; Wygnanski and Fiedler, 1969; Birch et al., 1978; Chevray and Tutu, 1978; Abramovich, 1963; List, 1982). The corresponding half spreading angle is from 4.29 ° to 6.28 ° . Similar to the centerline velocity decay rate, the spreading of the jet will not be linear if the jet has a strong coflowing stream.

As mentioned, conservation of momentum in turbulent jets has been a major topic in many papers. However, the role of the pressure term (in the absence of external pressure gradient) has not been resolved. The measurements taken by Barat (1954) and Maczynski (1962) seem to indicate this term is negligible compared to the other terms in the momentum equation. However, by substituting the other component momentum equation, Townsend (1976, p192) demonstrated that the pressure term contributed as much momentum as normal turbulent stress did. Miller and Comings (1957) also obtained the same results by measuring the static pressure inside the jet. The contribution of momentum by the pressure term given by Townsend was about 18 percent of the total axial momentum of the jet. Often, both the pressure term and the normal turbulent stress term are neglected in the integral momentum equation.

Some measurements indicated that the momentum decreased in the first few diameters downstream of the jet, but then increased and reached a constant value higher than the exit value further downstream (Hussain and Clark, 1977; Ramaprian and Chandrasekhara, 1985; Rankin et al., 1983). This phenomenon was due to the variation of the mean static pressure in the region near the jet exit (Hussain and Clark, 1977). Constant contributions to the axial momentum of the mean velocity term, normal fluctuation velocity term and pressure term were reached beyond $x / d = 40$.

1.3 Current investigation

The goal of the present study was to include several very slow background streams with the jet flow to asymptotically approach the free turbulent jet conditions by a confined turbulent jet. To do this required showing that self preservation could be approximately achieved in the confined turbulent jet as predicted by the theory for the free jet. The recirculation zone outside the jet can be eliminated by the background stream as long as the Craya-Curtet number is higher than the critical value. By measuring the jet flow with constant jet exit velocity and several different background velocities, the flow parameters, such as the spreading angle and decay rate, of the jet were determined. The spreading rate was characterized by the dimension of the half-velocity points which were computed from the excess axial mean velocity profiles by linear interpolation. A half spreading angle was computed from the spreading rate and used to explain the growth of the jet. The centerline velocity decay rate was determined by the slope of the line which was obtained by a linear least squares fit of the variation of the centerline velocity. The flow parameters of the free jet (with zero coflow) were calculated by extrapolating the data obtained in the present measurement (with nonzero coflow).

The concept of measuring the jet flow with several slow background streams and taking the limit to the free jet condition (no background stream) is first proposed and investigated in this study. No previous work has employed this method.

The scatter of the data in the previous free jet measurements at different flow facilities reflects the uncertainty produced by different amounts of recirculation outside the jet. This uncertainty can be greatly reduced by the extrapolation method and the problem of the recirculation zone which occurs without a background stream is avoided in the present study. The relationship between the minimum duct size and the background flow velocity was calculated with the critical Craya-Curtet number by using the extrapolated free jet parameters. This curve indicates the limitation of the dimension of the flow facility and the corresponding coflowing stream velocity. It can be used to determine the lowest value of the background flow velocity in a facility without recirculation and to design the jet experiments or flow facilities in the future work.

In order to avoid the seeding bias problem, the experiment was conducted in water. Thus, This project required the design and construction of facilities, including the water tunnel and water jet. Construction of the corresponding experimental instruments, such as signal amplifiers, frequency tracker, protection circuits and a one component frequency-shifted LDA system, were also major tasks in the present program. One component LDA is sufficient to measure the jet parameters (spreading rate, decay rate and entrainment rate). The instruments were calibrated and their performance evaluated during the testing phase. The computer programs for data acquisition and reduction were developed in Fortran. Axial mean velocity and turbulent intensity distributions were calculated from the measured data by the data reduction program. Momentum flux, centerline velocity decay rate, spreading rate and entrainment rate of the jet were

computed from the axial mean velocity profiles. The jet with several different velocity ratios, but all with very slow background flow (e.g. $U_s/U_j = 0.0034$), was measured. The measured data were stored in binary form by an AT compatible computer through a MetraByte 12-bit A/D converter board. Details of the facilities and instrumentation will be described in later chapters. The results presented in the following chapters include LDA measurements and results computed from them, e.g. entrainment rate and momentum flux were computed numerically by Simpson's rule integration of the excess axial mean velocity profiles. Uncertainty analysis of the measured and extrapolated data is given in the corresponding sections.

Chapter 2 Background Mathematics and Laboratory Jets

An axisymmetric turbulent jet submerged in still fluid and free from wall interference is hard to produce in a laboratory. A conceptual free jet, represented by a jet inside an infinite domain without background flow, behaves differently from any wall-constrained laboratory jet (any real jet). However, the free jet behavior could be approximated by applying a very slow external stream on the jet flow to eliminate the recirculation zone which occurs in all confined jets without background flow. The mathematical description is given in the present chapter.

The theory of ducted axisymmetric jets has been studied from 1950. The theory has as basic assumptions the boundary layer approximation on the jet flow and negligible energy loss in the coflowing stream (Craya and Curtet, 1955; Curtet, 1960). Before examining the equations for the confined jet, we will consider an

axisymmetric jet in an infinite domain without the external stream. For constant density fluid the flow across any cross-section in an infinite domain can be written as

$$\dot{Q}_{\infty} = 2\pi \int_0^{\infty} Ur\, dr \tag{2.1}$$

which represents the time-averaged volumetric flow rate across a plane normal to the jet axis. U is the mean velocity in the direction of the jet axis and r is the radial distance from the jet centerline.

If we consider the laboratory jet with the cross-section extending to the duct walls, refer to Figure 1, the time-averaged duct volumetric flow rate is constant along the axis. The jet flow grows downstream along the direction of increasing x. The time-averaged volumetric flow rate inside the jet flow, $\dot{Q}$, is also increasing downstream due to fluid entrained into the jet. Since the integral of volumetric flow rate remains constant along the duct, this implies that the gain of the jet is equal to the loss of the outer stream. If a coflowing stream with constant velocity equal to U_s is applied, the time-averaged volumetric flow rate in the duct is given as

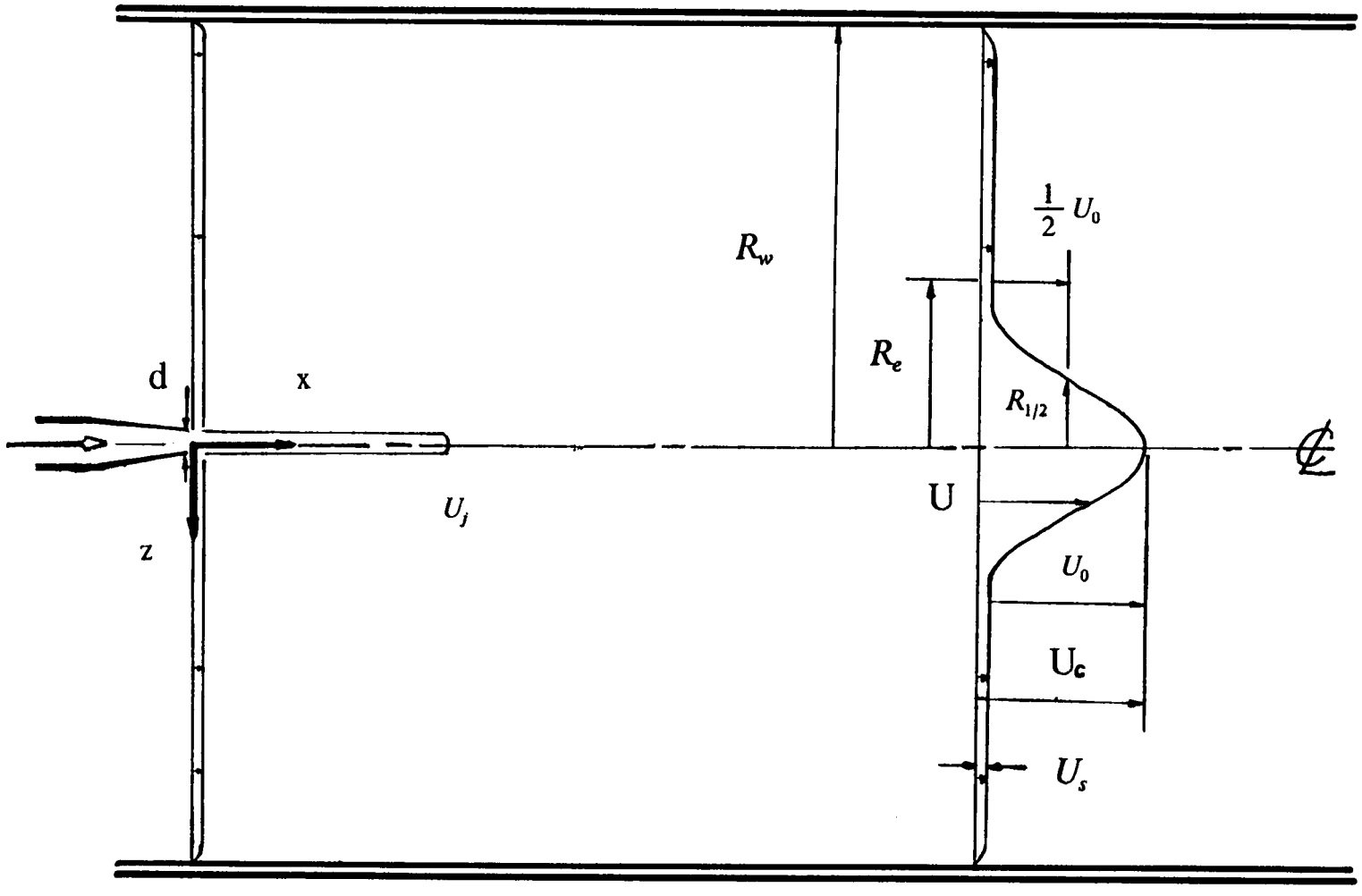

Figure 1 Definition of Variables.

$$\dot{Q}_w = 2\pi\int_0^{R_w} U r dr$$

$$= 2\pi\int_0^{R_e} (U - U_s)\, r\, dr + 2\pi\int_0^{R_e} U_s\, r\, dr + 2\pi\int_{R_e}^{R_w} U r\, dr \qquad (2.2)$$

$$= constant$$

The mean excess velocity is defined as $U - U_s$. U_0 is equal to $U_c - U_s$, U_c is the mean axial velocity at the centerline of jet. R_w is the distance from jet centerline to the wall. R_e is the distance between the jet centerline and the "edge" of the jet, which is defined to be a radius large enough so that the mean excess velocity, $U - U_s$, is within the measurement scatter. In general, R_e is much smaller than R_w . The time-averaged volumetric flow rate from the exit of the jet is given as

$$\dot{Q}_j = 2\pi\int_0^{\frac{d}{2}} U_j\, r\, dr \equiv \frac{\pi}{4} U_j\, d^2 \qquad (2.3)$$

U_j and d are defined as the jet exit velocity and the jet exit diameter, respectively. The half mean excess velocity is equal to half the mean excess velocity at the jet centerline, U_0 . $R_{1/2}$ is defined as the distance between the jet centerline and the point where the velocity reaches the half mean excess velocity. The first term in equation (2.2) is the time-averaged volumetric flow rate of the jet, $\dot{Q}$. The sum of the second and third terms is the time-averaged volumetric flow rate of the coflow.

The entrainment rate is defined as dQ/dx , which represents the change of the time-averaged volumetric flow rate inside the jet along the jet axis (Ricou and Spalding, 1961). For convenience, an entrainment coefficient is defined as

$$E \equiv \frac{\dot{Q} - \dot{Q}_j}{\dot{Q}_j} \tag{2.4}$$

which is a dimensionless parameter indicating the fractional increase of the jet volumetric flow rate. With the assumption of kinematic similarity, the mean axial velocity profile can be expressed

$$U = U_s + U_0 f(\eta) \tag{2.5}$$

where $\eta = r/R_{1/2}$ and $f(\eta)$ is the similarity shape function of jet mean excess velocity profile. The n'th integral of normalized mean excess velocity profile (or shape function) is defined (Antonia and Bilger, 1973) as

$$I_n \equiv \int_0^\infty [f(\eta)]^n \eta \, d\eta \tag{2.6}$$

The axial momentum flux of the jet in an infinite domain with coflow can also be described. We assume

$$\lim_{r\to\infty} [r\overline{u_r u_x}] = 0 \tag{2.7}$$

where the u_r is the radial velocity, u_x is the axial velocity and the overbar means time-averaged. Substituting the mass balance equation into the axial momentum equation and integrating radially, (Hinze, 1975) We obtain

$$\begin{aligned} \frac{M}{\rho} &= 2\pi\int_0^{\infty}[U(U-U_s)+\overline{u'^2}+\frac{P}{\rho}]\,r\,dr \\ &= constant \end{aligned} \tag{2.8}$$

where P is the mean static pressure and u' is the fluctuation velocity in the axial direction. As mentioned, the contribution of the pressure term is nearly the same but of opposite sign from the turbulent normal stress term $\overline{u'^2}$, see Miller and Comings (1957), Townsend (1976, p192) and Hinze (1975, p521). Equation (2.8) can be approximated as

$$\begin{aligned} \frac{M}{\rho} &= 2\pi\int_0^{\infty}U(U-U_s)\,r\,dr \\ &= constant \end{aligned} \tag{2.9}$$

The equations (2.8), (2.9) remain true in the case of the confined jet (integrating from 0 to R_e instead from 0 to infinity). With the new integration limits, equations (2.8) and (2.9) become

$$\begin{aligned} \frac{M}{2\pi\rho} &= \int_0^{R_e}[U(U-U_s)+\overline{u'^2}+\frac{P}{\rho}]\,r\,dr \\ &= constant \end{aligned} \tag{2.10}$$

$$\frac{M}{2\pi\rho} = \int_0^{R_e} U(U - U_s)\, r\, dr$$
$$= constant \tag{2.11}$$

If a recirculation zone is present outside the jet, the momentum flux outside the jet becomes important. Equations (2.10) and (2.11) are no longer true. Thus, we need to apply a coflowing external stream on the jet flow to move the recirculation zone downstream. An important variable which predicts the location of the recirculation zone is the similitude parameter, m, or equivalently the Craya-Curtet number C_t ($C_t = 1/\sqrt{m}$). The equation used to calculate the similitude parameter in a constant area square duct (Barchilon and Curtet, 1964) is

$$m = \frac{\dot{Q}}{\dot{Q}_w}\left\{1 + k\frac{U_0 L^2}{\dot{Q}_w} - \frac{3}{2}\frac{\dot{Q}}{\dot{Q}_w}\right\} \tag{2.12}$$

where L is the width of the duct, and k is the similarity shape factor defined as

$$k \equiv 2\int_0^{\frac{R_e}{R_{1/2}}} [f(\eta)]^2\, \eta\, d\eta \tag{2.13}$$

The equation (2.12) shows a smooth behavior when background flow is approaching zero and the duct size is approaching infinity. Thus, a confined jet with nonzero coflow can be used to extrapolate an ideal free jet. All the data measured for this thesis were computed by using the equations listed above. The

parameters computed from these were used to characterize the conditions of our jet. These results are given in Chapter 5.

Chapter 3 Flow Facility

3.1 Description of Flow Facility

The flow facility used in the present study was a horizontal closed-loop water tunnel and a water flow loop with a stainless-steel round jet. The jet was mounted inside the water tunnel. The facility was designed to be versatile. We wanted to use a wide range of background flow and jet exit velocities maintained at steady rates. The jet exit velocity (12 m/sec) produced no cavitation inside the jet. The ratio of background velocity to jet exit velocity was chosen to be small but with no backflow for at least 100 diameters downstream of the jet nozzle.

The water tunnel measures 7.32 meters by 4.88 meters, see Figure 2. The water tunnel was constructed with circular cross sections (0.457 m O. D. PVC pipe, elbow, Tee) except the test section and honeycomb-screen section. The flow was

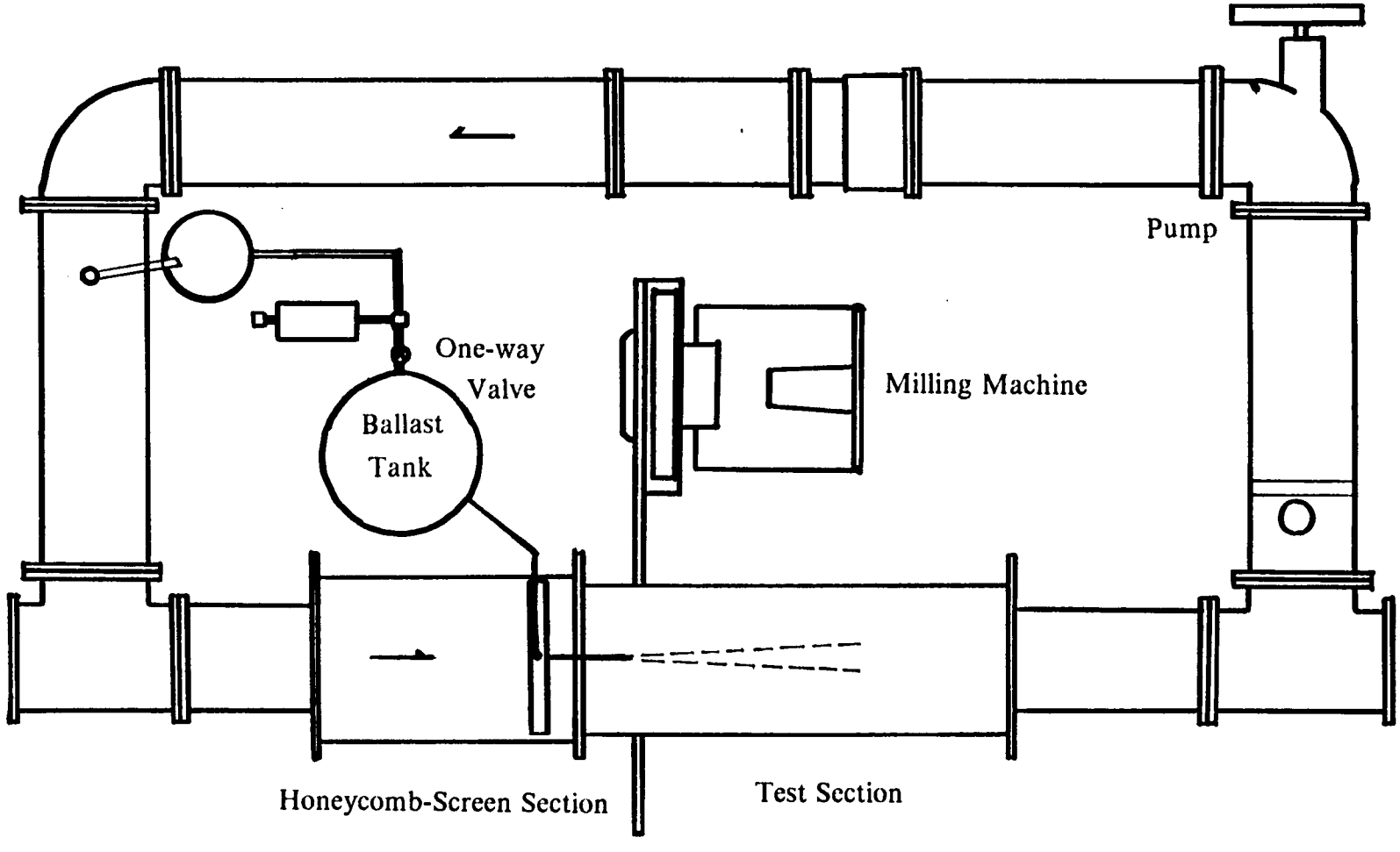

Figure 2 Flow Facility.

driven by a 0.46 m I. D. axial pump (donated by Ingersoll- Rand). A telescoping section was inserted at the charge side of the pump to adjust for length mismatch and to assist assembly. The pump was driven by a 3 phase, 10 hp induction motor with a Toshiba TOSVERT-130 H/H1 low acoustic-noise transistorized inverter. The speed of the pump was reduced 6 fold by a gear belt connecting the driving motor and the pump. A honeycomb was installed in the circular PVC pipe at the suction side of the pump to help isolate the test section from the pump. A 20 cm O. D. stand pipe was mounted upstream of the circular honeycomb. Another stand pipe, 10 cm O. D., was mounted at the opposite side of the tunnel as an over-flow. This overflow was the flow return for the jet and was used to calibrate the volumetric flow rate of the jet. When the flow reaches equilibrium, the volumetric over-flow rate is equal to the volumetric flow rate of the jet. Details of the calibration follow later in this chapter.

The square sections of the water tunnel were the test section and honeycomb-screen section. The open top test section was composed of three 1.27 cm thick by 2.44 m glass plates. The cross area of test section was 61.0 cm by 61.0 cm. A top wall for the test section was made by 1.27 centimeters thick Plexiglas and could be installed or removed, but the present study was conducted with free top surface. The test section could support up to 3000 kilograms, however, the total weight of the test section and water was 1500 kilograms. Two square, stainless-steel flanges were bolted at the ends of the test section to stiffen the section and to connect it to adjacent sections. The side walls were used to align the light beams. The difference of the distance between the side walls at the two ends of

the test section was less than 3 mm, a small fraction of the width of the test section. Therefore, the side walls of the test section were parallel enough to ensure the coincidence of the reflection and the incident light beams when the incident beam was normal to the side walls.

The honeycomb-screen section (1.524 m by 71.1 cm by 71.1 cm) was connected at the upstream end of the test section by stainless-steel flanges. This section consisted of Plexiglas plates and was held together by aluminun angles and silicon sealant. Ten square Plexiglas spacers (61.0 cm by 61.0 cm) were inserted inside the section. Between these spacers, eight screens and two square honeycombs in frames were installed to eliminate the vorticity and turbulence of the free stream. In order from the upstream end of the section were the two honeycombs, two coarse-grid screens, three medium-grid screens and three fine-grid screens.

The dimensions of each honeycomb were 66.1 cm by 63.5 cm by 7.6 cm thick. Each cell was about 0.5 cm from side to side. The honeycombs were coated with water-proof epoxy to prevent deterioration.

The screens were held by the Plexiglas frames. Tension force was applied to keep the screens rigid and uniform. The screens were made of stainless steel wires with different diameters according to the grid size.

Two Plexiglas double flanges were used to join the square sections with the circular sections. Although this configuration produced abrupt changes of area at

the upstream end of the honeycomb-screen section and the downstream end of the test section, the flow field at the upstream end of test section was not affected.

The jet apparatus consisted of a 3 hp DC motor, a 40 liter/min constant displacement gear pump, a one-way valve, a 292 liter ballast tank and a 130 liter holding tank. Water for the jet was pumped from the holding tank through the one way valve to the ballast tank. The water passed from there through a tube to the jet and into the water tunnel. Water spilled from the overflow tube of the tunnel back into the holding tank, so the fluid volume inside the water tunnel was kept constant. To achieve constant jet exit velocity the motor speed was monitored by a shaft-mounted optical encoder and Hewlett-Packard frequency counter. The motor was driven by a Sorensen model DCR150-15A DC power supply and a 5 amp Trygon Super Mercury DC power supply. The ballast tank (pressurized to 10 psig) and one way valve were used to further reduce fluctuations in jet velocity. This arrangement allowed continuous jet flow. The system required one hour equilibrium time before taking data.

The stainless-steel jet (total length 73.7 cm) was supported by two stainless-steel air-foil struts and installed in the middle of the honeycomb-screen section. The jet nozzle passed through three screens and extended 22.9 cm into the test section. At the upstream end of the jet was a 3:1 elliptical nose-cone (2.22 cm diameter) to reduce the disturbance to the coflow. The jet was aligned with the centerline of test section pointing downstream. The contraction angles of the jet were designed as 3 ° to ensure against separation. The jet exit diameter was 0.28 cm.

3.2 *Calibration of Flow Facility*

During calibration of the volumetric flow rate of the jet, we found it unnecessary to operate the coflow. The pump was set at various speeds to get a complete calibration curve of the jet flow rates including the one used later during the jet measurements. After the system reached equilibrium, the water level of the ballast tank, holding tank and water tunnel and the pressure inside the ballast tank were constant. Thus, the volumetric flow rate of the jet was equal to the volumetric flow rate of the overflow. To measure the flow rate, water from the overflow tube was diverted from the holding tank and collected in a graduated container for a measured time interval of about 30 seconds. All the calibration points were repeated 2 to 4 times to reduce the uncertainty and obtain the average volumetric flow rate of the jet. The calibration curves are plotted in Figure 3 and Figure 4. A linear relation between the air pressure in the ballast tank and the square of the volumetric flow rate or jet exit velocity was obtained. However, the variation of the jet exit velocity was not linear with respect to the speed of the pump. Other calibration curves such as the calibration of the frequency tracker and linear-variable-displacement transformer are given in the next chapter.

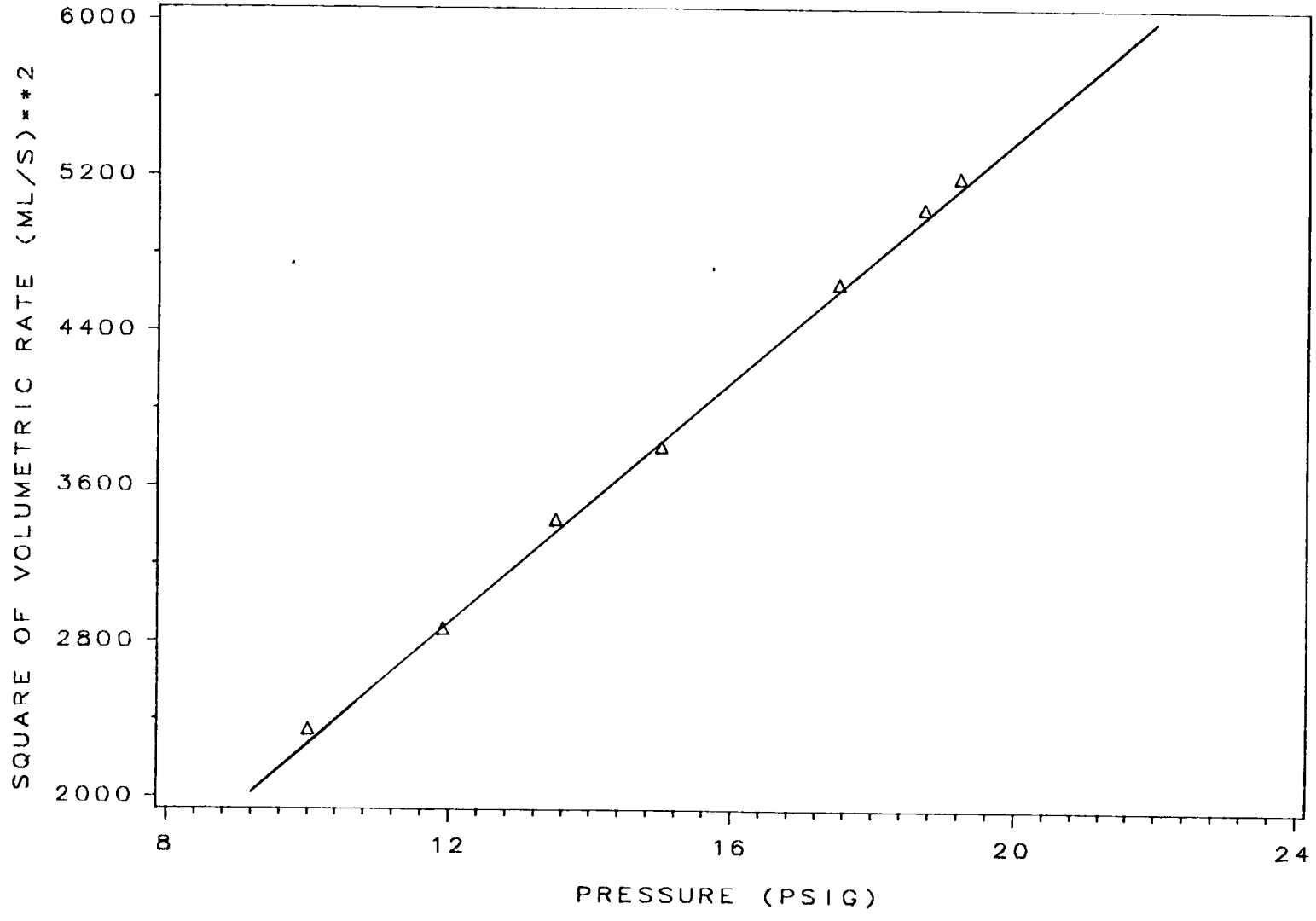

Figure 3 Tank Pressure vs. Jet Volumetric Flow Rate.

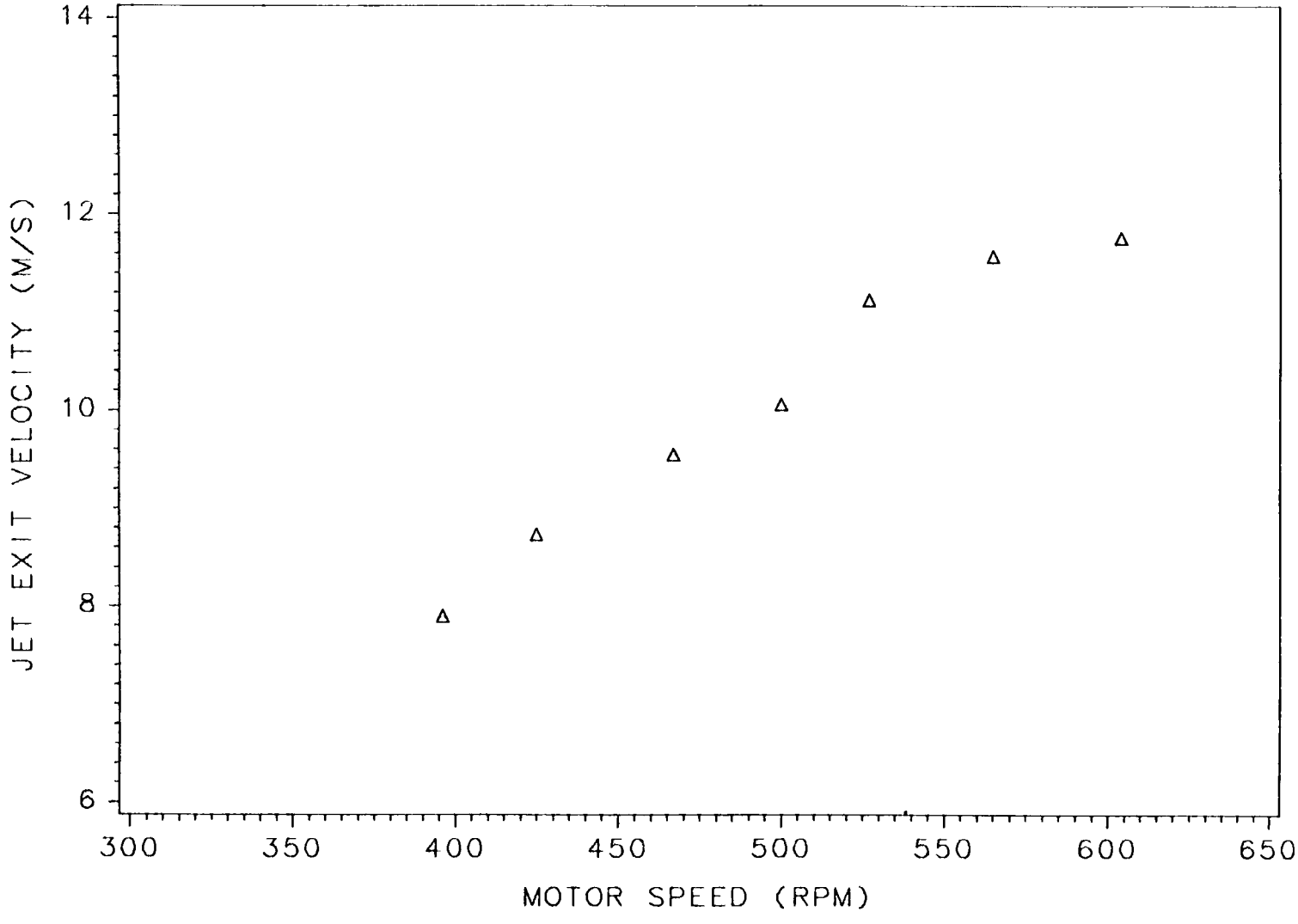

Figure 4 Jet Exit Velocity vs. Motor Speed.

The uncertainty of the flow rate calibration was less than 0.4 percent. Since the cross area of the jet exit is fixed, the variation of the jet speed was approximately 0.3 percent. This estimated uncertainty of the jet exit speed was obtained in the short period. The uncertainty due to the long term drift of the jet exit speed was not included. However, each velocity profile was measured in a short period (less than 1.5 hours), and the speed of the motor was monitored and adjusted to its nominal value constantly. Therefore, the effect of the long term drift is negligible for each profile. (it is shown by the symmetry of the profiles in the fifth chapter)

The testing parameters were summerized as follows :

Speed of motor	= 565	rpm
Volumetric flow rate of jet	= 71.0	ml/sec
Pressure in the ballast tank	= 18.7	psig
jet exit velocity	= 1160	cm/sec
jet exit diameter	= 0.28	cm
Laboratory temperature	= 25.0	° C
Reynolds number	= 32100	
Total momentum flux of jet	= 26130 $\rho\pi$	$cm^4/\ sec^2$

Chapter 4 Measurement Techniques

4.1 Laser Doppler Anemometry

The main components of the laser Doppler anemometer were a coherent 2 watt INNOVA 70 Ion laser, a beam splitter, mirrors, lenses, a TSI Model 9180A frequency shift system, two Matsushita acousto-optic light modulators (Bragg cells), and a photodetector. With these were built a dual-beam, frequency-shifted, forward-scatter laser Doppler anemometer (LDA). The configuration of the LDA system and the data acquisition system are sketched in Figure 5.

By now LDA is a well-known and well-developed experimental technique (see for example, Durst et al., 1976) A brief description of the technique follows.

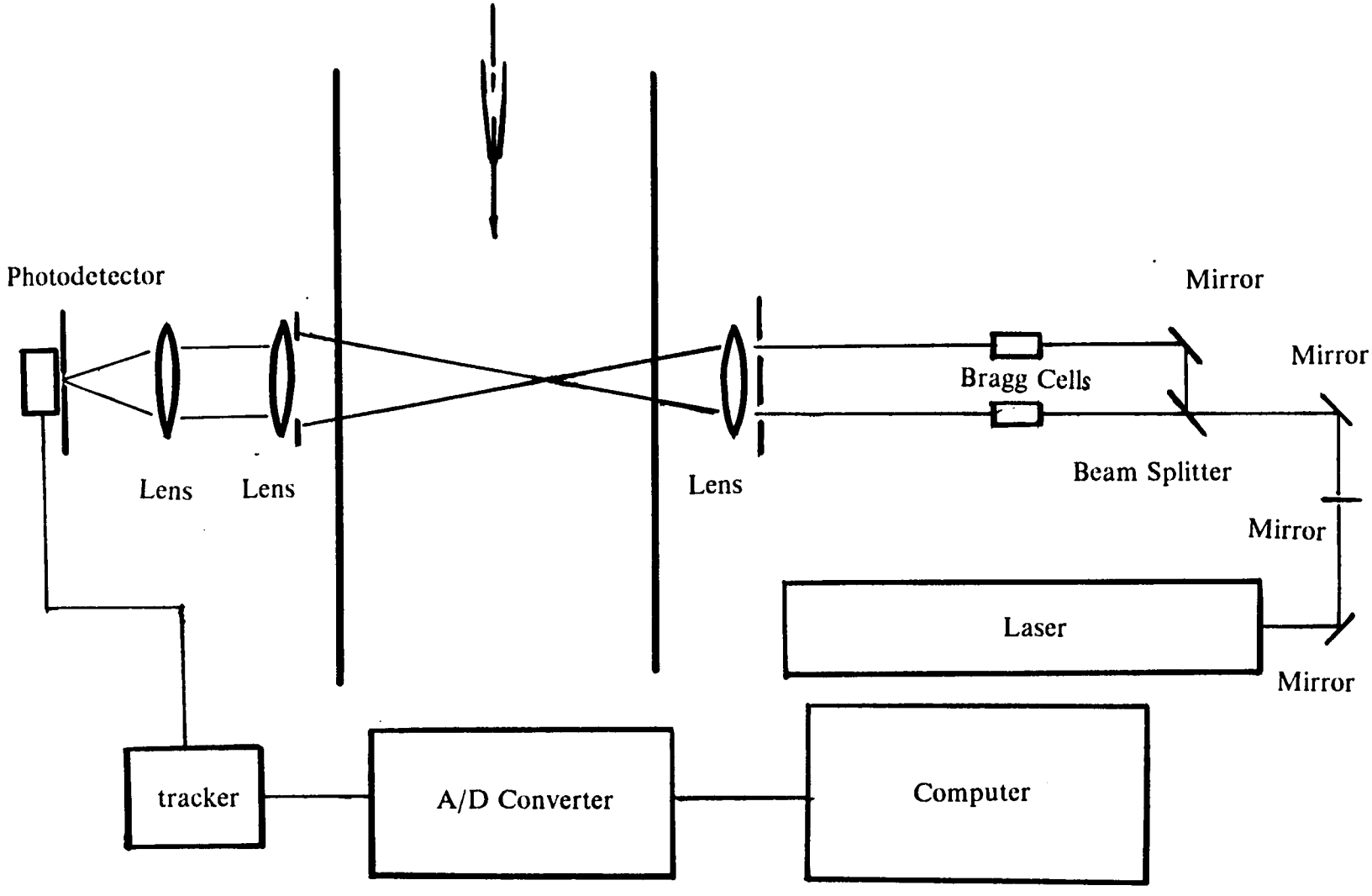

Figure 5 LDV Optics and Data Acquisition System.

Frequency-shifted LDA was introduced by Yeh and Cummins (1964). The frequency shift refers to adding an artificial frequency difference between two incident laser beams. One obtains a set of moving fringes at the intersection of the beams. If a stationary particle is located at the intersection, the scattered light produces a continuous Doppler frequency signal at the shift frequency. Consequently, a nonzero velocity reading is obtained even though the particle is stationary.

A pedestal is generated along with the Doppler frequency when a particle passes through the probe volume. The Doppler frequency is produced by the interference patterns of the light scattered from the two light beams from a moving center. The Doppler frequency contains the velocity information. The pedestal frequency was related to the time it takes for the particle to pass through the probe volume. The pedestal can be removed by frequency shifting which changes the Doppler frequency without changing the pedestal frequency. The pedestal can then be eliminated by a high pass filter. Frequency shifting is useful with any type of signal processor.

The equation relating the frequency and velocity of a particle without frequency shifting is

$$u = \frac{f\lambda}{2\ \sin(\frac{\theta}{2})} \tag{4.1}$$

where u is the velocity, f is the Doppler frequency, λ is the wavelength, and θ is the angle between the two incident light beams. The equation (4.1) shows that the particle velocity and the Doppler frequency are linearly related. The equation relating velocity and Doppler frequency with frequency shifting can be expressed as

$$u + u_{fs} = \frac{(f + f_s)\,\lambda}{2\,\sin(\frac{\theta}{2})} \tag{4.2}$$

where f_s is the shift frequency, and u_{fs} is the resulting shifted velocity.

The laser's green line (λ = 514.5 nm in air) was used. The single light beam was split to form two primary beams. After passing through two Bragg cells, two first-order beams (shifted approximately 40 MHz from the zero order beams) were intersected by an incident lens (38.1 cm focal length) to form the light scattering probe volume. A higher shift frequency, 2 MHz, was used between the two first-order incident beams, instead of the standard 500 kHz, because background noise generated by the driving motor of the tunnel was at the lower frequency. The optics arrangement produced a 2.73 ° half angle, $\frac{\theta}{2}$, in air. The method used to calculate the half angle is by projecting the intersected beam on the far wall(with measured known distance) and measuring distance between two beams. The uncertainty of the angle obtained is about 0.1 percent. A small half angle was used because of the size of the test section and the long focal length lens. The fringe spacing which resulted was 5.39 μm (in either air or water). The corre-

sponding uncertainty of the fringe spacing is 0.1 percent. The calculated (effective) dimension of the scattering volume at the intersection of the beams was about 150 μm by 3000 μm . The estimated length was considered an upper bound as it does not include the effects of the receiving optics, the restriction of the effective measuring volume by an aperture on the photodetector. There were about 30 fringes in the probe volume. Ambiguity noise was negligible inside the jet due to this high fringe number.

The seeding particles were made from an emulsion of vegetable oil in water (1 ml/liter) which was allowed to separate until particles were the desired size. The maximum particle size, as estimated by Stokes' Law, was 1.7-2.4 μm. The minimum detectable size for Mie scattering is approximately equal to the wavelength of the light, or 0.5 μm. The total volume of the emulsion used was 700 ml per water tunnel volume. To avoid the velocity bias problem described by McLaughlin and Tiederman (1973), a highly seeded water flow and a frequency tracker were used. The biased seeding problem (Barnett and Giel, 1975) which occurs in jet measurements in gases was negligible because of the high concentration of seeding particles. The velocity signals could be processed as continuous signals (like hot-wire signals) instead of the discrete signals in air.

The receiving optics were mounted in a forward scatter configuration. The two incident beams were blocked at the first of two receiving lenses. Each receiving lens had the same focal length as the incident lens. The focused light was detected by a UDT PIN 3D photodiode in a hybrid cascode circuit (Walker, 1984)

through a 300 μm pinhole. The Doppler signal was filtered and amplified 500 times and demodulated by a 1 MHz 4th order Butterworth high pass filter, three inverting amplifiers and a frequency tracker. The final signal was adjusted to values ranging between -5 volts to +5 volts and then digitized at a rate of 500 samples/sec by a MetraByte 12-bit A/D converter and stored in an AT compatible computer. 10000 samples were taken at each measurement point. All the data were later transferred onto a DC2000 40 megabyte mini-cartridge streaming tape.

Some frequency broadening occurs in LDA measurement which distorts the velocity probability density function (Durst et al., 1976). The instrument broadening was estimated during the calibration of the instruments. The calibration demonstrated that the broadening caused by the resolution of the instruments could be neglected. Details of the calibration of the instruments will be discussed later in this chapter. Another broadening effect, velocity gradient broadening, results when the mean velocity varies significantly within the size of the scattering volume. A small half angle, which caused longer probe length in the transverse direction, may introduce larger velocity gradient broadening. In contrast, a greater half angle increases transit time broadening as it reduces the velocity gradient broadening. None of these broadening effects were significant, except in the flow field outside the jet where the turbulence intensity was low.

4.2 *Traverse Equipment*

The optics were mounted on a triangular (Ealing) optical bench clamped to two I-beams. The optical assembly and laser were mounted on the table of a milling machine base (Cincinnati Milling Machine Co., Serial No. 5A2U1P-44) to allow precise traversing in three directions while maintaining the alignment. The uncertainty of the traverse mechanisms of the milling machine was within 0.05 mm. A 15.3 cm Linear-Variable-Displacement Transformer (LVDT) was mounted on the milling table to detect the distance along the transverse direction (horizontally, across the flow) or the z axis.

The position of the LDA probe volume moved at $N_{water} / N_{air} = 4 / 3$ times the mechanical traverse displacement due to refraction when traversing in the z direction. This was taken into account for motion in the z direction. No correction was necessary for the other traverse axes.

The signal of the LVDT was filtered, adjusted to output values ranging from -5 volts to +5 volts by a 1 kHz 4th order Bessel low pass filter and a voltage divider, and then digitized by the A/D converter at a rate of 500 samples/sec. 1000 samples were taken at each location. The output voltage from the circuit was also monitored by a Keithley 175 multimeter to ensure that there were no bad connections in the circuit. The calibration of the LVDT is given together with the calibration of the frequency tracker in a later part of this chapter.

4.3 *Instrumentation*

Construction of some electronic circuits was required to conduct this research. Schematic diagrams of filters, amplifiers and the protection circuit for the A/D converter are shown in Appendix A. The block diagram of the frequency tracker is shown in Figure 6. Detailed discussion of the frequency tracker follows.

The circuit invòlved two major branches. The first branch of the circuit functioned as a frequency-to-voltage converter. The last stage of this branch contains an output range adjustment element. The output of this branch was calibrated by a function generator to obtain the relationship between the input frequency and the output voltage.

The second branch was a voltage discriminator. Its output signal indicated whether or not a Doppler signal was present and enabled the frequency-to-voltage converter. The discrimination level could be adjusted by changing the threshold of the discriminator. Therefore, background noise could be avoided by increasing the threshold above it.

The design of the frequency tracker differed from commercially available trackers. Most commercial frequency trackers contain a phase locked loop. The present tracker combines a track and hold technique and amplitude discrimination, but without a phase locked loop. Even with low signal-to-noise ratio, the present tracker worked well. The track and hold feature operates by latching the

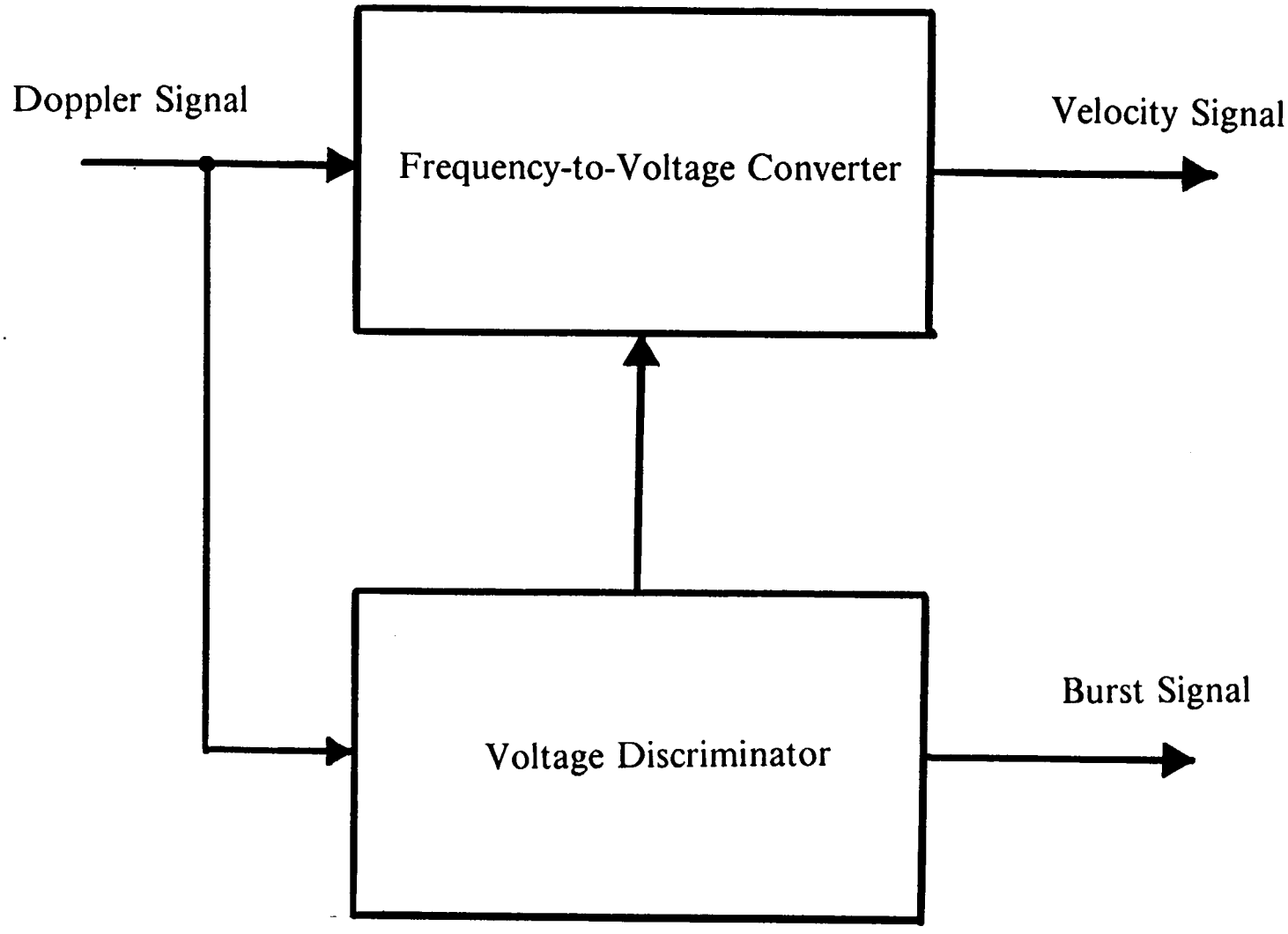

Figure 6 Block Diagram of Frequency Tracker.

voltage at its last valid level as the Doppler signal is lost due to noise or a void of seeding particles, i.e. "drop-out." The drop-out time is also minimized by increasing the concentration of the seeding particles in the flow. For more discussion about signal processing and this tracker design refer to Walker (1986 and 1988).

The performance of the tracker deteriorates on turbulence measurements in flows with low turbulence intensity such as the background flow in the present experiment. Spikes occur during the transition of the drop-out. This broadens and skews the measured velocity probability density function and can result in a bias of the mean velocity and a higher value of turbulence. However, the spikes were adjusted to be symmetric about the mean (upward and downward spikes were nearly equal) in the present frequency tracker. Thus, no skewness of the probability density function occurred, only broadening in the background flow measurement. This broadening effect was insignificant inside the jet flow because of high turbulence intensity.

The frequency tracker was designed to respond to input Doppler frequencies up to 5.0 MHz. The response of the tracker was tested. The output of the tracker was linear only up to 4.3 MHz input frequency because of the limitation of the bandwidth, slew rate and linearity of some electronic elements used in the circuit. However, the frequency range used in the present study was between 2.0 MHz to 3.0 MHz which is within the linear range of the tracker. The output voltage was adjusted to get the full scale response for this frequency range. Conse-

quently, the uncertainty introduced in digitizing the output signal of the tracker by the A/D converter was reduced considerably.

4.4 Calibration of the Traverse and Instruments

The LVDT was calibrated by using the read-out of the scale dial of the milling table traverse mechanism. One thousand samples were taken and digitized at the rate of five hundred samples/sec by the A/D converter and stored in the computer. The read-out was recorded at different positions and stored in the computer. The linear portion of LVDT output signals were calibrated. A least-squares fit gave the calibration curve that related the output voltage to the position. The calibration correlation coefficient was 0.99996. The calibration curve is plotted in Figure 7. The deviations of each sampling group at various positions is plotted in Figure 8. The uncertainty of the mean position reading of the LVDT was less than 0.002 mm.

The frequency tracker assembly was calibrated by using a BK Precision Model 3030 function generator and a Hewlett Packard 5300A frequency counter. Continuous sine waves at various frequencies were generated by the function generator, filtered and amplified through the filter and amplifier circuits, and then converted to voltage by the frequency tracker. Ten thousand samples of the output signal of the tracker were taken and digitized at the rate of five hundred

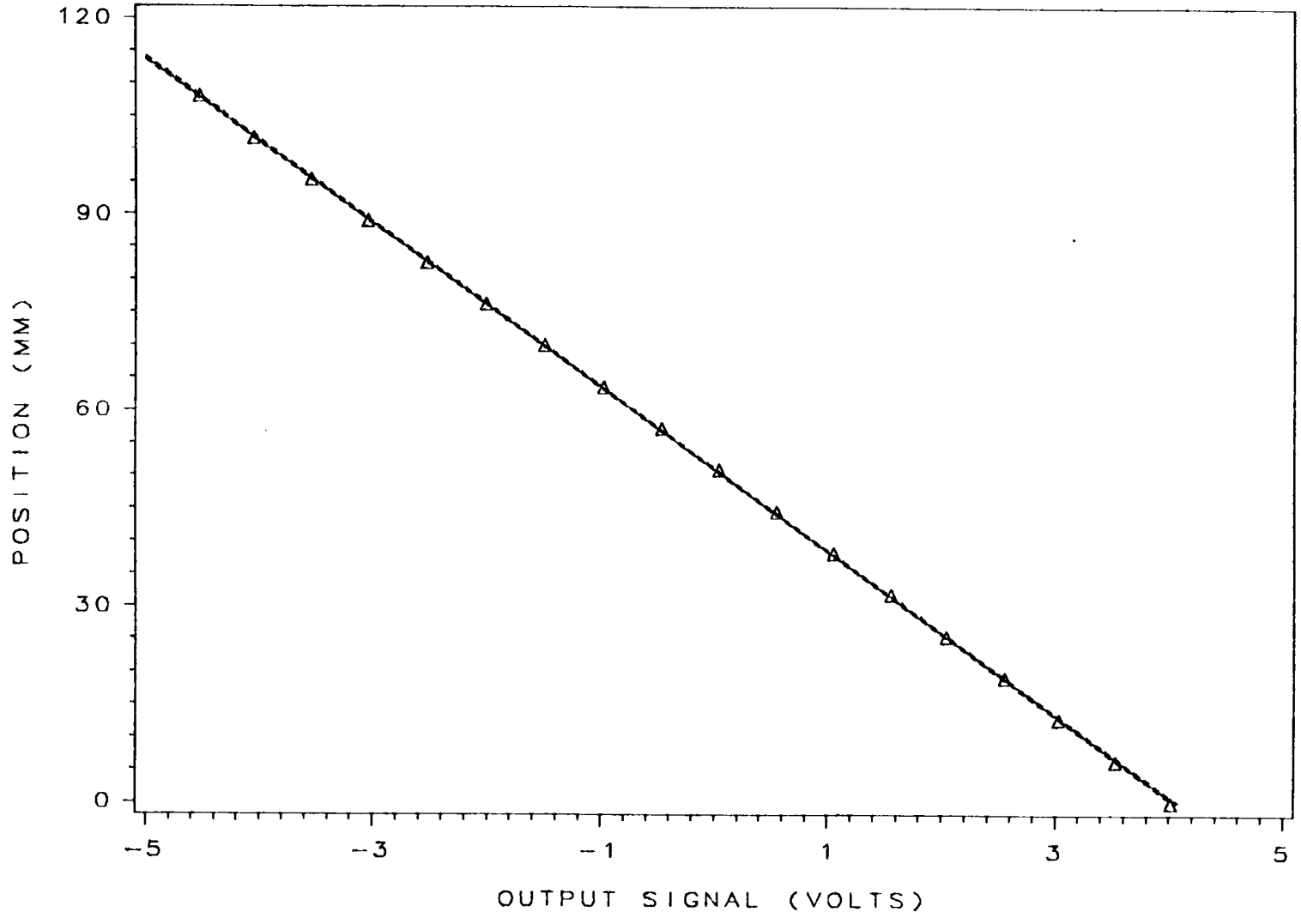

Figure 7 Calibration Curve of LVDT.

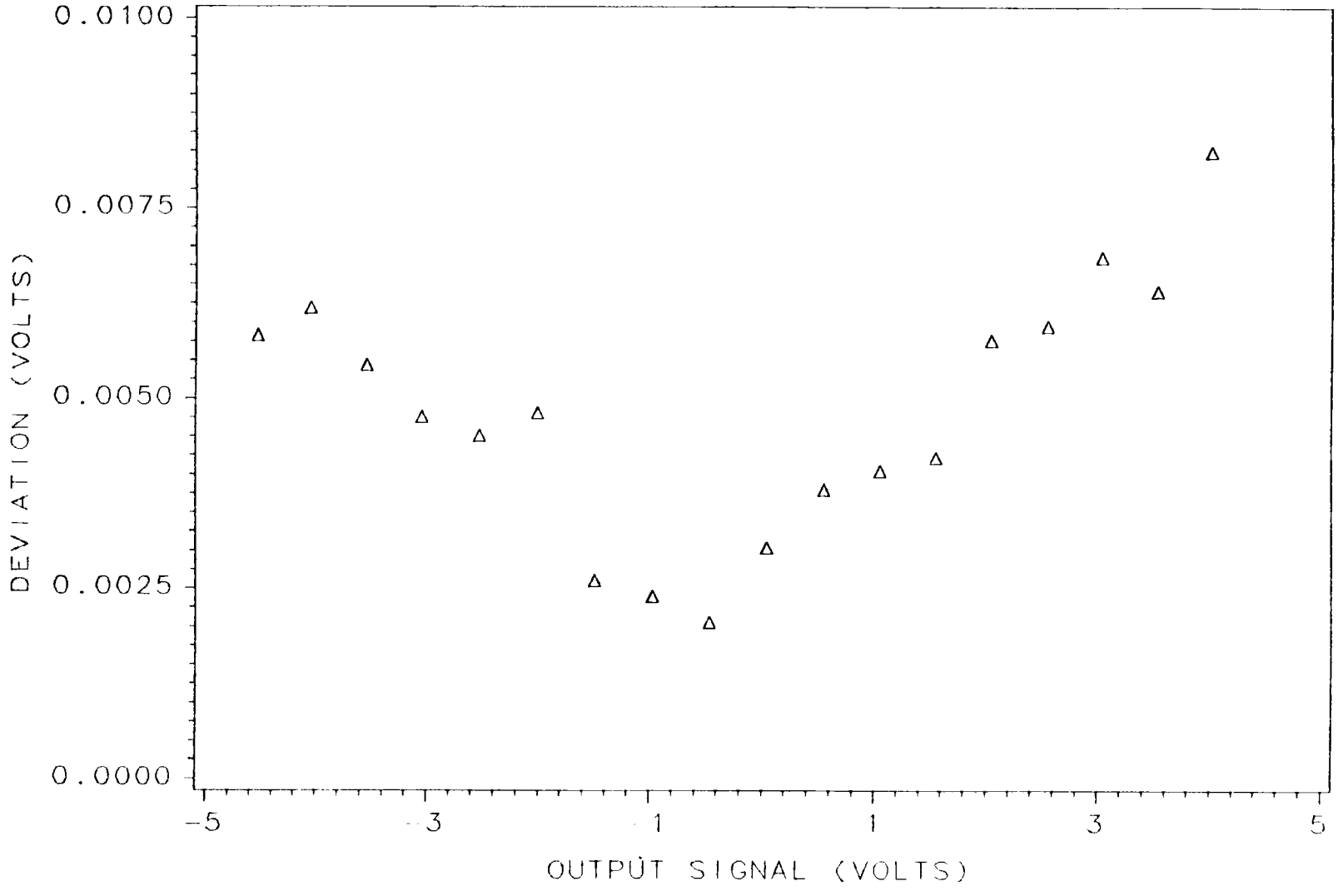

Figure 8 Calibration Deviation of LVDT.

samples/sec by the A/D converter. The sine wave frequencies were monitored by the counter and recorded by the computer. Both full range (600 kHz to 4.3 MHz) and the range from 1.8 MHz to 3.3 MHz were calibrated, see Figure 9 and Figure 10. The deviations at various frequencies in Figure 9 and Figure 10 are presented in Figure 11 and Figure 12 respectively. A least-squares analysis was applied to get the calibration curve between output voltage and input frequency. The correlation coefficient of full range calibration curve was 0.9999976 and for the range from 1.8 MHz to 3.3 MHz was 0.9999982. The linearity of the frequency tracker was shown by the full range calibration. The second calibration curve, Figure 10, was used in all the measurements. The uncertainty based on the mean squared error of the second calibration curve is about one significant bit of the A/D converter. Therefore, the uncertainty of the velocity measurements, if the Doppler signal is strong and continuous, is approximately equal to the uncertainty of the frequency-voltage conversion. The corresponding velocity value of this uncertainty is 0.025 mm/sec.

The uncertainty estimated from the calibration is the lowest reference uncertainty of the velocity measurements because the tracker was calibrated by strong, continuous signals from the function generator, instead of the weak, quasi-continuous Doppler signals scattered by the seeding particles. The uncertainty due to the alignment of the optics (mostly is due to the uncertainty of the half angle) is much larger than the uncertainty introduced by the frequency-voltage conversion. By including these uncertainties, the corresponding uncertainty of the velocity measurement is 0.2 percent of the measured velocity value (from

Kline and McClintock equation). The estimation of the uncertainty for the mean velocity measurements will be given from the measured velocity profiles in next chapter.

4.5 Measurement and Data Reduction Processes

The water tunnel facility and jet were equilibrated for at least one hour before measurements were made. The ballast tank was pre-pressurized to 10 psi by filling with compressed air. The jet flow loop was opened and powered by turning on the 3 hp DC motor. The motor speed was set at 565 rpm and was monitored by the frequency counter through the optical encoder. The speed of the water inside the water tunnel was controlled by tuning the frequency of the AC induction motor speed controller. The laser Doppler anemometer and instruments were turned on and tested after the flow system reached its equilibrium state. The raw Doppler signal and the output signal of the frequency tracker were monitored by a BK Precision 1590A 100MHz oscilloscope to ensure that the signal and the circuits were operating correctly. The drop-out rate of the frequency tracker was less than 8 percent.

Each profile was started at the same z location and traversed in one direction (from positive z to negative z). One thousand samples of the output signals from the LVDT and ten thousand samples of the output signals from the frequency

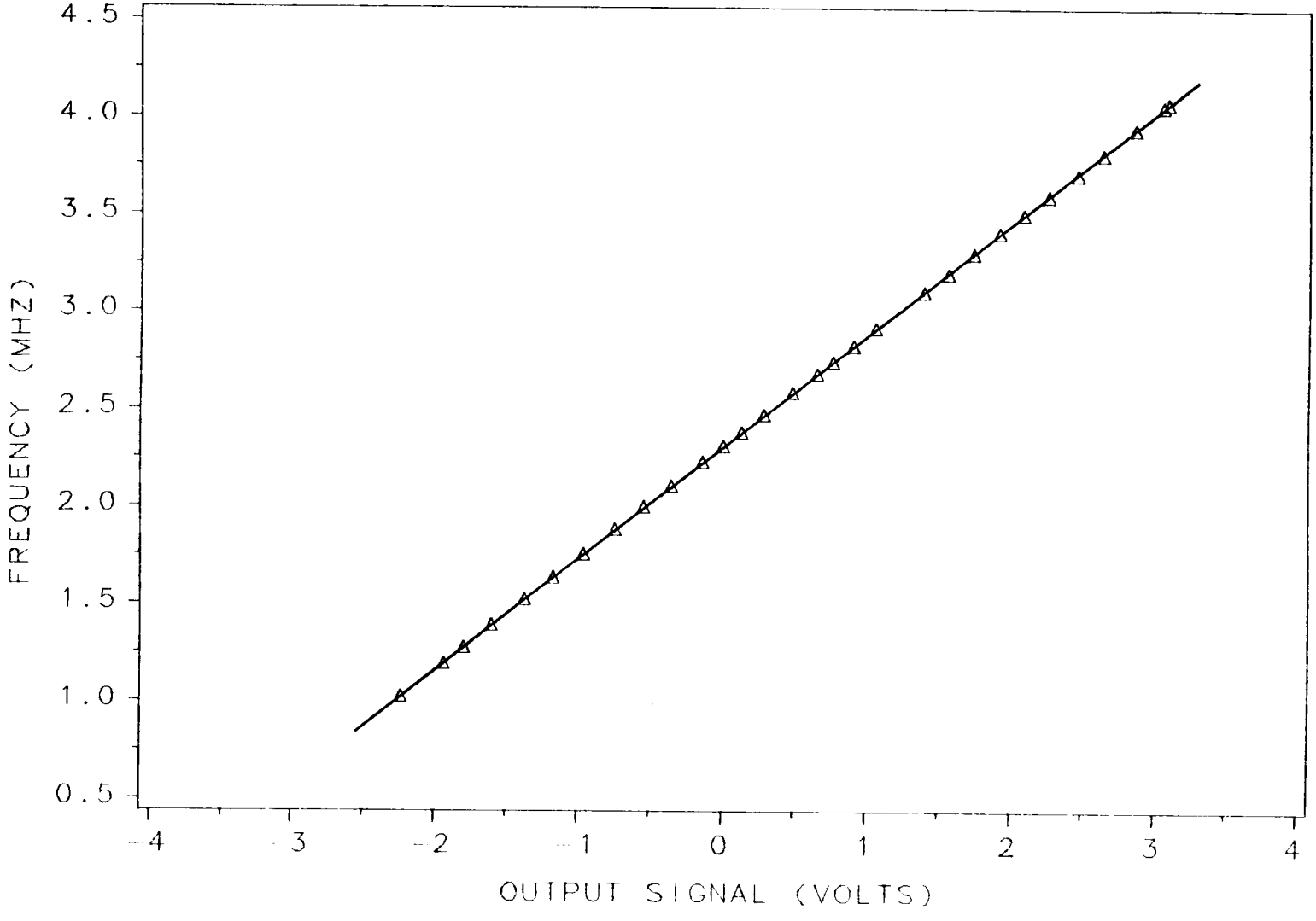

Figure 9 Full Range Calibration Curve of Frequency Tracker.

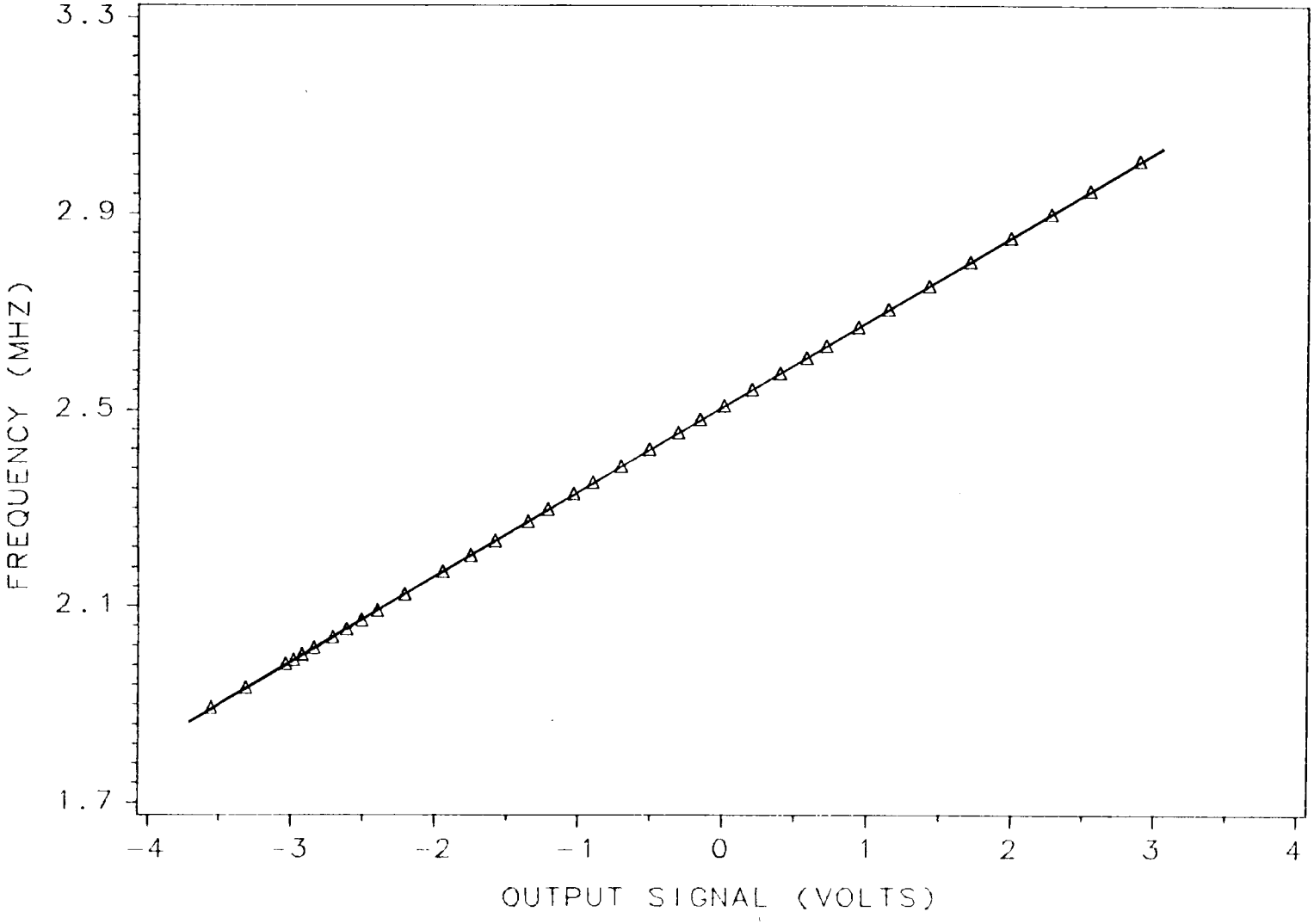

Figure 10 Calibration Curve of Frequency Tracker within 1.8 - 3.3 MHz.

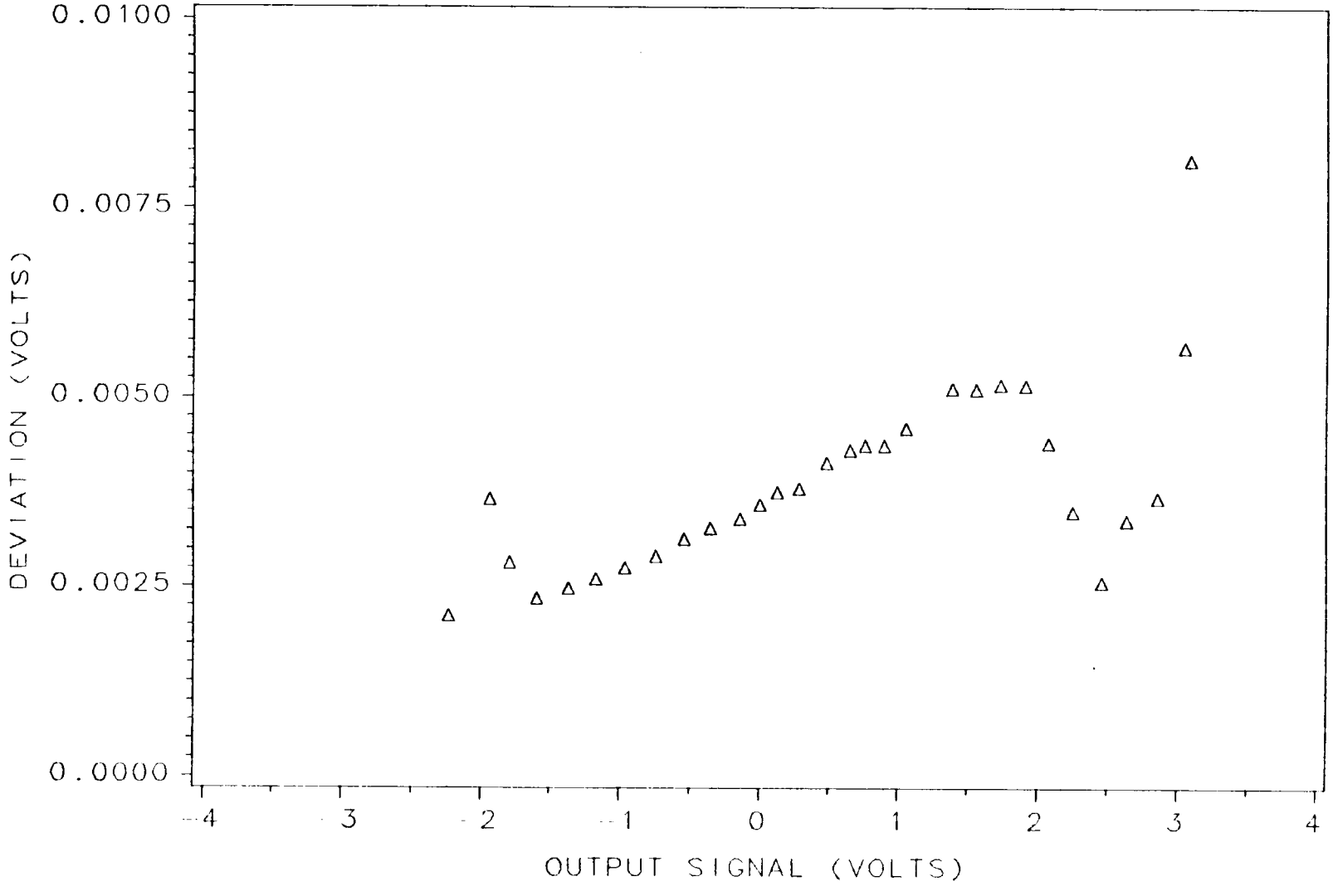

Figure 11 Full Range Calibration Deviation of Frequency Tracker.

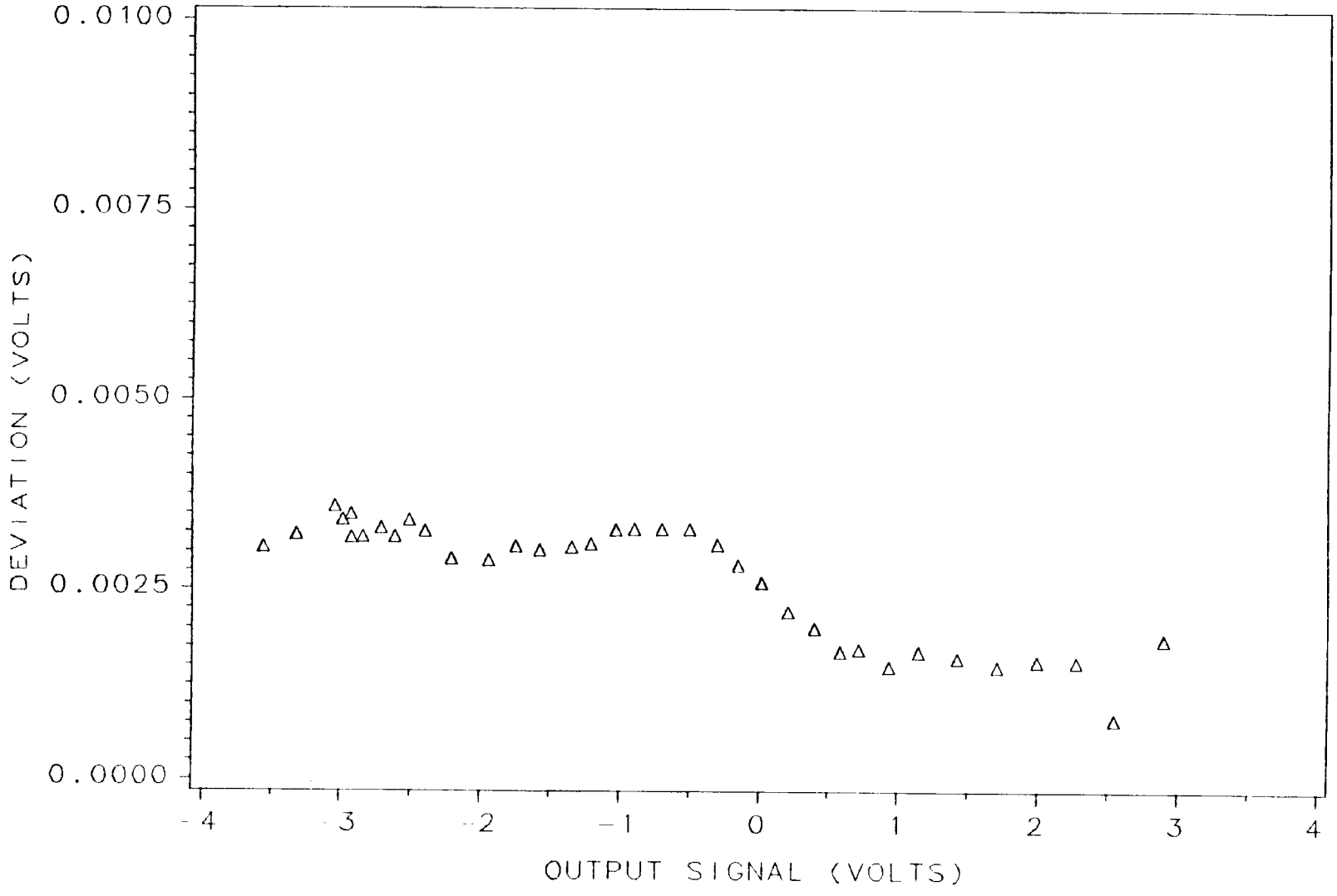

Figure 12 Calibration Deviation of Frequency Tracker within 1.8 - 3.3 MHz.

tracker were digitized at a rate of 500 samples/second by the A/D converter in Direct Memory Access (D.M.A.) mode, and then saved in binary form on the hard disk of the computer. The data files were then transferred to a streaming tape. Each file corresponded to one location and contained 20 KB of velocity data and 2 KB of position data.

The program used to collect data, control the experiments including data sampling, calibration, least-square fitting and data reduction was written in Fortran and compiled by the Microsoft 4.01 Compiler. The subroutines used to control the A/D converter and data I/O were supplied by the MetraByte Corporation. Only a brief description is given here about the data reduction. Refer to Holman (1984) for the details of the statistical analysis involved in data reduction.

Frequency and position data files were processed in the same way. The routine was as follows: Each data file was divided into several subsets. The number of samples in each subset could be arbitrarily assigned. 100 samples per subset was used here. The mean of each data file was computed by averaging the sum of all the subsets. Integer format was used in summing the samples to reduce the round-off error that occurred in real format summation. However, the reduction of the frequency data was more complicated due to the noise generated by the drop-out of the frequency tracker.

Each data file, 10000 samples, contained the velocity information at one position. Before reducing the data files, several files were chosen to compute the probabil-

ity density function. The samples within the main envelope of the probability density function (nearly Gaussian distribution) were used to compute the mean and rms values of the Doppler frequency. The samples outside three deviations were truncated during the data reduction. The typical probability density function is shown in Figure 13.

After the mean and the rms of the frequency were obtained, the mean velocity could be computed by using the equation (4.2), in which the shift frequency was subtracted from the mean frequency to get the real Doppler frequency. As mentioned before, the shift frequency was set at 2 MHz. The shift frequency was measured to ensure its accuracy by moving the scatter volume to the side wall of the test section. A continuous Doppler frequency was generated by the stationary wall and was equal to the shift frequency. Three repeated measurements were made, processed and averaged to get the value of the shift frequency after each complete velocity profile measurement. The shift frequencies were found to deviate 10 kHz from 2 MHz.

The mean and rms velocity and the position data were combined after data reduction. The final velocity profiles and other calculated results such as the spreading rate, and entrainment rate are presented in next chapter.

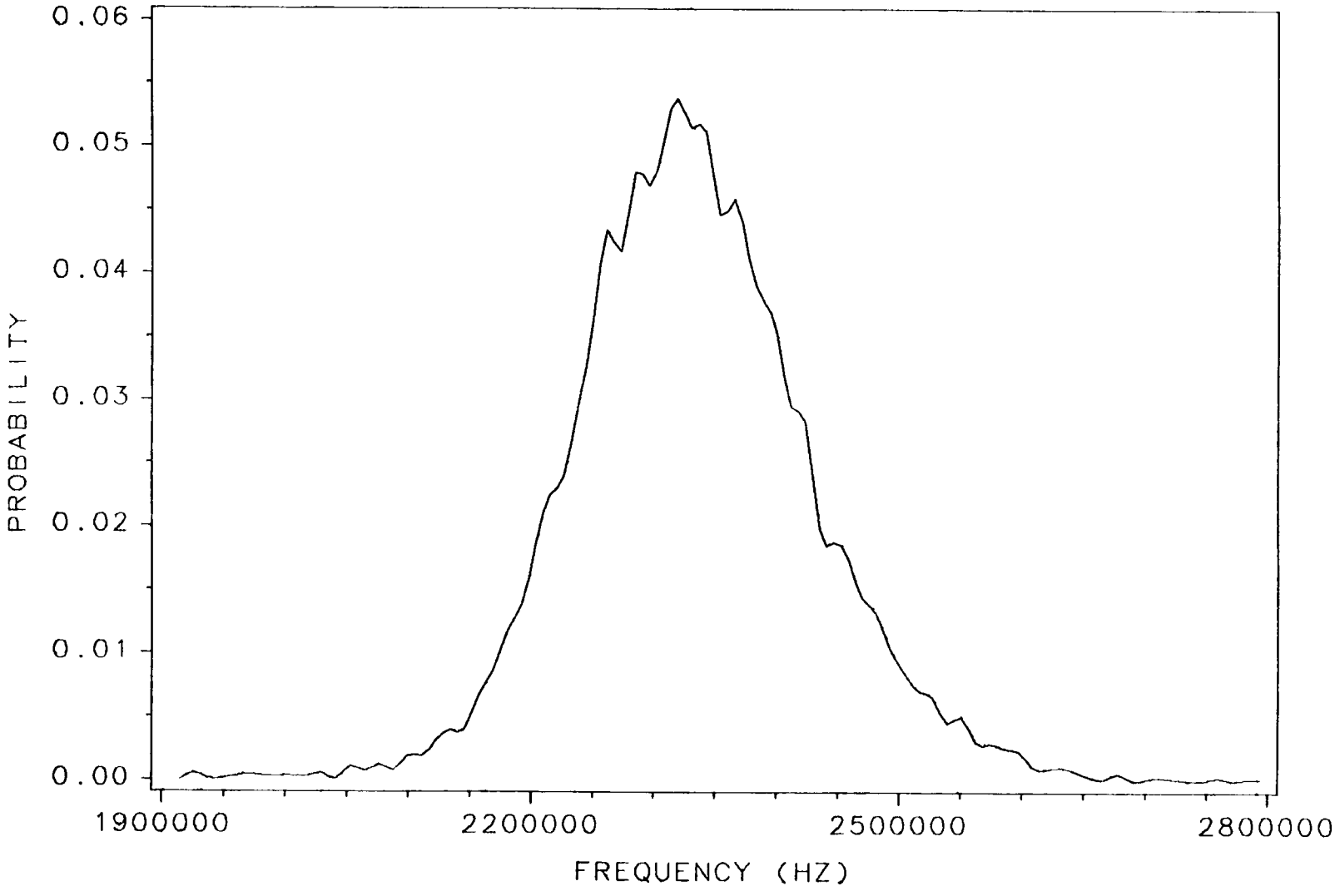

Figure 13 Probability Density Function of Samples at Centerline of the Jet, $x/d = 30$.

Chapter 5 Result and Discussion

A jet flow with several different coflowing streams (U_s/U_j = 0.0034, 0.0071, 0.009 and 0.0136) was measured. The results have been calculated and are presented in the following sections. The quantities deduced from the mean velocity profiles are shown and discussed first. The rms velocity distributions of the jet flow are given in the latter part of the chapter.

5.1 Axisymmetric Measurements of the Jet Flow

A calibration measurement of the jet flow was made to locate the centerline axis of the jet and verify the jet symmetry. The probe volume of the LDA was traversed in both the vertical (y) and horizontal (z) directions at the axial location x/d

= 40.5 downstream of the jet exit. After the peak value of the axial mean velocity in both directions was found, a full velocity profile was established in both vertical and horizontal directions. There was a difference at the peak of the profiles between the measured axial mean velocity profiles in z and y directions of 3 percent. This may be due to the long term drift of the jet exit velocity. Therefore, these two mean velocity profiles were rescaled by their centerline excess mean velocities U_0 and half widths $R_{1/2}$ and plotted in Figure 14 to show the symmetry of the jet. The measured rms velocity distributions in both directions are plotted in Figure 15.

The slight difference between the rms velocity distributions in the y direction versus the z direction near the axis of the jet may be due to velocity gradient broadening since the probe volume is longer in the z direction. However, generally the rescaled axial mean velocity profiles and measured rms velocity distributions coincided very well. While these do not prove axisymmetry; they indicate that the jet is not elongated in the y or z directions - a strong indication of axisymmetry. This also allows us to take measurements in a single direction. In this case the horizontal direction , z, was chosen.

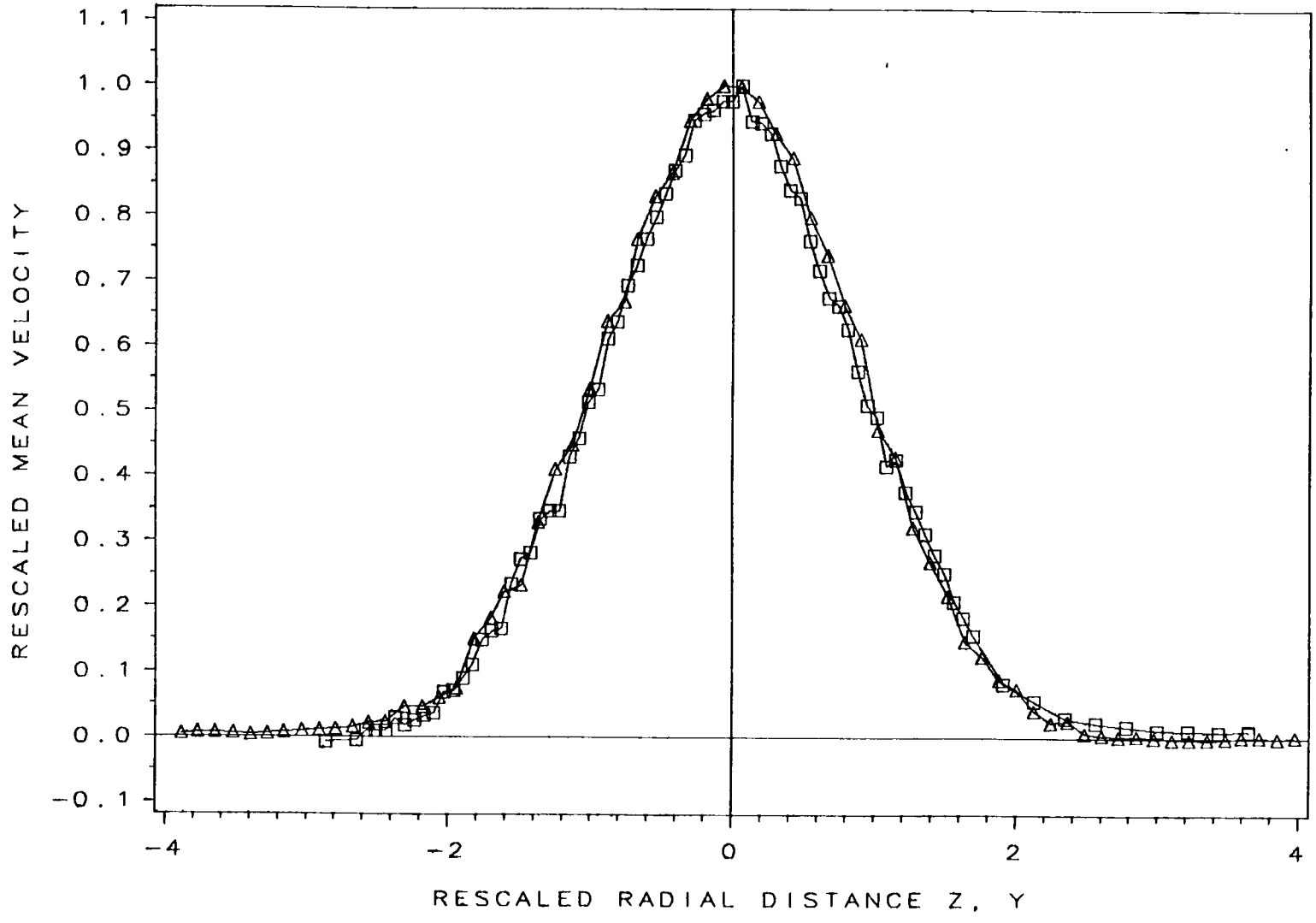

Figure 14 Mean Velocity Profiles on Z and Y axis with U_i/U_j = 0.0136.

△, z axis; □, y axis.

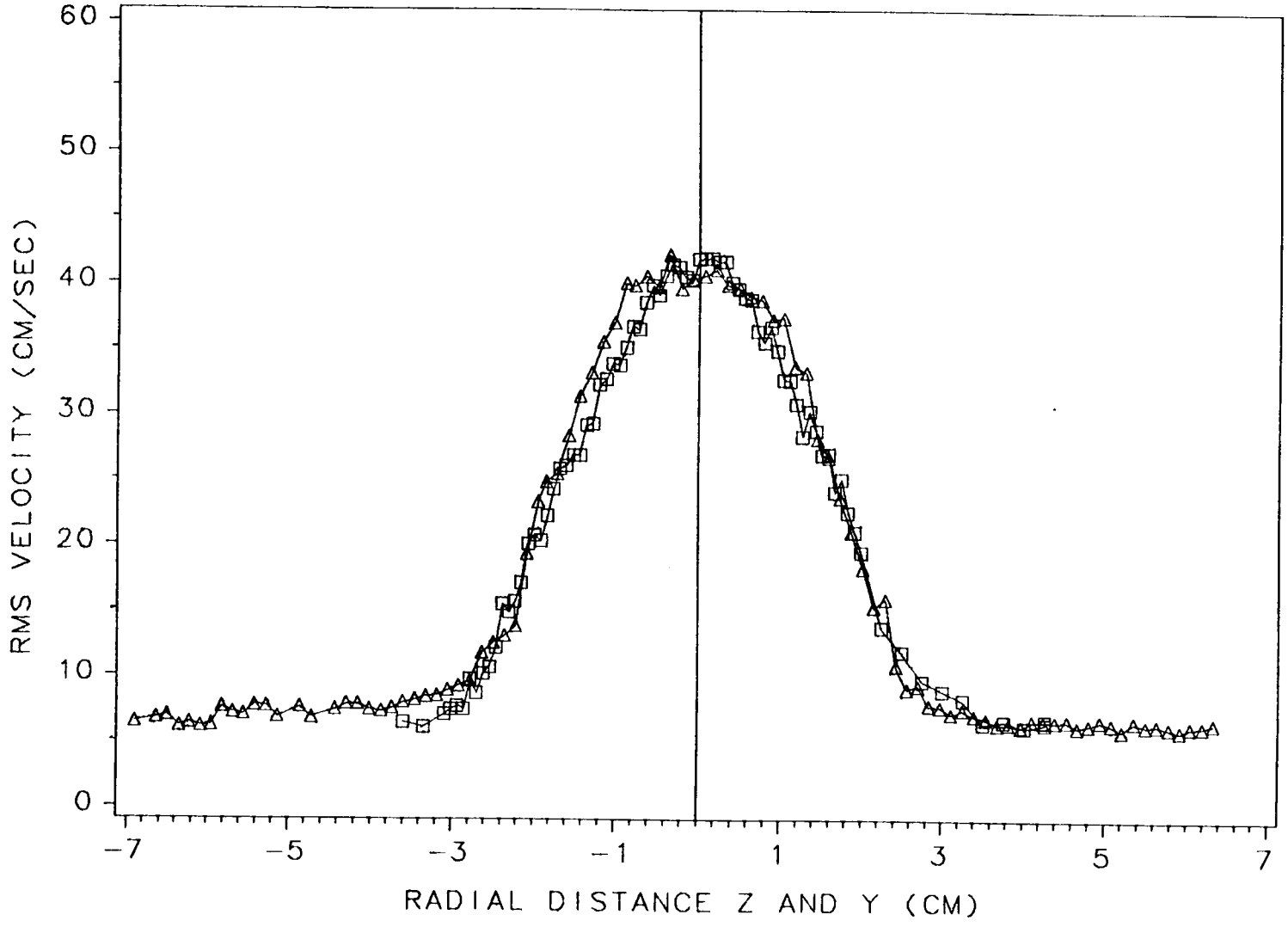

Figure 15 RMS Velocity Distributions on z and y axis with U_s/U_j = 0.0136.

△ , z axis; □ , y axis.

5.2 *The Axial Mean Velocity Profiles*

Axial mean velocity profiles were measured at the axial locations x/d = 30, 40.5, 60 and 100. Several different background flow velocities were used. The measured axial mean velocity profiles under the conditions U_s / U_j = 0.0034, 0.009 and 0.0136 were plotted in Figures 16, 17 and 18 respectively. A symmetric axial mean velocity profile with the characteristic nearly Gaussian shape was shown at each measurement location.

Upstream profiles had less scatter compared to profiles far downstream. There are thought to be two reasons: 1. The difference between the jet velocities and background flow become much smaller and harder to resolve. 2. Due to larger scales and lower velocities much longer averaging times are required to reach the same level of uncertainty. In the present study the sampling time was adequate for our purposes. In the high shear region of the profiles, intermittency and increased turbulence intensity (based on the local mean) also contributed to increased scatter.

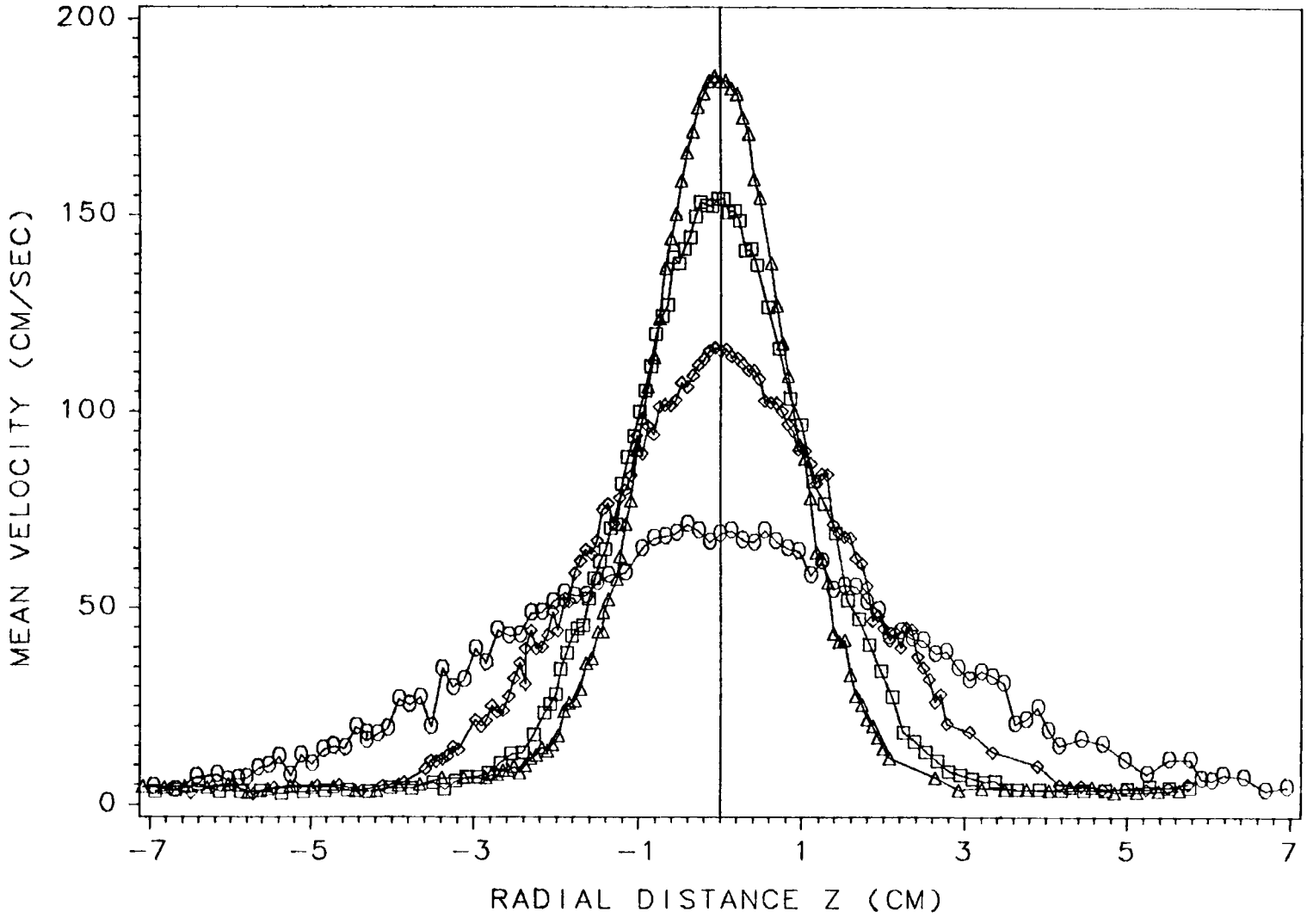

Figure 16 Mean Velocity Distributions with U_i/U_j = 0.0034.

△ , x/d = 30; □ , x/d = 40.5; ◇ , x/d = 60; ○ , x/d = 100.

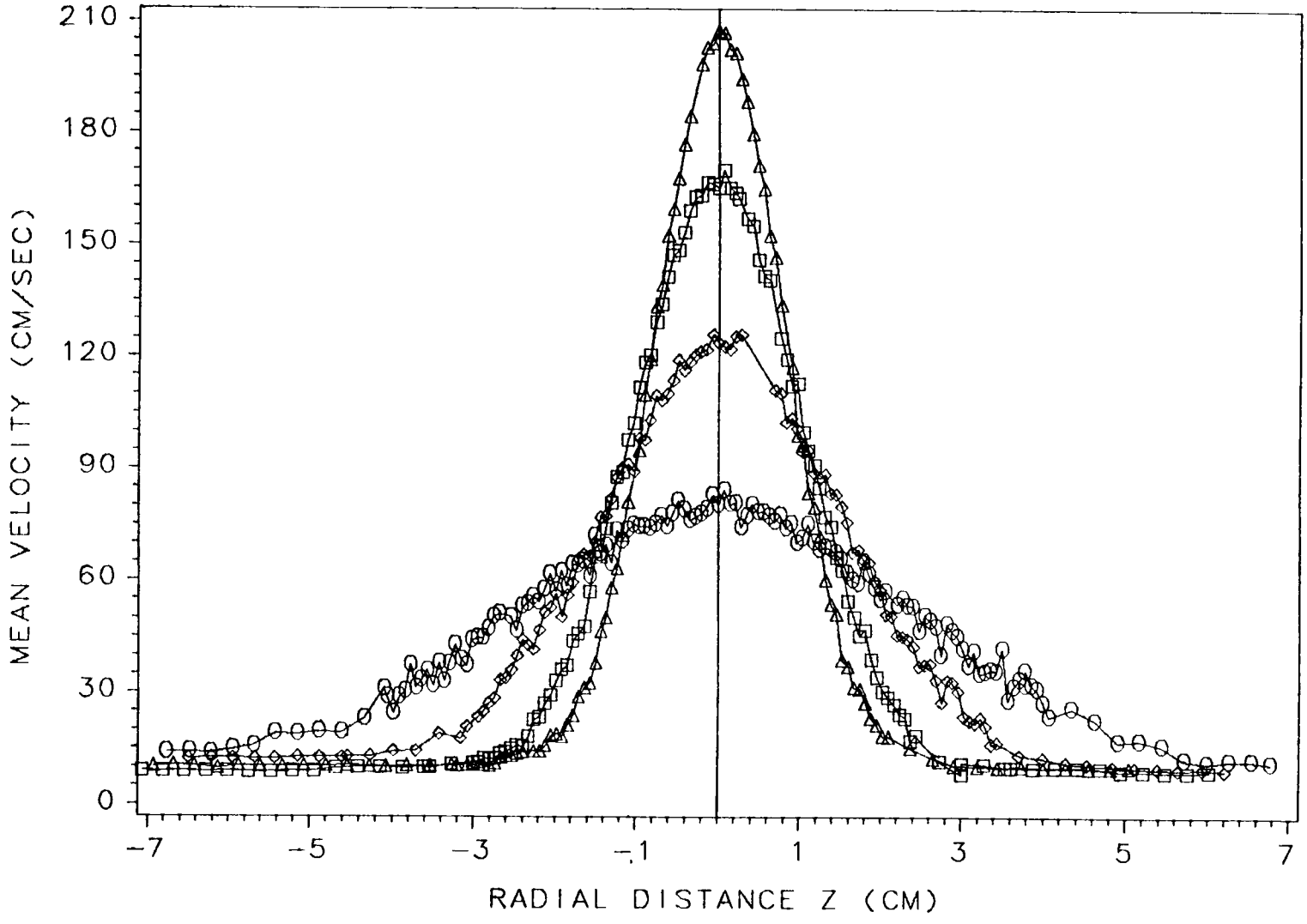

Figure 17 Mean Velocity Distributions with U_s/U_j = 0.009.

△ , x/d = 30; □ , x/d = 40.5; ◇ , x/d = 60; ○ , x/d = 100.

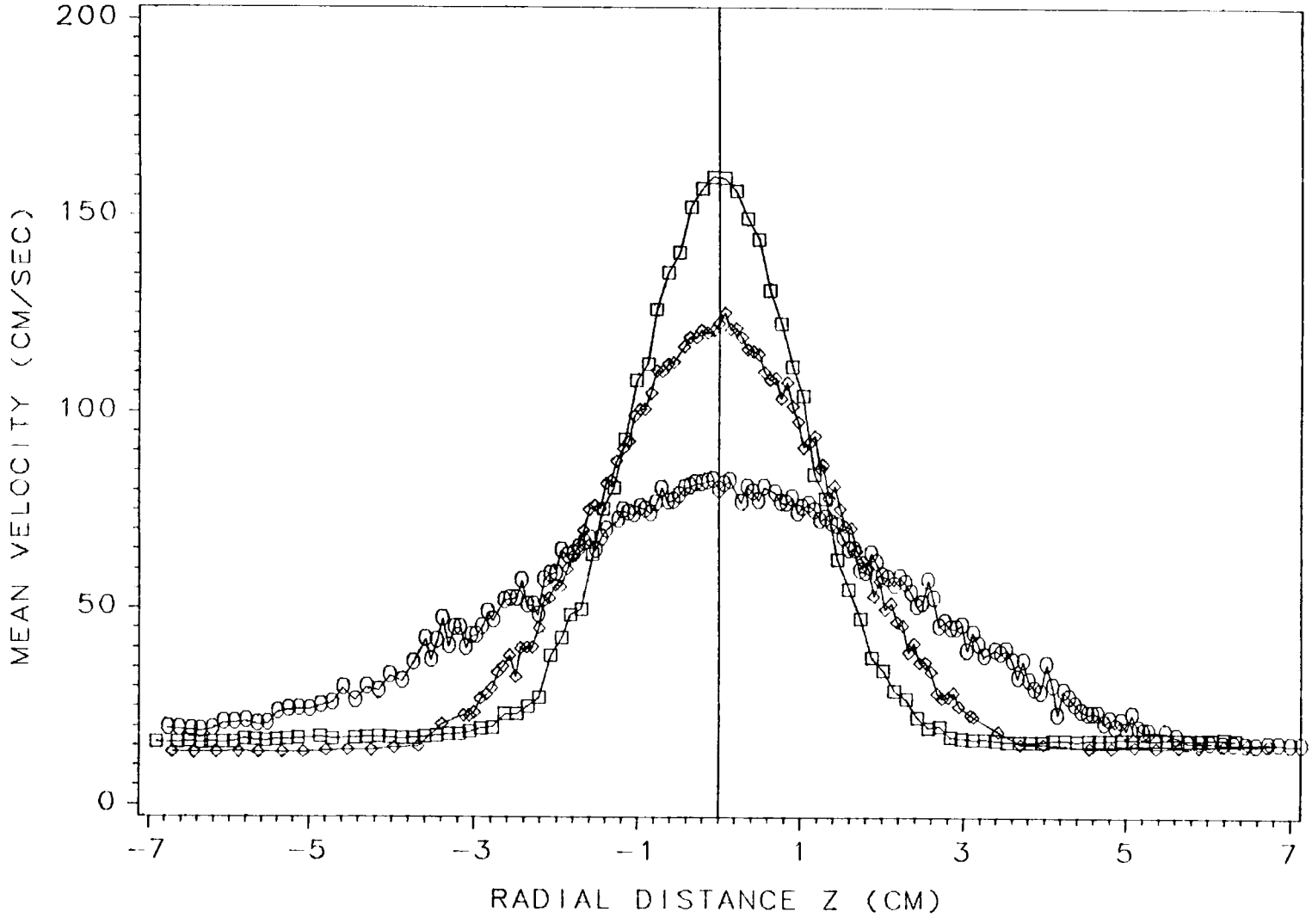

Figure 18 Mean Velocity Distributions with U_s/U_j = 0.0136.

□ , x/d = 40.5; ◇ , x/d = 60; ○ , x/d = 100.

5.3 *The Half Width Variation of the Jet Flow*

The half width of the jet was determined as the distance between the centerline of the jet and a point in the z direction at which the excess axial mean velocity of the jet flow was half the value of the centerline excess axial mean velocity. The following procedure was used to locate the half width: First because the profile was nearly Gaussian, replacing r with $\log(r)$ should be approximately parabolic. Then a parabolic least squares fit in the neighborhood of the half width was used to locate the point. Because the half width is found by a least squares fit to points in the vicinity, it is not sensitive to the uncertainty of individual points. The measured half width at different measurement stations and background flow velocities in the present study and the data taken by other investigators are presented in Figure 19.

The linear increase of the half width with respect to the axial distance from the virtual origin (not necessarily at the jet exit plane) was consistent with the prediction of the axisymmetric turbulent jet theory based on the self-preservation assumption. The linear growth of the axisymmetric jet flow agrees with the data taken by other researchers with and without a slower coflowing stream.

In Figure 19, the data taken by Antonia and Bilger (1973) with a strong coflowing stream ($U_s / U_j = 0.22$ and 0.33) show a nonlinear variation of the half width. This can be contrasted with other researchers who used a slower

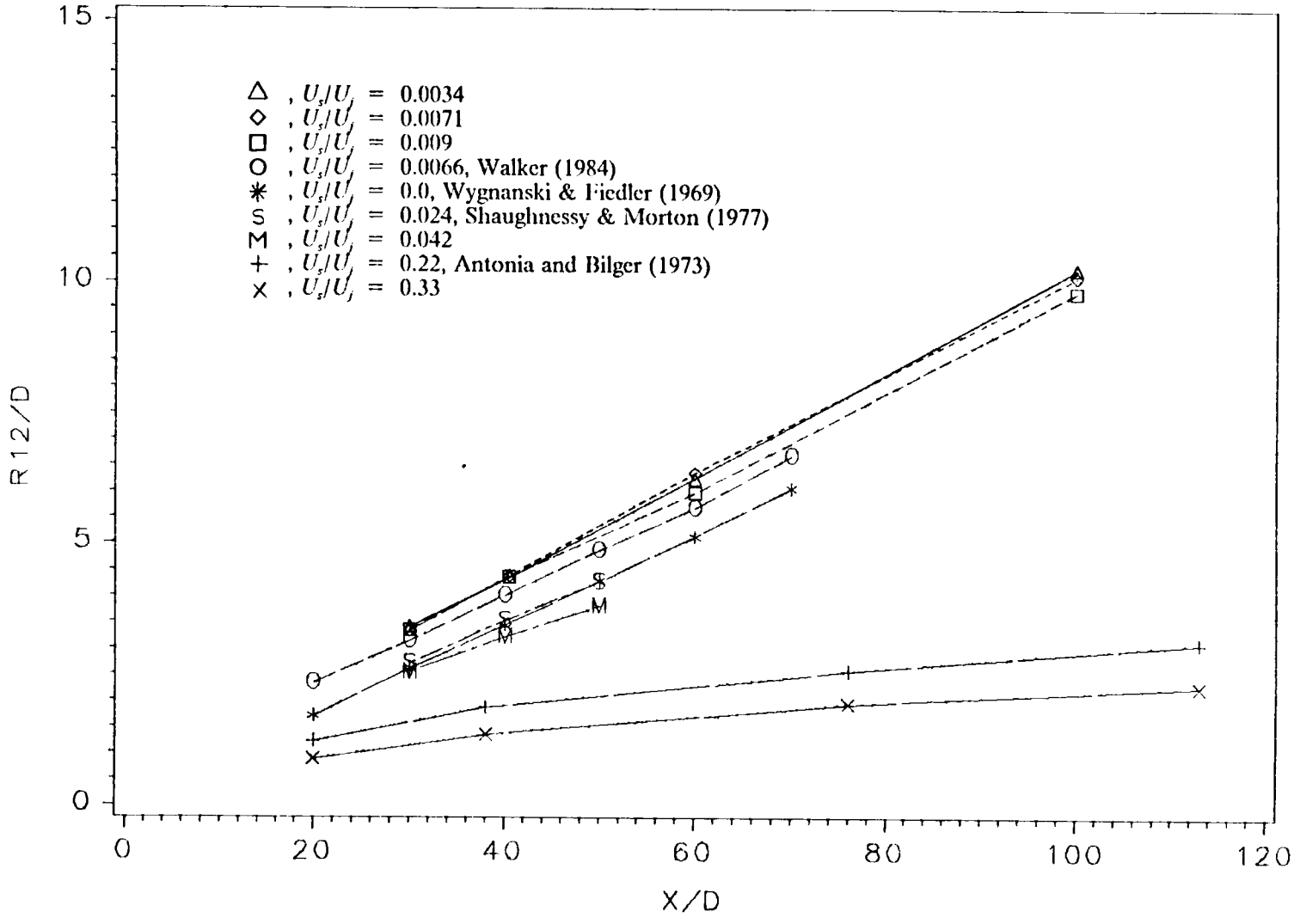

Figure 19 Variation of Profile Half Width, $R_{1/2}$.

coflowing stream and found a linear growth of the half width in measurements of an axisymmetric jet. (Walker, 1984; Komori and Ueda, 1985)

A regression analysis of the data taken at various stations was used to find a linear expression for the growth of the half width of the jet flow. The spreading rate was defined as the slope of the line, $\frac{dR_{1/2}}{dx}$, regardless of the location of the virtual origin. A half spreading angle was obtained by taking the arc-tangent of the spreading rate and used to describe the flow to give a clear picture about the growth of the jet. The present results of the half spreading angle with different coflowing streams and the other investigators' data are shown in Figure 20. An error bar representing the standard error of the linear regression of the half spreading angle is given at each velocity ratio for the present study. There is some scatter of the half spreading angle data which was taken previously by other investigators. This demonstrates the difficulty of producing a free jet flow in the laboratory.

Although a straight line extrapolation cannot be proven analytically to describe the functions for small velocity ratio (U_s / U_j), there are two arguments to justify linear extrapolation to zero velocity ratio. First, as the velocity ratio approaches zero, there are three possible cases: 1. the function goes to zero or infinity 2. a finite nonzero limit exists 3. no limit exists. The third of these corresponds to "pathological" functions, such as sin(1/b) as b approaches zero. This case is not considered likely here. There is no reason to expect such behavior and the data points which exist lie close together. The first case does not appear to occur either since no trend toward zero or infinity appear and all of the present data fall

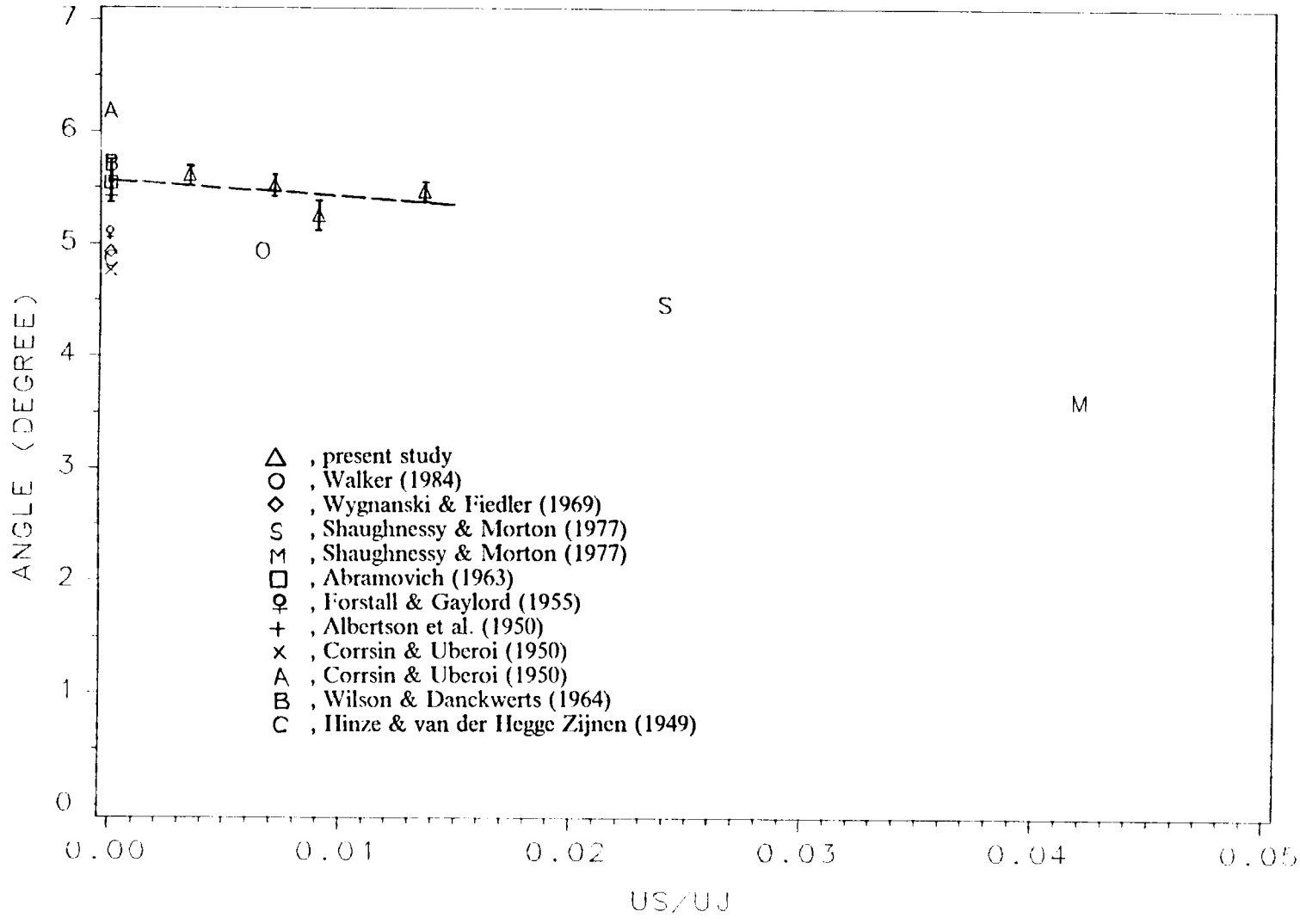

Figure 20 Variation of Half Spreading Angle.

within the range of experimental uncertainty for zero coflow data. Therefore, it seems reasonable to assume that a finite nonzero limit exists.

If a finite nonzero limit exists, then the function can be expanded in a Taylor series about zero coflow. As long as the velocity ratio is small, the leading terms of the Taylor series will be a good approximation to the function. From the data even the first term, a constant, is not a bad approximation, using the second, linear term should be better.

The second argument is more pragmatic. Higher order least-squares fits require more data points. Although a parabolic fit can be found with four points, the goodness of fit parameter (see e.g. Gerald, 1978) indicates that there is no statistically significant improvement of fit to the data available.

The next question to be answered is "what is the uncertainty of the limit thus obtained?" That also must be answered statistically. It is not reasonable to use the maximum error at each point to estimate the uncertainty of the extrapolated limit (Holman, 1984) because the combination of the extreme errors is the most unlikely condition. The method used to compute the uncertainty of each half spreading angle and the extrapolated value is given in the section of Uncertainty Analysis.

The half spreading angle of the free jet can be extrapolated from the data obtained in the present study to zero coflow by linear regression. The angle obtained is 5.6

° with a standard error uncertainty of 2.9 percent, shown by the error bar in Figure 20 for the extrapolated free jet half spreading angle. This uncertainty is about one third the scatter of previous free jet data.

The reason there has been scatter in the measurement of the half spreading angle in previous free jet measurements is that there is a recirculation zone inside the flow field (Barchilon and Curtet, 1964). The confined jet with the addition of a very slow coflowing stream has no recirculation zone for at 100 jet diameters downstream. Therefore, it is believed that the value of the half spreading angle obtained in our present study is a better estimate than any previously obtained.

The distribution of the half spreading angles also presents an interesting phenomenon. The higher the speed of the coflowing stream, the smaller the spreading of the jet flow. In addition, from our observations and those made by other reseachers in Figure 20, it is clear that higher coflowing stream velocities would restrict the development of the jet flow. The growth of the large structure vortex motion is limited by the stronger background flow. It is of little wonder that the data taken by Antonia and Bilger (1973), whose velocity ratios were 0.22 and 0.33, resulted in a totally different growth pattern of the axisymmetric confined jet with a coflowing stream.

5.4 *Centerline Excess Mean Velocity Variation*

An exchange of momentum takes place as the jet grows downstream. External non-turbulent fluid is entrained by the large structure vortex motion of the jet flow. Momentum is transfered to this newly entrained slow speed fluid. Consequently, this results in the decay of the velocity and increase of the width of the jet flow.

The centerline excess mean velocity, U_0 , is used as a velocity scale for describing the jet flow (scaling the mean velocity profiles). Its variation along the axial direction becomes an important characteristic of the jet flow. Using the self-preservation assumption, the axisymmetric turbulent jet theory predicts a linear inverse relation between the centerline excess mean velocity and the axial location, i.e. $U_0 \sim x^{-1}$. Our data and that of other investigators are plotted in Figure 21. Most of the data, including ours, shows a linear decay of the U_0 and is clustered in a narrow band up to $\frac{x}{d} = 100$. In contrast, the data taken by Wygnanski and Fiedler (1969) shows a jump in slope at the location near $\frac{x}{d} = 60$. The data measured by Antonia and Bilger (1973) show a strange decay at the velocity ratio $\frac{U_s}{U_j} = 0.33$. The data taken by Capp (1983) and Rodi (1975) appears to have some scatter. Only the data taken by Walker (1984), Komori and Ueda (1985) and the present study show a linear decay of the centerline excess mean velocity. The measurements conducted without a coflowing stream or with a very strong background flow are all adversely affected

by the flow conditions outside the jet flow. There are recirculation zones when there is no coflowing stream in a flow facility with finite dimensions. On the opposite side a strong coflowing stream causes the growth of the jet flow to be slower. These effects not only result in inconsistencies between experiments done in different flow facilities but also make it difficult to compare different measurements.

Finally, the data taken by Komori and Ueda (1985) differ from the results of Walker (1984) and the present study even though their data show a linear decay of U_0 . The data of Komori and Ueda (1985) were taken at the velocity ratio $\frac{U_s}{U_j} = 0.0093$. Their data indicate a faster decay of the centerline excess mean velocity with respect to the axial locations. This decay rate is not consistent with the results obtained in Walker (1984) and the present study. The velocity ratio used by Komori and Ueda (1985) was higher than that used by us. The Craya-Curtet number in their measurements at the location $\frac{x}{d} = 50$ is 1.58. This implies that there is no back flow in their flow field. The inconsistency may be due to the lower Reynolds number (9280) in their measurements. The Reynolds number dependence of the centerline velocity decay rate has not yet been answered. However, the influence of Reynolds number may account for the discrepancy. The entrainment depends on the Reynolds number when the Reynolds number is lower than 25000 (Ricou and Spalding, 1961; Hill, 1971). Its value is larger with smaller Reynolds number(the length scale of the eddies is larger, the eruption and engulfment motion is stronger). Higher entrainment implies that more low speed external fluid was entrained. The momentum distribution inside

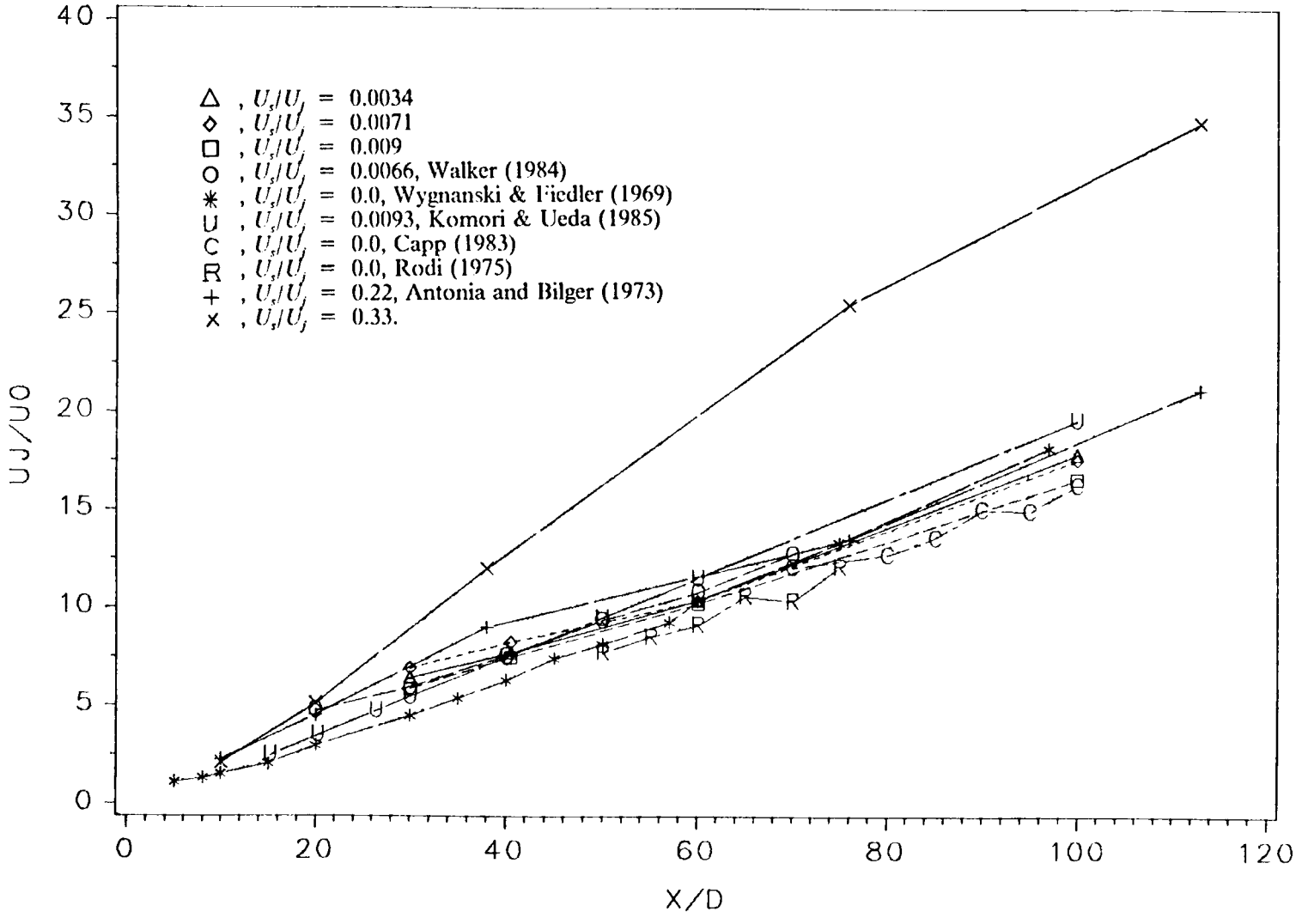

Figure 21 Centerline Mean Velocity Variation.

the jet will be more uniform. This suggests that the centerline velocity will decay faster. The data of Walker (1984) and the present study are consistent. The data of Komori and Ueda (1985) are different. It is possible that, under higher Reynolds number, and with a faster coflowing stream, the momentum of the jet concentrates more closely within the jet. The distribution of the velocity is more compact. Consequently, the width of jet is narrower and the decay of the centerline velocity is slower.

The centerline excess mean velocity variation along the axial direction of the jet is sensitive to the long term drift of the jet exit velocity even though the effect is negligible for each single mean velocity profile. The standard error of the least squares fit of the centerline excess mean velocity on the axial distance x can be used to estimate the uncertainty of the mean velocity measurements which is due to the long term drift of the jet exit velocity. Details will be given in a later section.

5.5 Centerline Excess Mean Velocity Decay Rate

The linear decay of the centerline excess mean velocity can be normalized and written as

$$\frac{U_j}{U_0} = \frac{1}{B_u}\left(\frac{x}{d} - VO\right) \tag{5.1}$$

where the parameter B_u is the decay rate of the centerline excess velocity, VO is the location of the virtual origin and varies with different flow conditions. The virtual origin is the intercept with the independent axis when the straight line describing the decay rate is projected back to the origin. The virtual origin is very sensitive to the initial conditions of the jets and the development of the jet flow. The locations of the virtual origin for the spreading and the decay of the jet flow do not necessarily coincide.

The decay rate B_u was determined by using a least squares linear fit of the data. The decay rates of the centerline excess velocity for different background flow velocities measured in our present study and from the investigations of other researchers are presented in Figure 22. The asymptotic decay rate for the free jet flow can be calculated by linear extrapolation based on the same reasons discussed in the section of the spreading rate of the jet. Similar to the half spreading angle, an error bar is given for each B_u at each velocity ratio including the extrapolated value for the free jet in the present study. The scatter is bigger than that of the half spreading angle because the decay rate is more sensitive to the long term drift of the jet velocity. **The extrapolated value of the decay rate B_u for the free jet is equal to 5.9.** This value agrees with the number, 5.8, predicted by Seif (1981). In addition, the decay rate suggested by Capp (1983) was within 5.8 to 6.0. However, the decay rate is equal to 7.06 if the linear regression is taken

on Capp's data. The uncertainty of this extrapolated value is about 2.1 percent, corresponding to approximately one-sixth the scatter of previous results. The method used to estimate the uncertainty of the decay rate is given in the section of Uncertainty Analysis.

Refer to the data in Figure 22. As discussed in the previous section, the decay of the centerline excess velocity is faster with lower background velocity. This implies that the value of B_u is smaller when the coflowing stream is slower. However, the decay rate, B_u, obtained by Komori and Ueda (1985) is much smaller than the number obtained by other investigators with or without a coflowing stream. As reasoned in a previous section, this suggests that the decay of the jet in the experiment of Komori and Ueda (1985) is too fast even when the measurements were conducted with a slow coflowing stream.

The large scatter in the decay rate in previous free jet measurements shows that the jet is effected by the flow conditions outside the jet. The presence of recirculation zones affect the growth of the jet. This implies that the decay of the jet velocity and the spreading rate of the jet are very sensitive to the flow conditions outside the jet. Careful control of the outside flow field is necessary and it is not sufficient to simply increase the size of the facility since it still contains recirculation zones. Therefore, the use of a very slow coflowing stream on a confined jet is apparently a better approximation of a free jet. The recirculation zone can be eliminated by the coflowing stream. A limiting process on the velocity ratio U_s / U_j can be obtained by using several slow coflowing streams on the confined

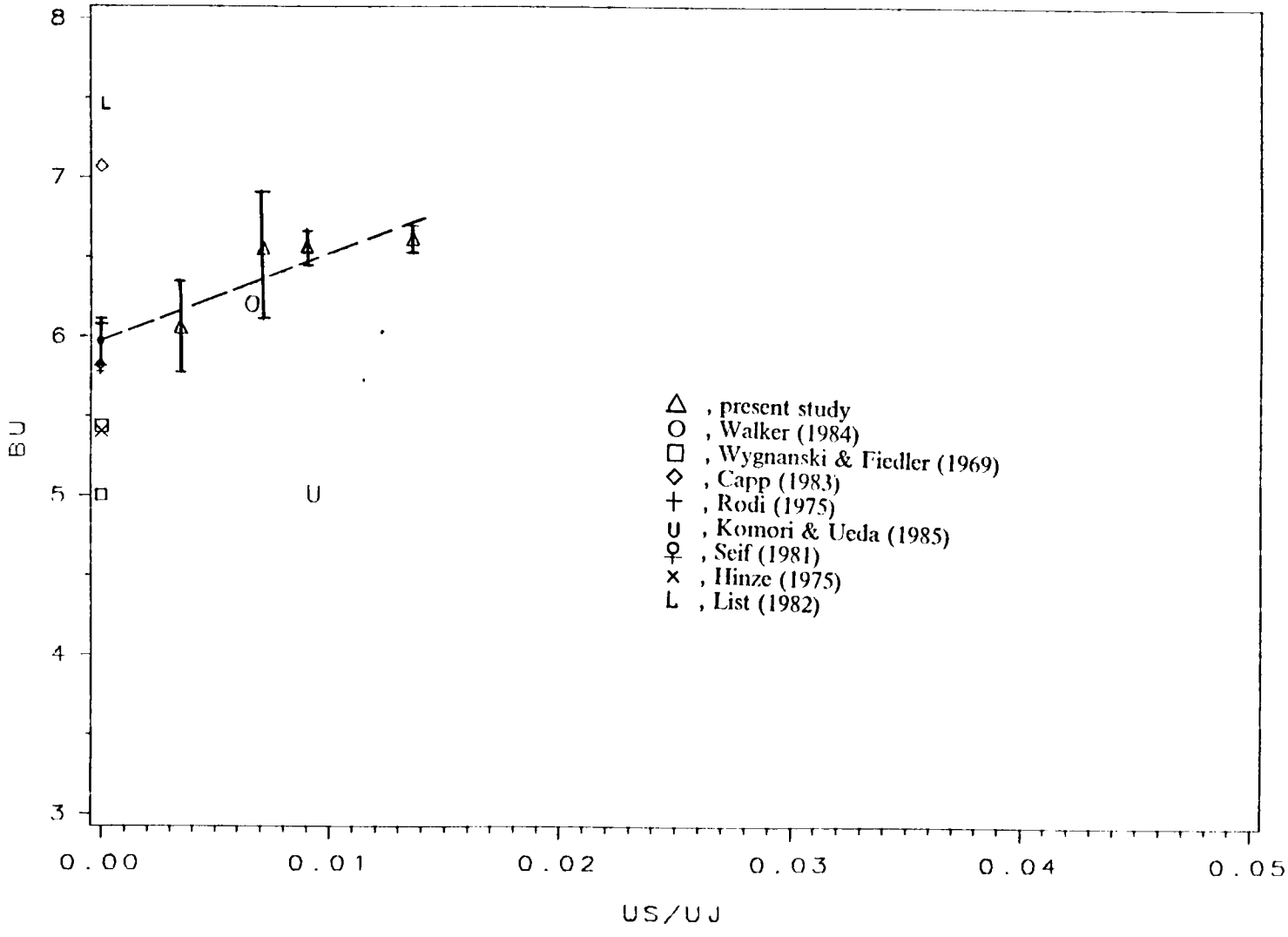

Figure 22 Variation of Centerline Velocity Decay Rate, B_u.

jet. It provides a more reliable method to extrapolate to the conditions of the free jet. It is also believed that the inconsistency among different facilities can be greatly reduced if the jet experiments can be conducted with the method proposed in the present study.

5.6 *Centerline Momentum Velocity Variation*

The term "momentum velocity" is the integrand of the equation for the conservation of the axial momentum. It converts the centerline momentum velocity to a reasonable velocity scale for scaling the turbulent fluctuation velocity when the jet flow has a background flow (Walker, 1984). The linear decay of the momentum velocity in the present study supports the fact that self-preservation is well-approximated not only in the free jet but also in the confined jet with a slow coflowing stream.

The centerline momentum velocity is defined as

$$U_{M0} = [\, U_0 (U_0 + U_s)]^{1/2} \tag{5.2}$$

and the jet exit momentum velocity is given as

$$U_{Mj} = [\, U_j (U_j - U_s)]^{1/2} \tag{5.3}$$

The ratio between U_{M0} and U_{Mj} versus $\frac{x}{d}$ is plotted in Figure 23. Note that $\frac{U_0}{U_j}$ is equal to $\frac{U_{M0}}{U_{Mj}}$ when the background flow velocity, U_s, is equal to zero, or the condition of the free jet.

The data taken by Antonia and Bilger (1973) represents a nonlinear decay of the momentum velocity. Other data taken under free jet conditions or confined jets with slow coflowing streams including ours shows a linear decay of the momentum velocity. The conclusion drawn by Antonia and Bilger (1973) is that the confined jet with coflowing stream was not even approximately self-preserving. It is concluded that this is true only for the jet with a strong coflowing stream. It is also concluded that their flow was not simply a jet flow, but instead was a combination of a jet and a wake.

5.7 Rescaled Mean Velocity Profiles

The distribution of the jet mean velocities at various stations with two velocity ratios $U_s / U_j = 0.0034$ and 0.009 were scaled by using the half width and centerline excess mean velocity and were plotted with rescaled velocity profiles taken by other researchers in Figure 24 and Figure 25, respectively. The rescaled mean velocity profiles of the present study collapse and show good agreement

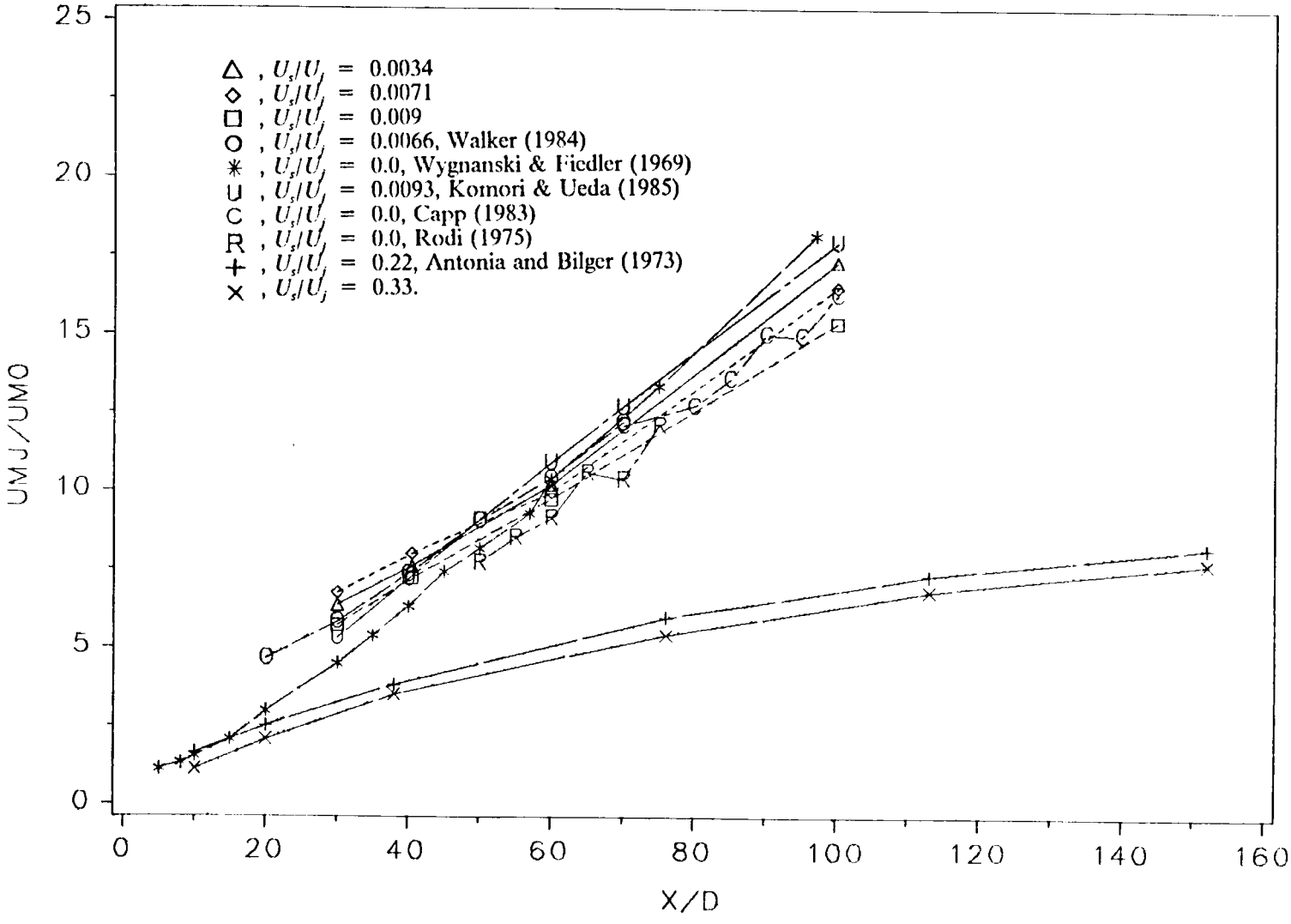

Figure 23 Centerline Momentum Velocity Variation.

with the data of other researchers except in the outer region where their data is suspect because of the presence of the reverse flow.

The collapse of the rescaled mean velocity profiles again supports the claim that self-preservation is a good approximation for this flow for $x/d < 100$. A universal profile can be obtained to describe the velocity distribution. Differences where they exist were produced by the limitation of the instruments, flow facilities and the flow conditions outside the jet, for example, this is the case for the profiles measured by Antonia and Bilger (1973).

The reason for improvement here requires an examination of the measurement techniques. Previous measurements have been conducted by hot-wire anemometers, LDA in air, and LDA in water. Hot-wire anemometers have advantages at low turbulence intensities. However, at high turbulence intensities, even with great care (see for instance, Rodi, 1975) including measuring all three components and correcting for nonlinearities, they produce undependable results. In the reversing flow found with most free jet experiments, the problem is worse since they cannot identify flow direction.

LDA has occasionally been used in jets (see for example Barnett and Giel, 1975; Walker, 1984). Frequency-shifting is recommended even in the absence of reversing flow due to the high turbulence intensities. LDA in water rather than air also seems to have advantages. In air seeding bias can occur and data rates are not generally high enough to reconstruct the time history of the velocity. In

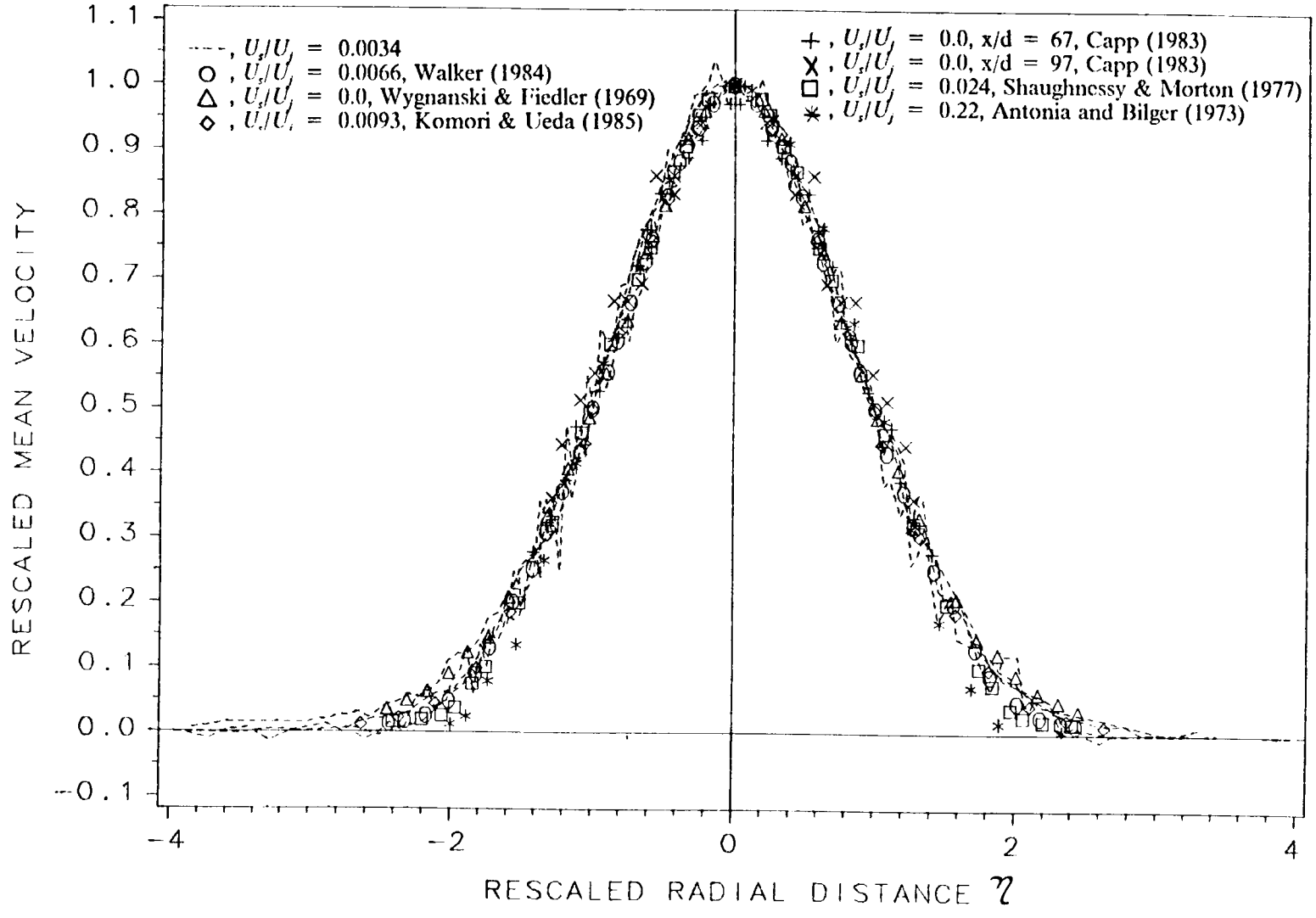

Figure 24 Rescaled Mean Velocity Distributions.

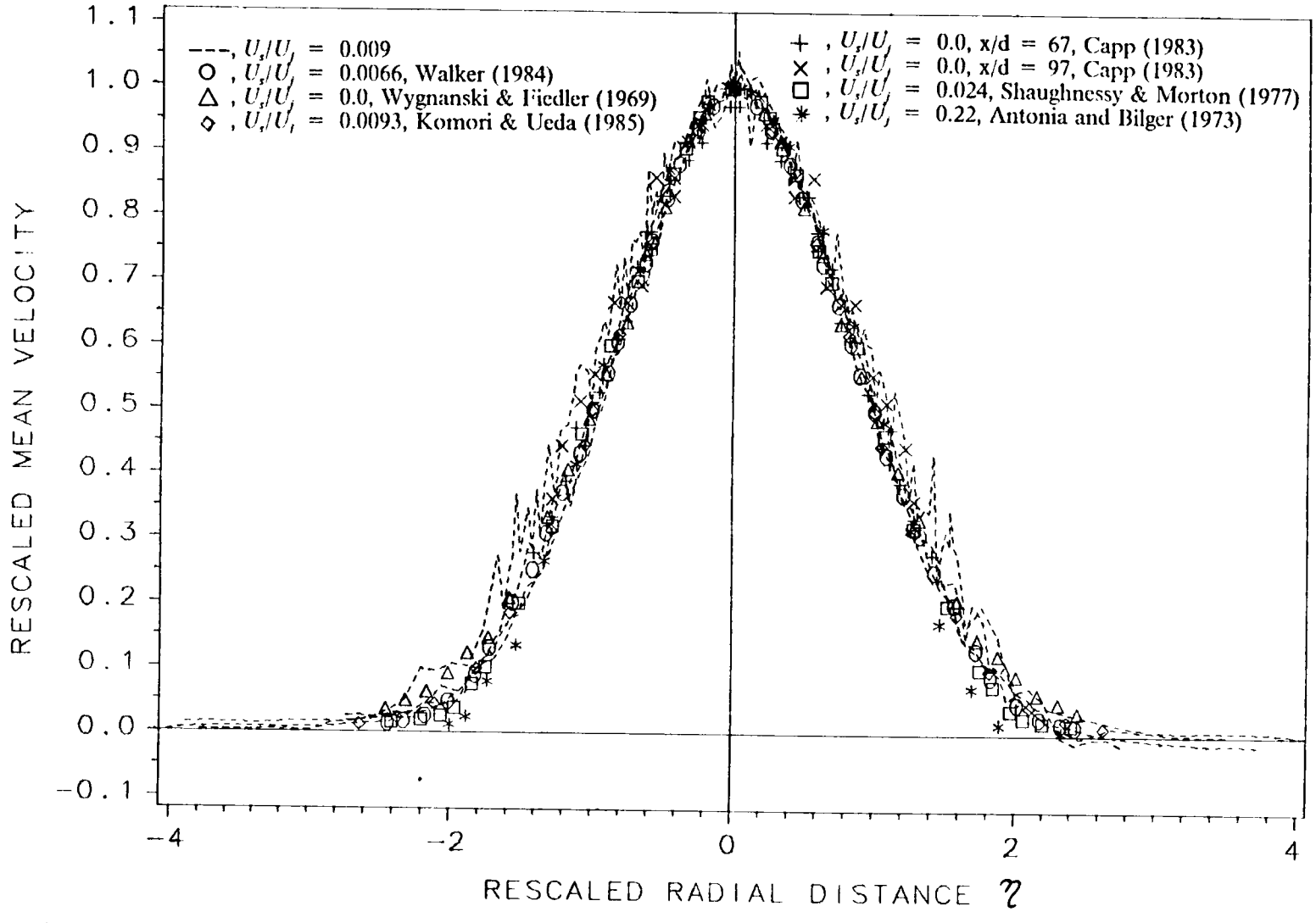

Figure 25 Rescaled Mean Velocity Distributions.

water the data rates are high enough to reconstruct velocity and avoid seeding bias. In air the seeding particles also less likely to follow the flow than in water.

According to Capp (1983), the profiles measured by hot-wire anemometers were narrower than the LDA measurements. No satisfactory explanation has been given yet. It may be due to the presence of the back flow, especially near the edge of the jet. Momentum flux is decreasing downstream due to the narrow velocity profiles measured by hot-wire anemometers.

5.8 Entrainment Coefficient

The entrainment was calculated by integrating the mean velocity distributions. The integration limit used was 2.75 times the half width (Walker, 1984). The constancy of the integrated value was verified by increasing the limit. By using the equation (2.4), the entrainment coefficients at each measurement station was determined. The results are plotted with the data of Ricou and Spalding (1961) in Figure 26.

The entrainment coefficients obtained in our present measurements are larger than those of Ricou and Spalding (1961). Their method for measuring the entrainment coefficients differed from ours. They did not measure and integrate the mean velocity profiles inside the jet flow to get the entrainment coefficients.

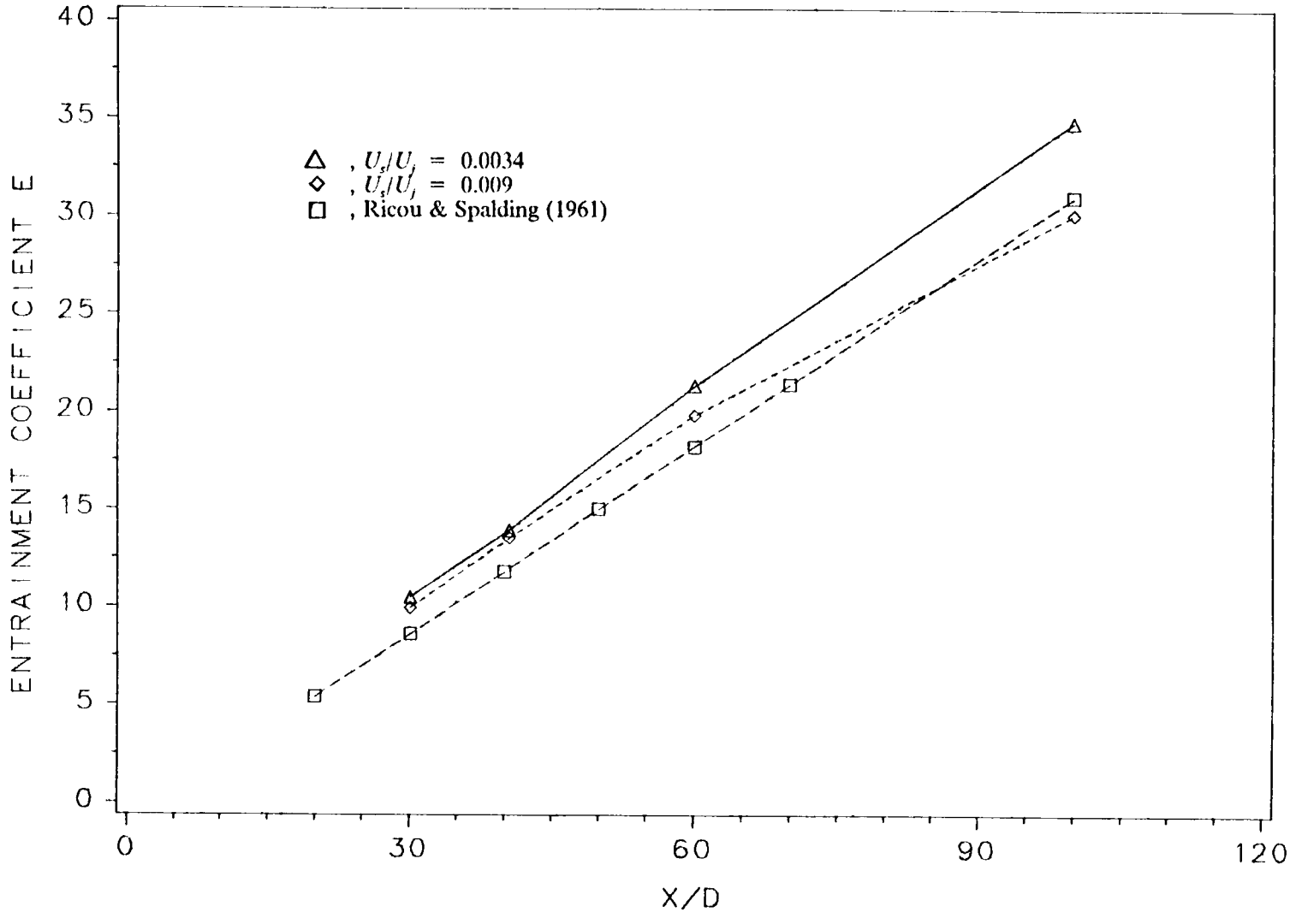

Figure 26 Variation of Entrainment Coefficient.

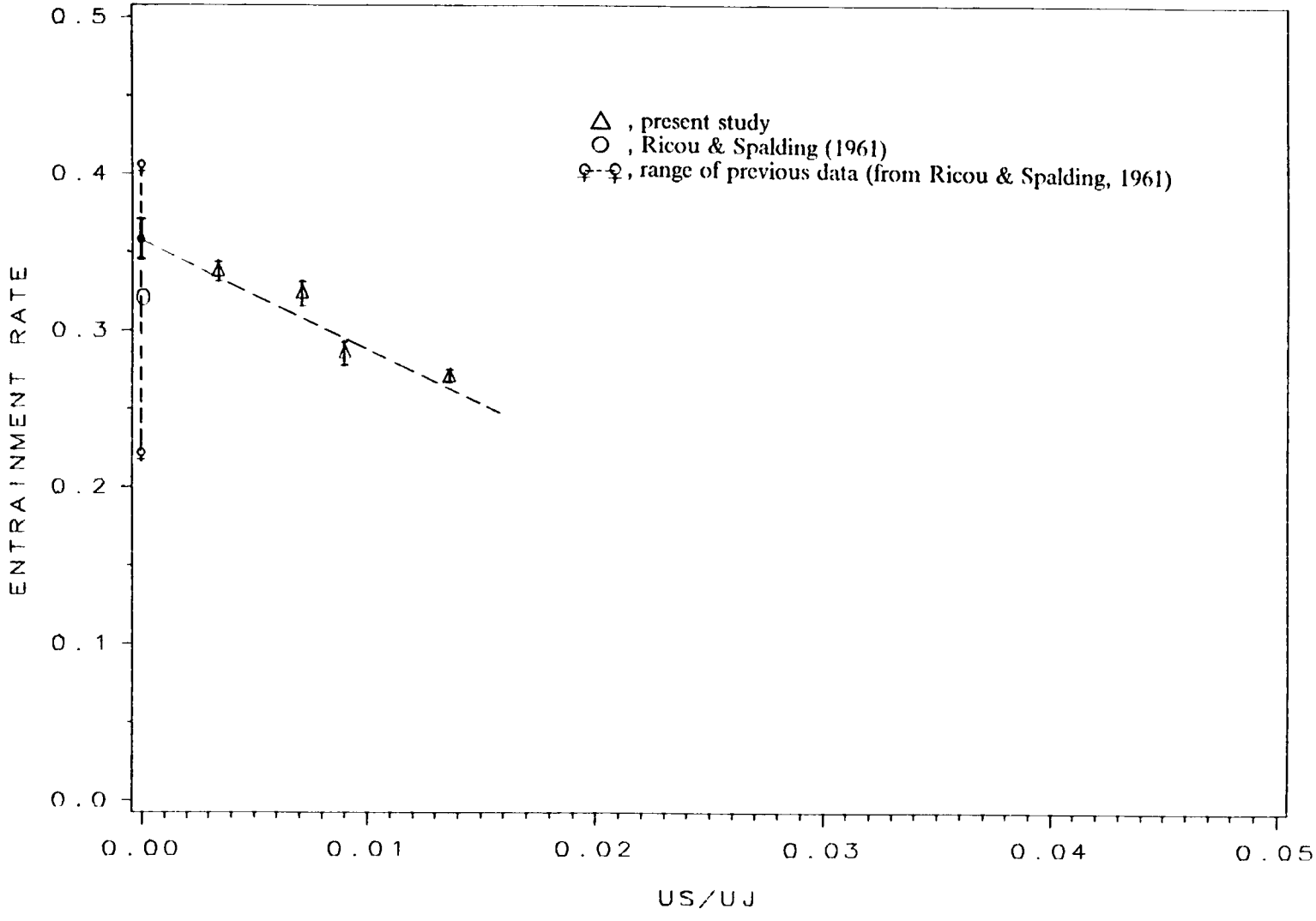

Figure 27 Variation of Entrainment Rate.

Instead, their jet was surrounded by a porous-walled cylindrical chamber, and air is injected through the wall. The flow rate through the porous wall was varied until no axial pressure graidents can be detected. They measured this flow rate which was presumed to be equal to that entrained by the jet. The entrainment coefficient was then obtained by this indirect method. However, the overall slope of the entrainment coefficients versus axial distance in the present study is in agreement with those of Ricou and Spalding (1961). The present method (measuring the jet with several background coflows) gives a reliable way to estimate the entrainment of the free jet. The entrainment rate $\frac{dE}{d(x/d)}$ versus velocity ratio U_s/U_j is shown in Figure 27. An error bar representing the standard error of the linear regression of the entrainment rate is given at each velocity ratio. The entrainment rate of the free jet can be extrapolated from the data obtained in the present study to zero coflow by linear regression. The value obtained is 0.36 with a standard error uncertainty of 3.5 percent, shown by the error bar in Figure 27 for the extrapolated free jet entrainment rate. This uncertainty is about one-tenth the scatter of previous free jet entrainment rate which varied from 0.22 to 0.404. (Ricou and Spalding, 1961) The method used to estimate the uncertainty of the entrainment rate is given in the section of Uncertainty Analysis.

The entrainment of the turbulent jet is very sensitive to the flow conditions outside the jet flow. From our present measurements, the jet flow with a higher background flow velocity was found to have a smaller entrainment coefficient and the spreading of the jet flow was less with a high coflow than with a slow coflow.

5.9 *The Axial RMS Velocity Distributions*

The axial rms velocity distributions for $U_s / U_j = 0.0034$, 0.009 and 0.0136 are plotted in Figure 28, Figure 29 and Figure 30, respectively.

It is shown that the peak rms velocity is not at the centerline of the jet. The peak is located at a point near the highest shear. The turbulence production is zero at the centerline of the jet flow because of the symmetry of the flow. These off-axis peaks of the rms velocity decrease relative to the centerline value as the x-distance increases. It has been suggested (e.g. Corrsin, 1943; Kobashi, 1952) that the decrease in the peak values results from the initial region before the jet becomes fully-developed. As shown in the present study, the peaks become indistinguishable by $x/d = 100$ for all of our velocity ratios. Some measurements done by other researchers, e. g. Antonia and Bilger (1973), indicate the persistence of the peaks to x/d greater than 200. Since this is far beyond the initial region of the jet, it seems likely that increased jet flapping (the growth of the eddies) is the reason. It is suggested that more measurements are needed in this area.

The distribution of rms velocities are sensitive to the flow conditions outside the jet and the initial conditions of the jet. The uncertainty of rms velocity is larger

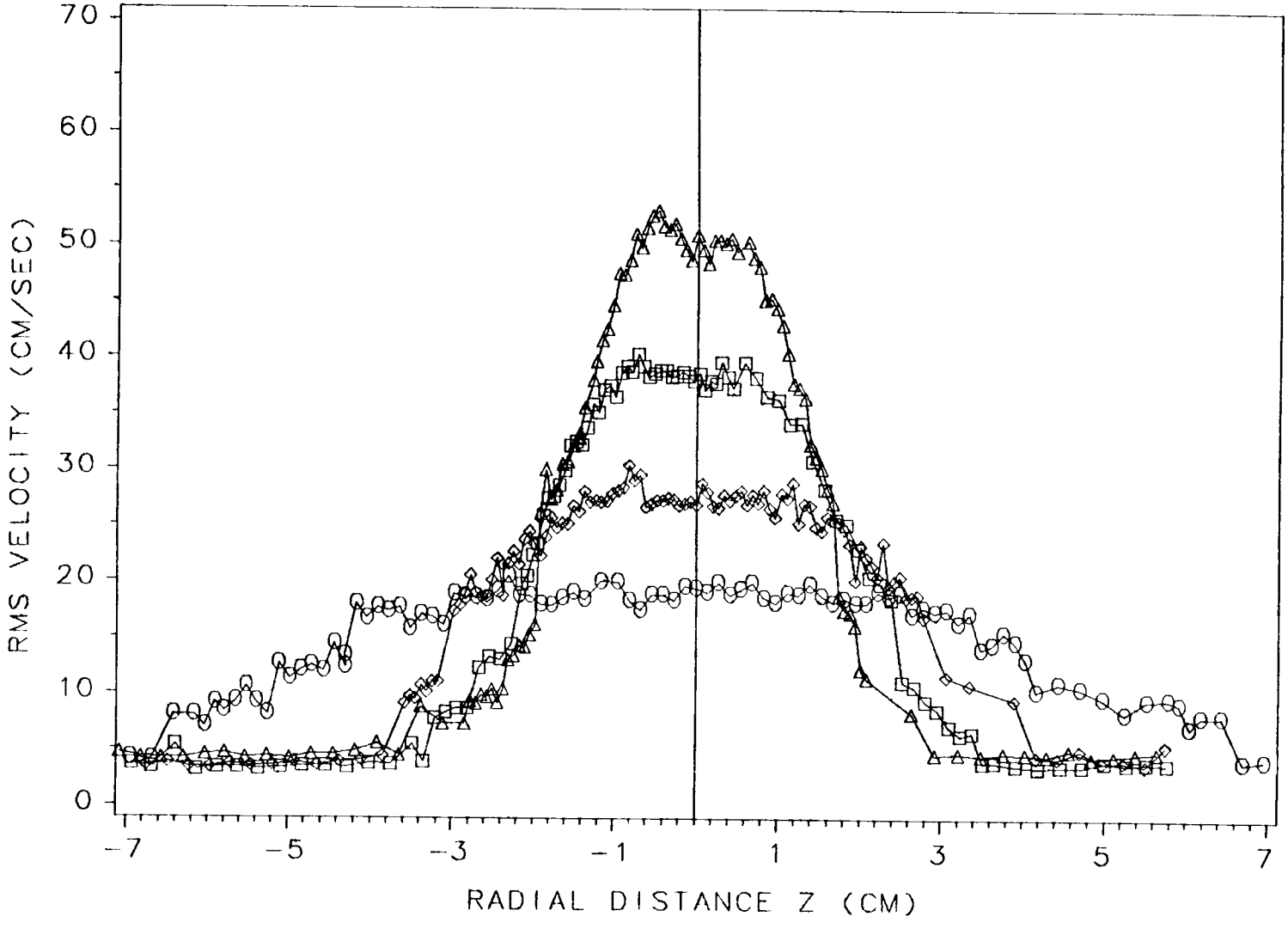

Figure 28 RMS Velocity Distributions with U_s/U_j = 0.0034.

△ , x/d = 30; □ , x/d = 40.5; ◇ , x/d = 60; ○ , x/d = 100.

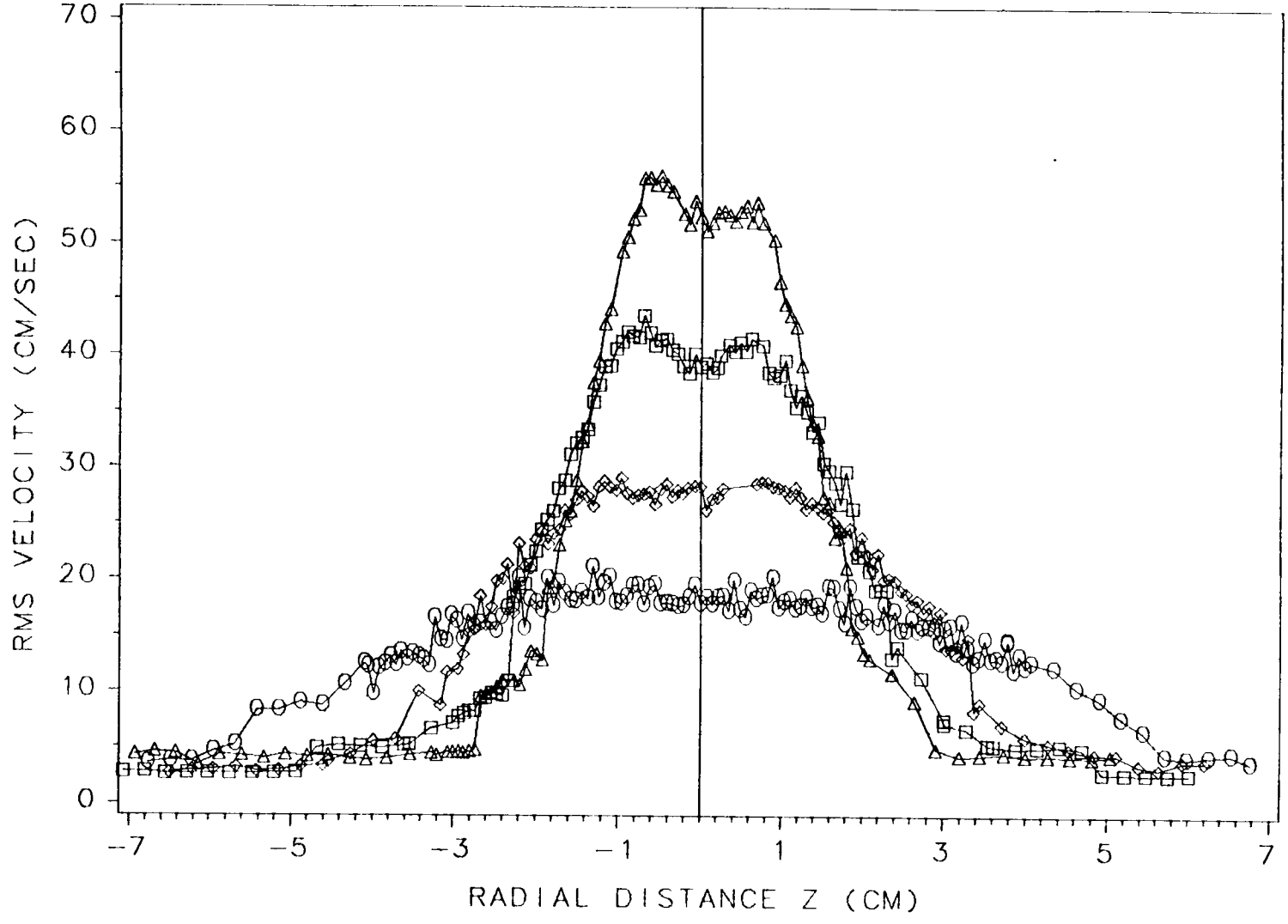

Figure 29 RMS Velocity Distributions with U_i/U_j = 0.009.

△ , x/d = 30; □ , x/d = 40.5; ◇ , x/d = 60; ○ , x/d = 100.

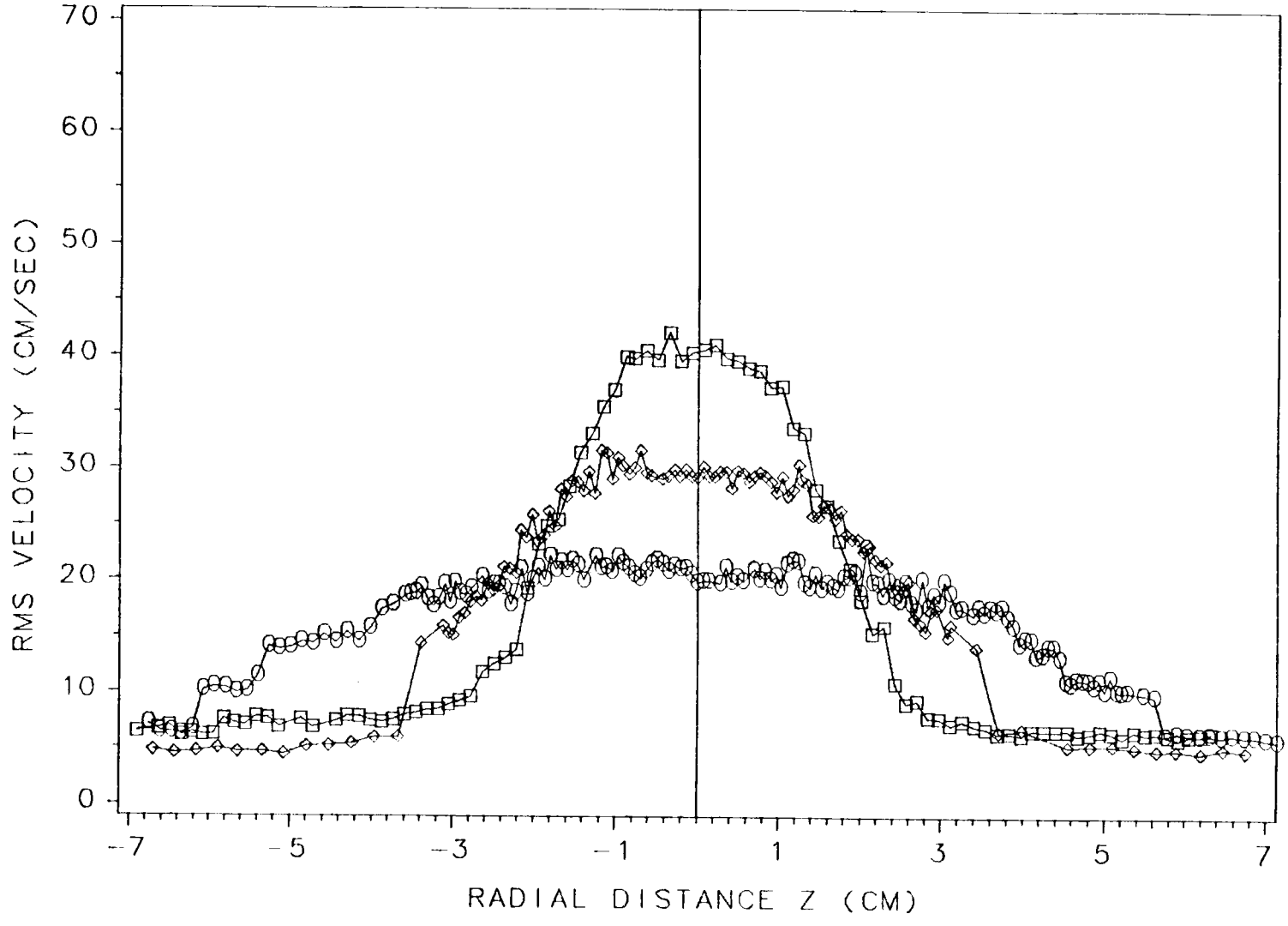

Figure 30 RMS Velocity Distributions with U_r/U_j = 0.0136.

□ , x/d = 40.5; ◇ , x/d = 60; ○ , x/d = 100.

than the mean velocity because it is a second order term. The uncertainty increases near the edge of the jet because the sensitivity of the frequency shifted LDA and the tracker is decreasing. The rms levels in the free stream represent the resolution of the instrument, notably the A/D converter, not the actual free stream turbulence level. Free stream turbulence was too low to be measured with the present set-up but was conservatively expected to be less than 1 percent (measurement region is far downstream of the screen). A subsequent study using hot-film anemometers is presently under way. The rms data were "corrected" for instrument broadening and both uncorrected and corrected results are presented. A comparison demonstrates that the results are indistinguishable except in the freestream and at the very edge of the jet.

5.10 The Centerline RMS Velocity

The centerline rms velocity was normalized with the local momentum velocity and plotted with respect to the axial locations in Figure 31. The data presented in this figure indicated that the higher the background flow velocity, the lower the values at the centerline. Even though there is some scatter as the background flow velocities diminish, this is a definite trend, which emphasizes that at higher background flow velocities less turbulence is produced.

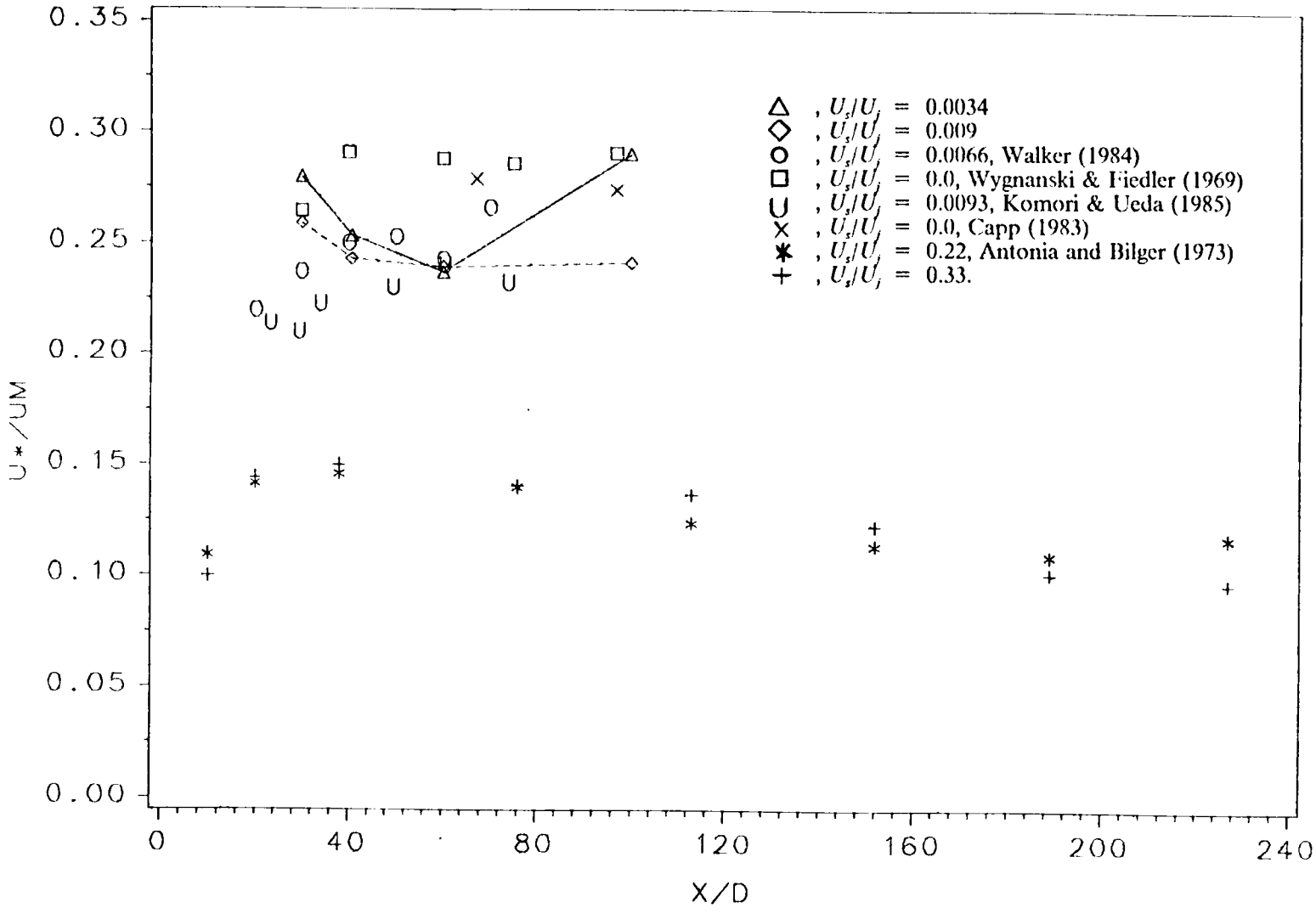

Figure 31 Centerline RMS Velocity Variation.

The normalized centerline rms velocity measured by Wygnanski and Fiedler (1969) was 0.29 in the region of fully-developed free jet flow. Capp (1983) measured 0.27. Our estimates are in agreement. The normalized rms velocity should be constant if the flow is self-preserving. The data taken at $U_s / U_j = 0.009$ shows a constant around 0.24. For $U_s / U_j = 0.0034$, the value varies from 0.24 to 0.29. An averaged value of 0.265 is our estimate of this constant at this time. Details will be given in next section.

5.11 The Rescaled RMS Velocity Distributions

The rms velocity distributions at various stations with different coflowing streams were scaled by the centerline momentum velocity and the half width of the jet flow. The normalized profiles were plotted in Figure 32 and Figure 32 for $U_s / U_j = 0.0034$ and 0.009, respectively.

The normalized rms velocity distributions in our present study collapse very well. A similar shape for the normalized rms velocity profile was obtained in the jet. Thus, the rms quantities of the jet flow are also consistent with approximate self-preservation in the confined jet with slow background flow. The uncertainty of velocity measurement increases with increasing x/d because of the decrease in speed.

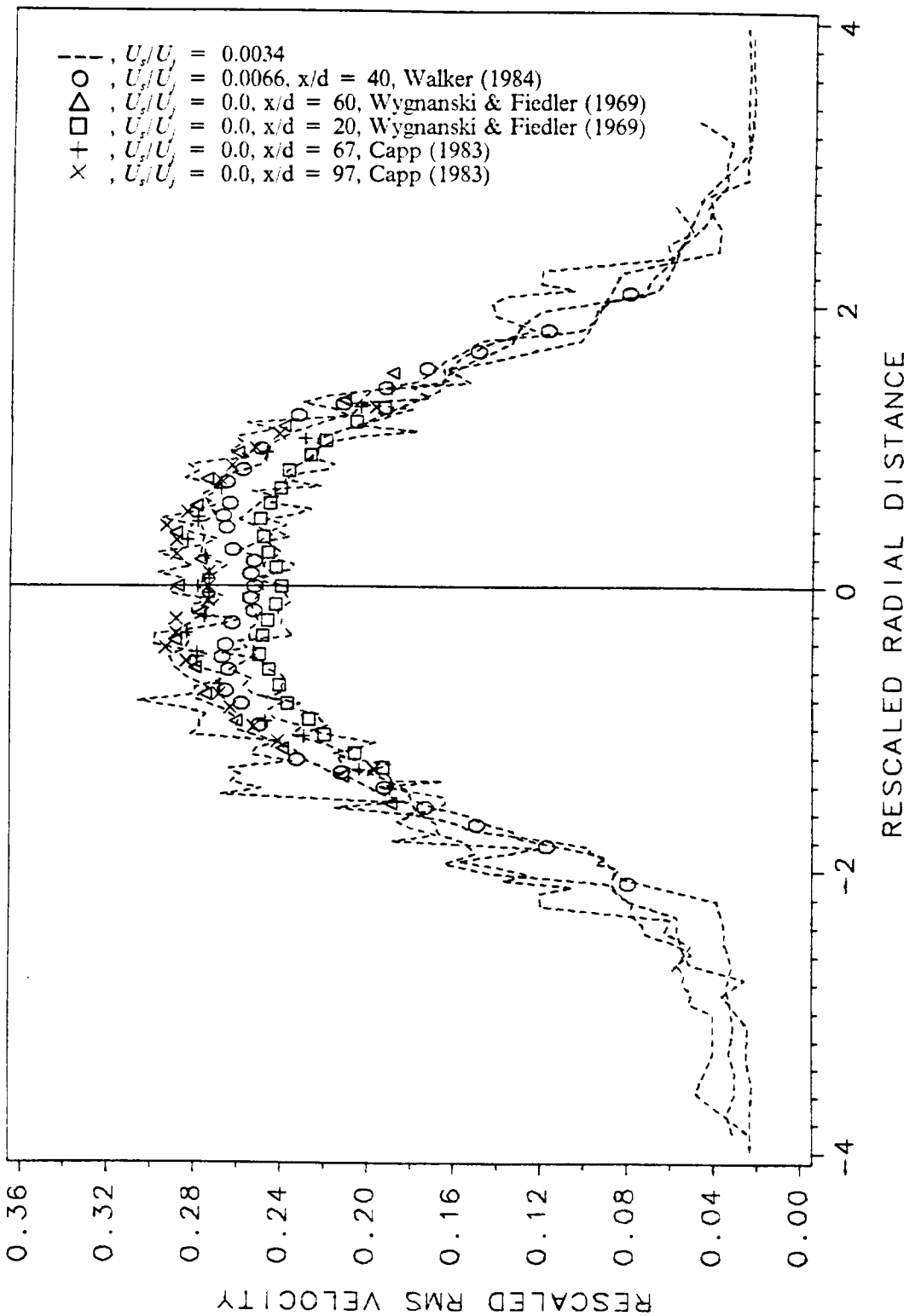

Figure 32 Rescaled RMS Velocity Distributions.

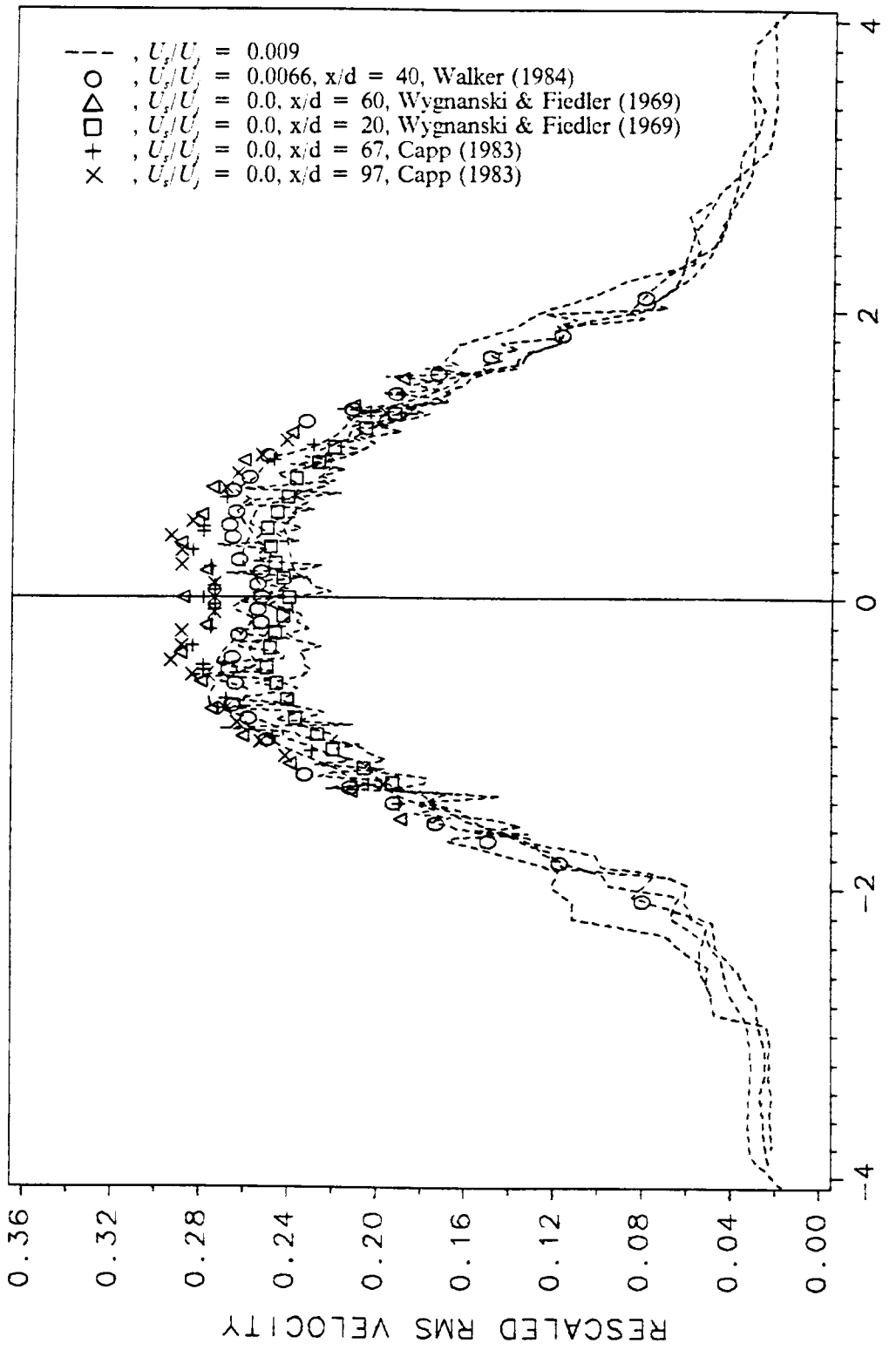

Figure 33 Rescaled RMS Velocity Distributions.

The normalized rms velocity profiles coincide with those of other researchers taken with a free jet or confined jet with slow background flow. But none of the previous measurements except Walker (1984) have measured far enough away from the centerline of the jet. Most only measured turbulence out to the half width. The reason is due to the limitation of their measurement probes (hot-wire anemometer) in the outer region, where the local turbulent intensity is high, between the half width and the edge of the jet. It is also in this region that reverse flow occurs due to the recirculation zone. As discussed in the previous section, the frequency-shifted LDA is capable of measuring the high turbulent flow. Therefore, the rms velocity in the present study can be measured much closer to the edge of the jet to form a complete distribution. For each flow in the present investigation, a universal profile for the normalized rms velocity is obtained. The values of the normalized rms velocity obtained here are slightly lower than those obtained in previous studies because the coflow, even so slow, restricts the growth of the eddies.

The rms velocity measured in the free stream is approximately equal to the standard deviation of the mean velocity measurements if the free stream turbulent intensity is significantly less (the expected case as described earlier). Thus, the uncertainty of the mean velocity measurements can be estimated from this standard deviation. The standard deviation is approximately 5 cm/sec for various velocity ratios (Figure 28, 29 and 30) used and measurement locations in the present study. From the statistical analysis and the sample number of the experiment, the uncertainty of the mean velocity measurements is one hundredth

of the standard deviation. The uncertainty estimated for the mean velocity is equal to 0.5 mm/sec. However, this estimate of the uncertainty does not include the uncertainty due to the long term drift of the jet velocity. The method used to estimate the uncertainty of the long term drift will be given in the next section.

Under the assumption of zero turbulent intensity in the free stream, the corrected rescaled rms velocity distribution is shown in Figure 34 and 35. The correction is only significant in the region very near the edge of the jet and vanishes at the center of the jet.

5.12 *Uncertainty Analysis*

The equations used to determine the uncertainty of the linear regression is as follows: Suppose a linear equation $Y = a + b\,X$ is the least squares fit to a set of data points (X_i, Y_i), $i = 1, 2, \ldots, n$ and $\hat{Y}$ is the estimated value on the line for a given X value. The standard error of the estimate of Y on X is defined as

$$S_{Y,X} = \sqrt{\frac{\sum (Y_i - \hat{Y}_i)^2}{n-2}} = \sqrt{\frac{\sum Y_i^2 - a\sum Y_i - b\sum X_i Y_i}{n-2}} \tag{5.4}$$

The standard error of the regression coefficient a is

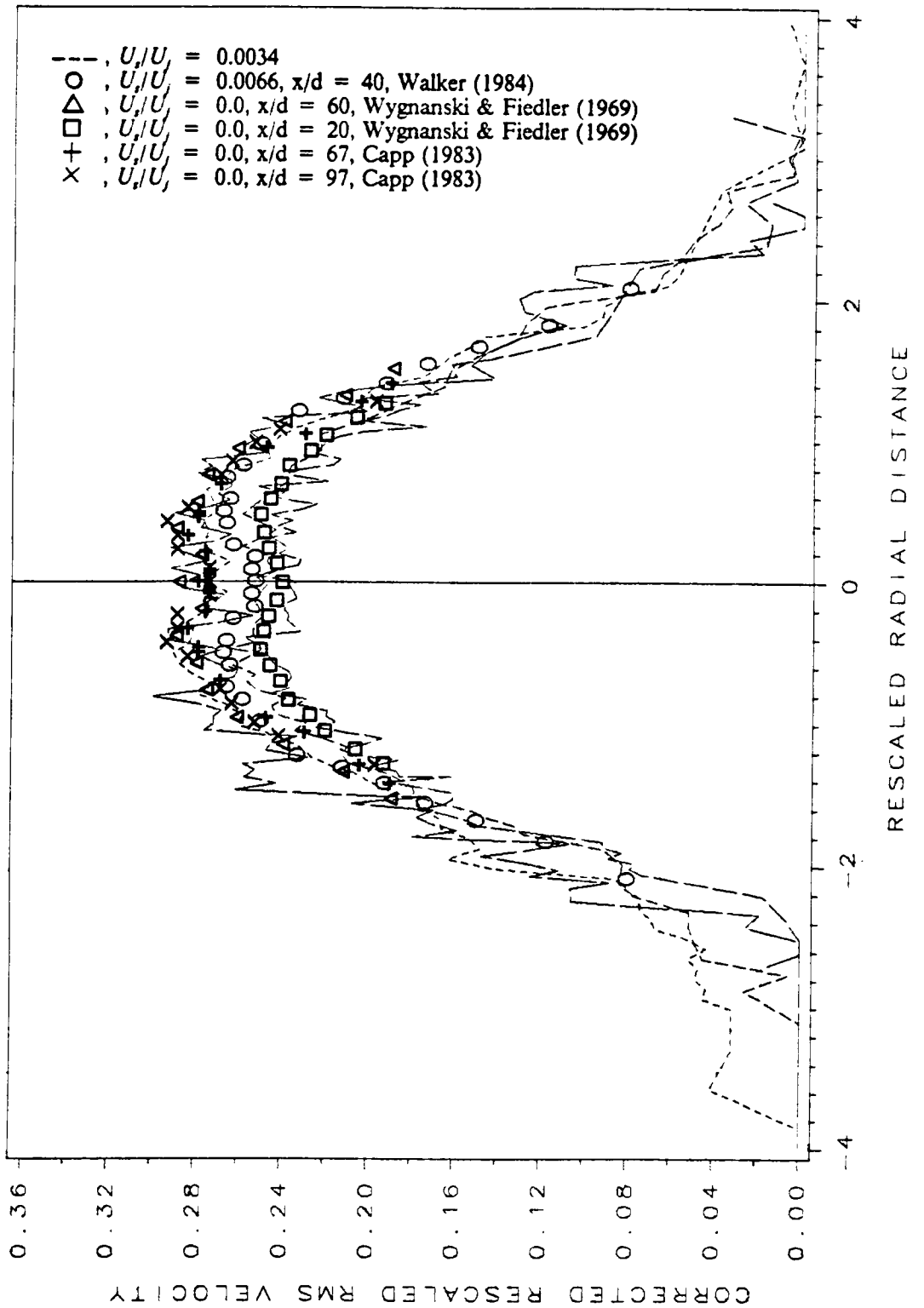

Figure 34 Corrected Rescaled RMS Velocity Distributions.

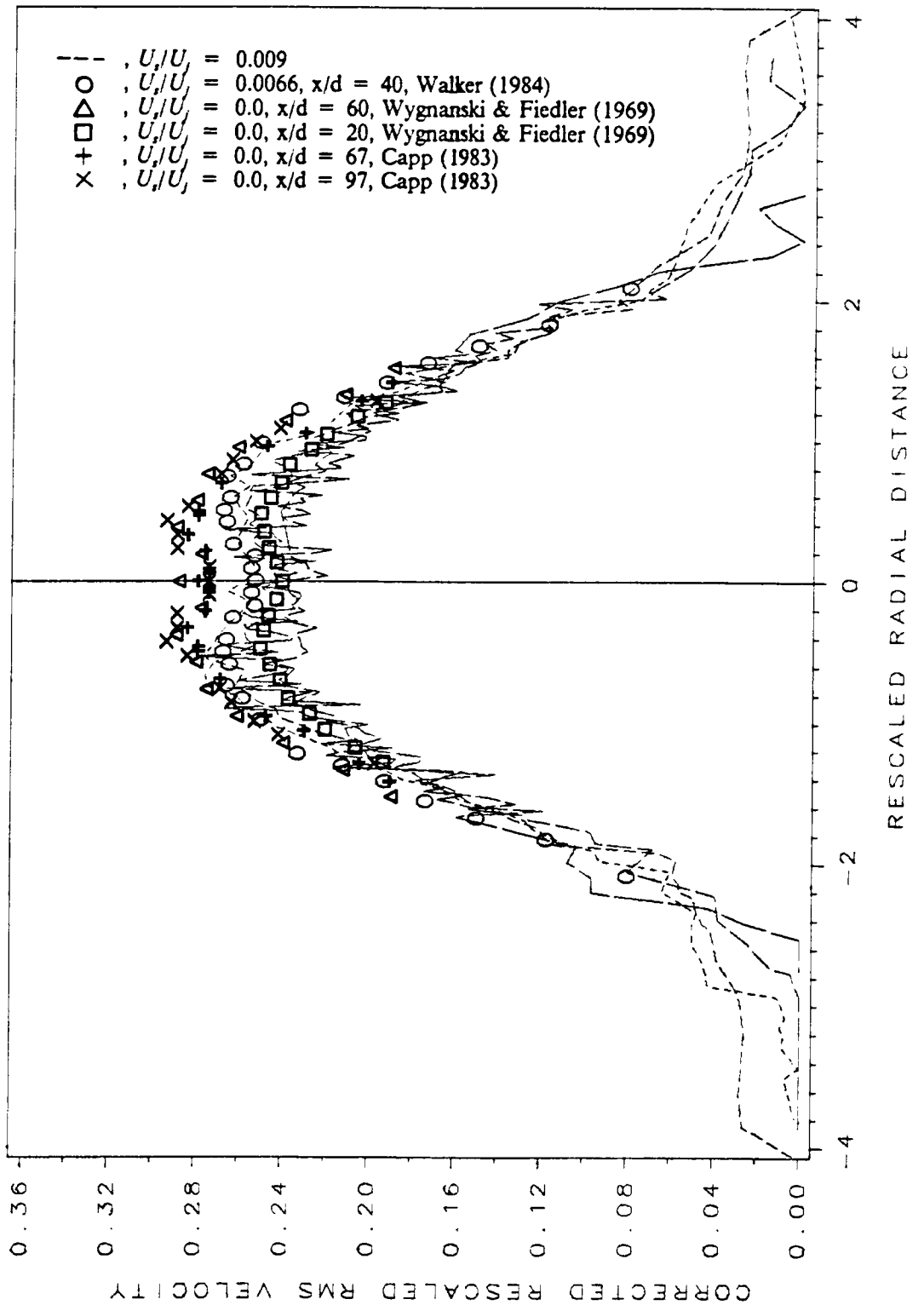

Figure 35 Corrected Rescaled RMS Velocity Distributions.

$$S_a = S_{Y,X} \frac{\sum X_i^2}{\sqrt{n\left[\sum X_i^2 - \frac{\left(\sum X_i\right)^2}{n}\right]}} \tag{5.5}$$

The standard error of the regression coefficient b is

$$S_b = \frac{S_{Y,X}}{\sqrt{\sum X_i^2 - \frac{\left(\sum X_i\right)^2}{n}}} \tag{5.6}$$

where n is a positive integer larger than 2. For details refer to Draper and Smith (1966).

Equation (5.4) is used in the linear regression of the variation of the jet centerline excess mean velocity versus axial distance to estimate the long term drift of the jet velocity. This standard error of the estimate of the least squares fit is taken to approximate the uncertainty of the long term drift of the jet exit velocity. Consequently, this estimation indicates that the long term drift is about 3.5 percent. It is the major source of the uncertainty of the decay rate (e.g. the longer error bar shown in Figure 22).

The error bars of the points in Figure 20, 22 and 27, except the limiting points at $U_s/U_j = 0$, were determined by equation (5.6). The standard error of the regression coefficient, b (the slope of the line), was taken as its uncertainty. The extreme error combination of each point in the figures is the most unlikely con-

dition during the extrapolation. Also, statistically, if a linear regression is used to extrapolate to a limiting value the uncertainty of the individual points are expressed as the mean squared deviation from the line. They needn't be accounted for separately. The uncertainty of the limiting value can be approximated by the standard error of the regression coefficient, a (the intercept). Therefore, the limiting values of the half spreading angle, decay rate and entrainment rate in the Figure 20, 22 and 27 were obtained by linear regression and the uncertainties of them were computed by the equation (5.5).

5.13 The Conservation of the Axial Momentum

The axial momentum was obtained from equation (2.11) and plotted with respect to the axial locations in Figure 36. The averaged values show the distribution of the momentum. The axial momentum reaches a constant after $x/d = 40$ in Figure 36. The momentum value is smaller at the location $x/d = 30$. This may be due to the variation of the mean static pressure upstream. The momentum decreases if the static pressure at the exit of the jet is smaller than the pressure outside the jet nozzle and increases to a fixed value when the pressure decreases to a constant downstream. The pressure term is then equal but in opposite sign to the normal stress term. These two terms can be neglected in the equation of the conservation of momentum (Townsend, 1976; Hinze, 1975). This variation of the pressure in

the axial direction was measured by Hussain and Clark (1977). The fact that their momentum is conserved is indicated by the constant contribution of the mean velocity term beyond their initial region. This constant is not necessarily equal to the reference exit momentum which was computed by assuming a uniform mean velocity profile at the exit of the jet. The momentum variation in the present study follows the same tendency. A constant was achieved downstream. This implies that the momentum is conserved in the present study. Very few previous free jet measurements satisfied the conservation of the momentum (Kotsovinos, 1978). Their momentum flux was decreasing downstream. This implied that the recirculation zone must have occurred in their flow field. Some scatter of momentum was found in Figure 36. The error due to the integration method (Simpson's rule) is small. However, the part of the velocity profile that contributed most of the momentum for the integration was the outer part of the profile. Refer to Figure 37. Therefore, the integrated value for the momentum is more sensitive to the quantities measured in the outer region where uncertainty are greater.

The momentum of the jet flow with respect to the background flow velocity at the location $x/d = 60$ is plotted in Figure 38. The momentum of the jet flow is approximately conserved regardless of the different background flow velocities used in the experiment.

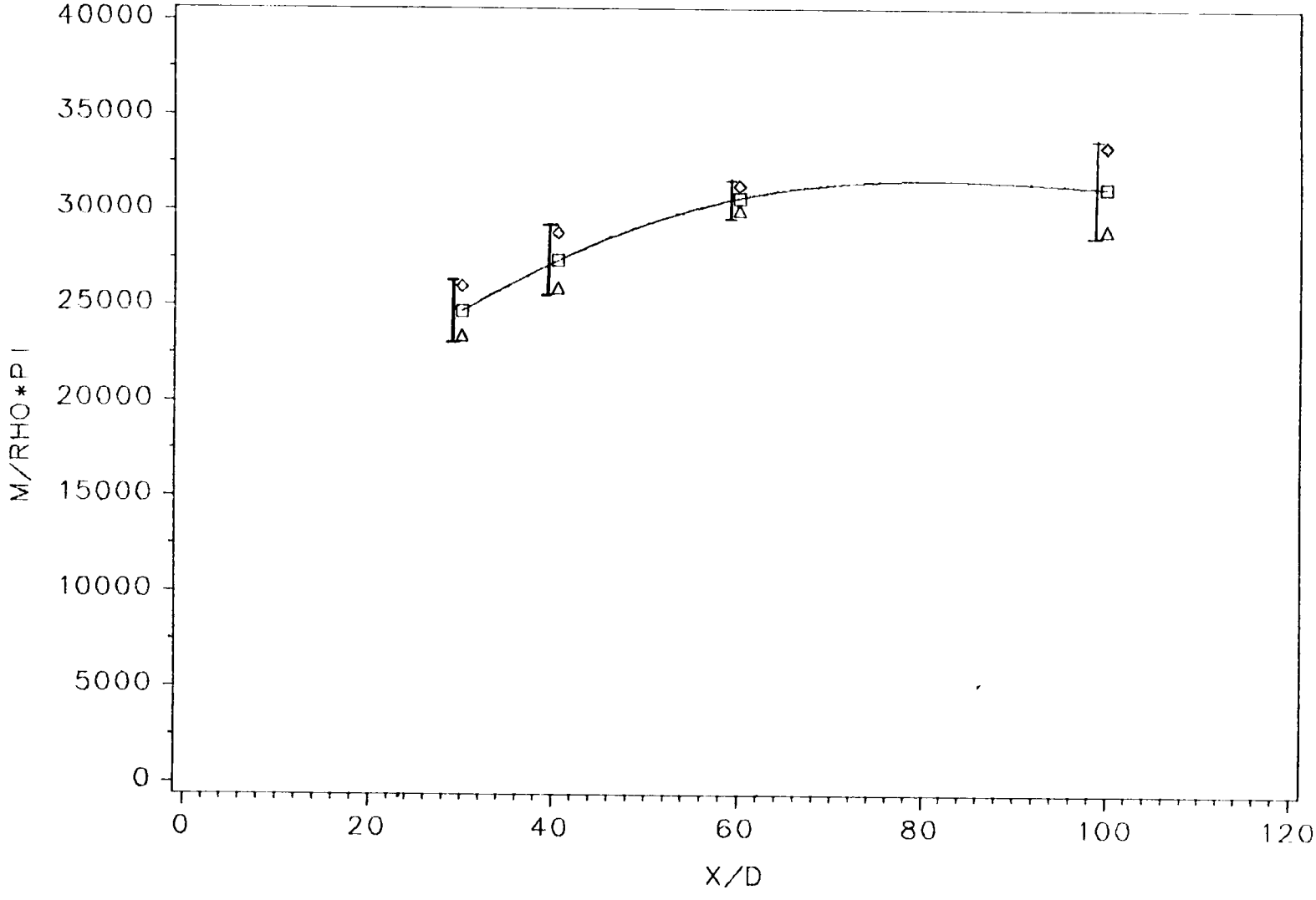

Figure 36 Variation of Integral Momentum.

△ ,U_s/U_j = 0.0034; ◇ ,U_s/U_j = 0.009; □ , Mean.

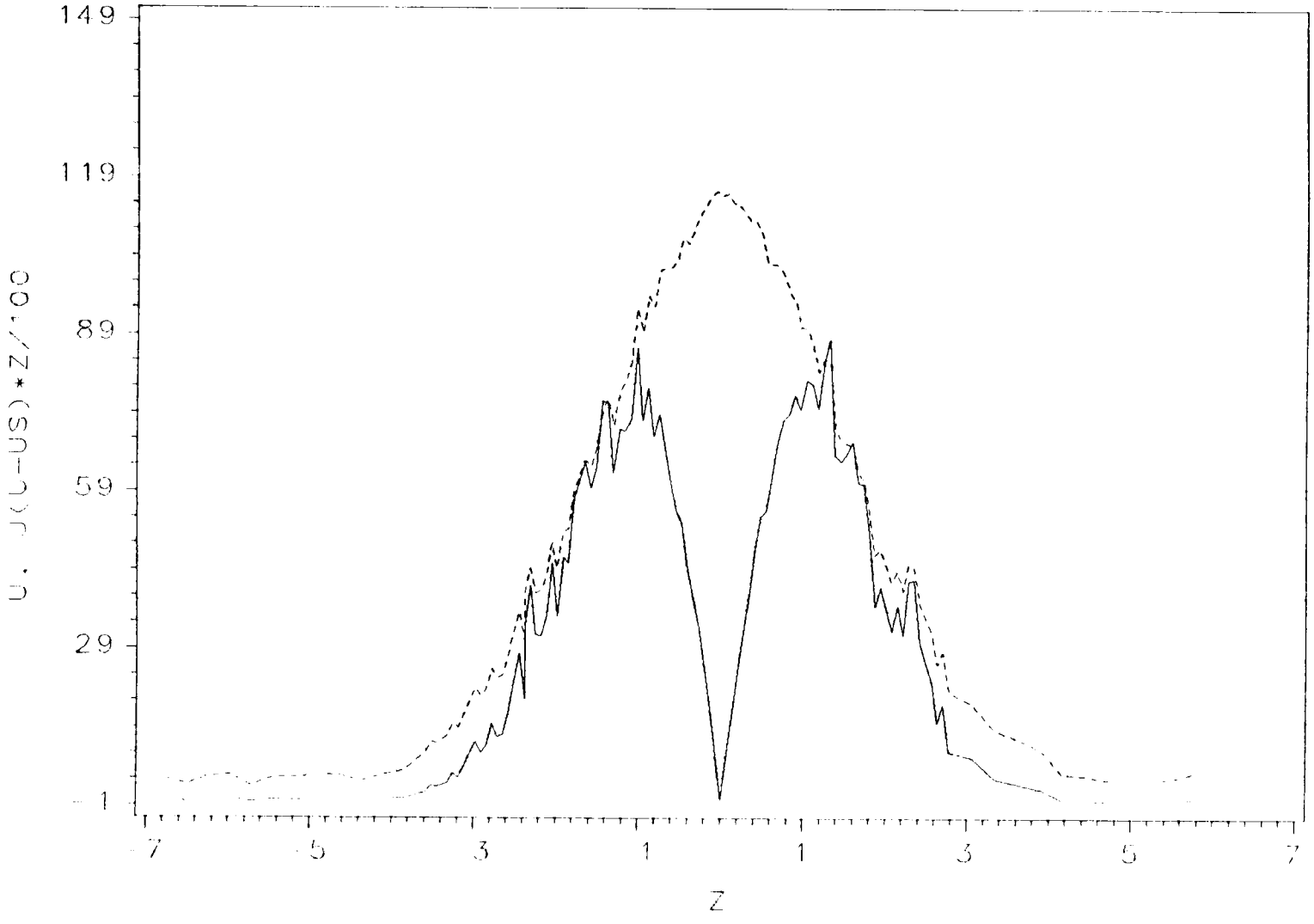

Figure 37 Momentum Contribution in z Direction at x/d = 60.

—, Momentum; - - -, Velocity.

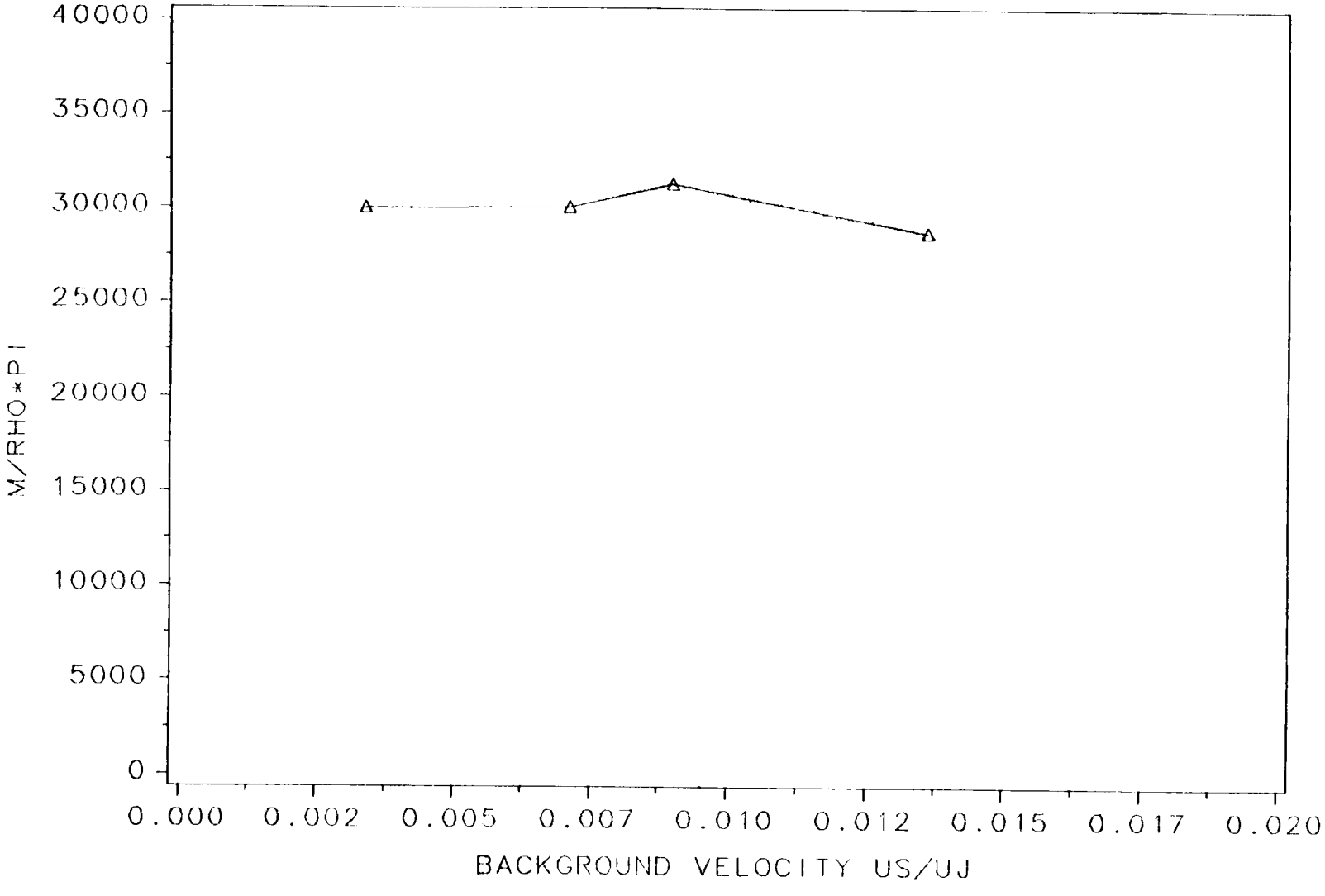

Figure 38 Integral Momentum Versus U_s/U_j at x/d = 60.

5.14 *The Craya-Curtet Number*

The Craya-Curtet number, C_t, defined in equation (2.12) which indicates the presence of the recirculation zone was plotted versus axial location in Figure 39. It represent the momentum ratio between the jet flow and the background coflow and can be expressed by the intake condition of the flows. The lower the background flow velocity, the smaller C_t becomes. Furthermore, the farther downstream, the smaller C_t. C_t was approximately equal to 0.72 at $x/d = 100$ for the case $U_s / U_j = 0.0034$. The critical value for C_t was around 0.73 to 0.81 (Rajaratnam, 1983). In our case C_t is very close to the critical value at $x/d = 100$ which indicates that there may be some recirculation there. If a recirculation zone is present there, it is very weak and small (Barchilon and Curtet, 1964).

We found, by calculating Craya-Curtet number, that it is not possible to maintain critical values of C_t while reducing $\frac{U_s}{U_j}$ indefinitely. The limitation of the tunnel can be determined by substituting the critical value of Craya-Curtet number (0.73) and the estimated entrainment of the free jet at the location $x/d = 60$ in the present study into equation (2.12). A simple approximate formula about the limitation of the confined jet experiment in the particular flow facility can be given as

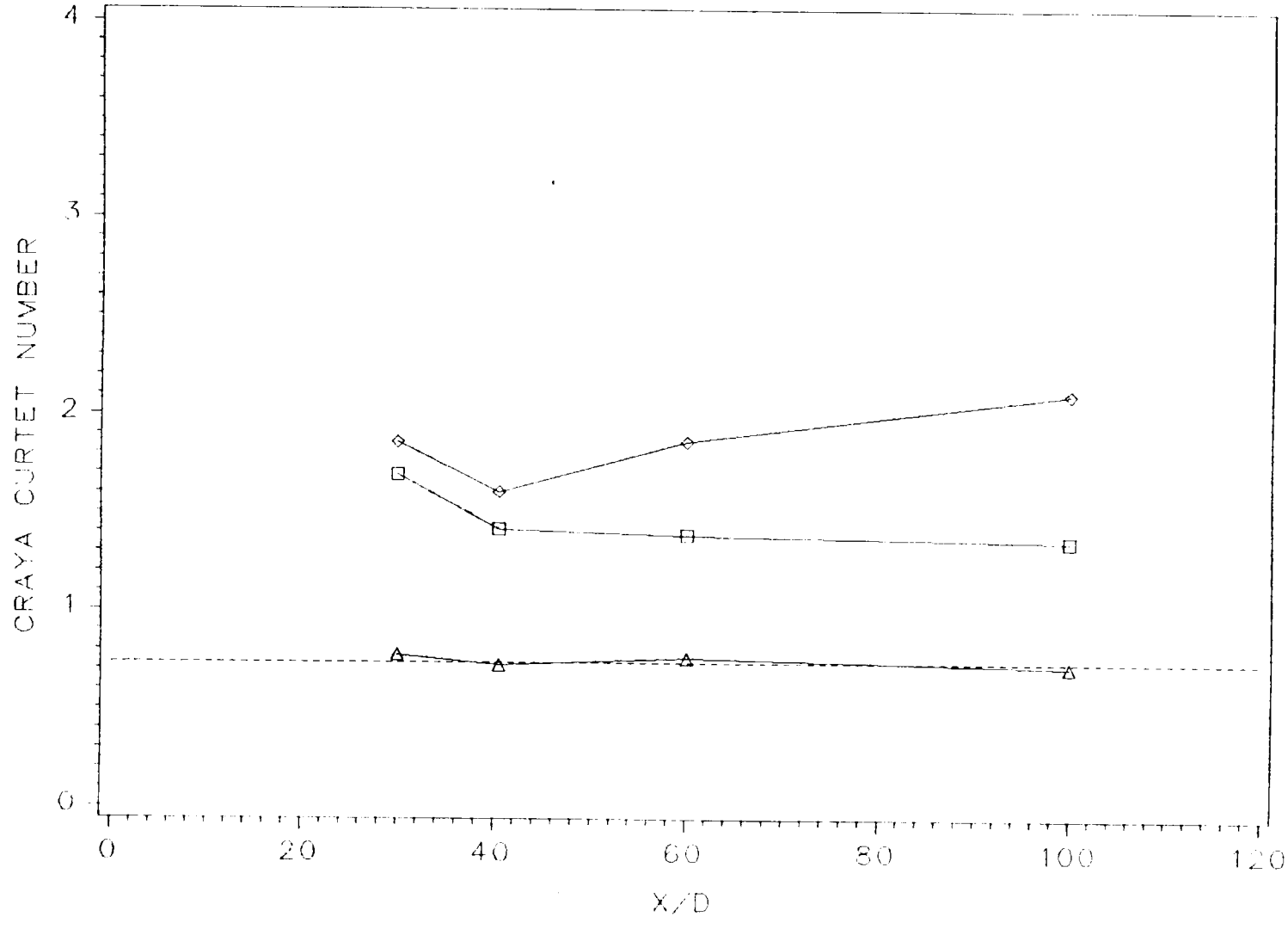

Figure 39 Variation of Craya-Curtet Number.

Δ ,U_i/U_j = 0.0034; $\square$,U_i/U_j = 0.0071; $\diamond$, U_i/U_j = 0.009.

$$\frac{L}{d} = \frac{1}{1.12\left(\frac{U_s}{U_j}\right)\left\{0.43 - 15.97\frac{U_s}{U_j} + \left[344.4\left(\frac{U_s}{U_j}\right)^2 - 13.72\frac{U_s}{U_j} + 0.18\right]^{1/2}\right\}^{1/2}} \tag{5.7}$$

This minimum ratio between the duct size and nozzle diameter L / d versus the velocity ratio U_s/U_j was plotted in Figure 40.

The tendency of the curve supports the fact that the cross area of the duct need to be increased four times in order to decrease the velocity ratio to its half value at a fixed Craya-Curtet number. This relation indicates that it is not possible to reduce the velocity ratio to an arbitraily small value without backflow because the duct must become impractically large. This suggests that the measurements of the jet flow with a coflowing stream is best done at several velocity ratios and extrapolated to $U_s / U_j \rightarrow 0$. It also give us a reliable estimation in the future research about how far the jet experiment can go in a known facility before the actual experiment is started. Consequently, A better understanding about the design of the jet experiment can be obtained.

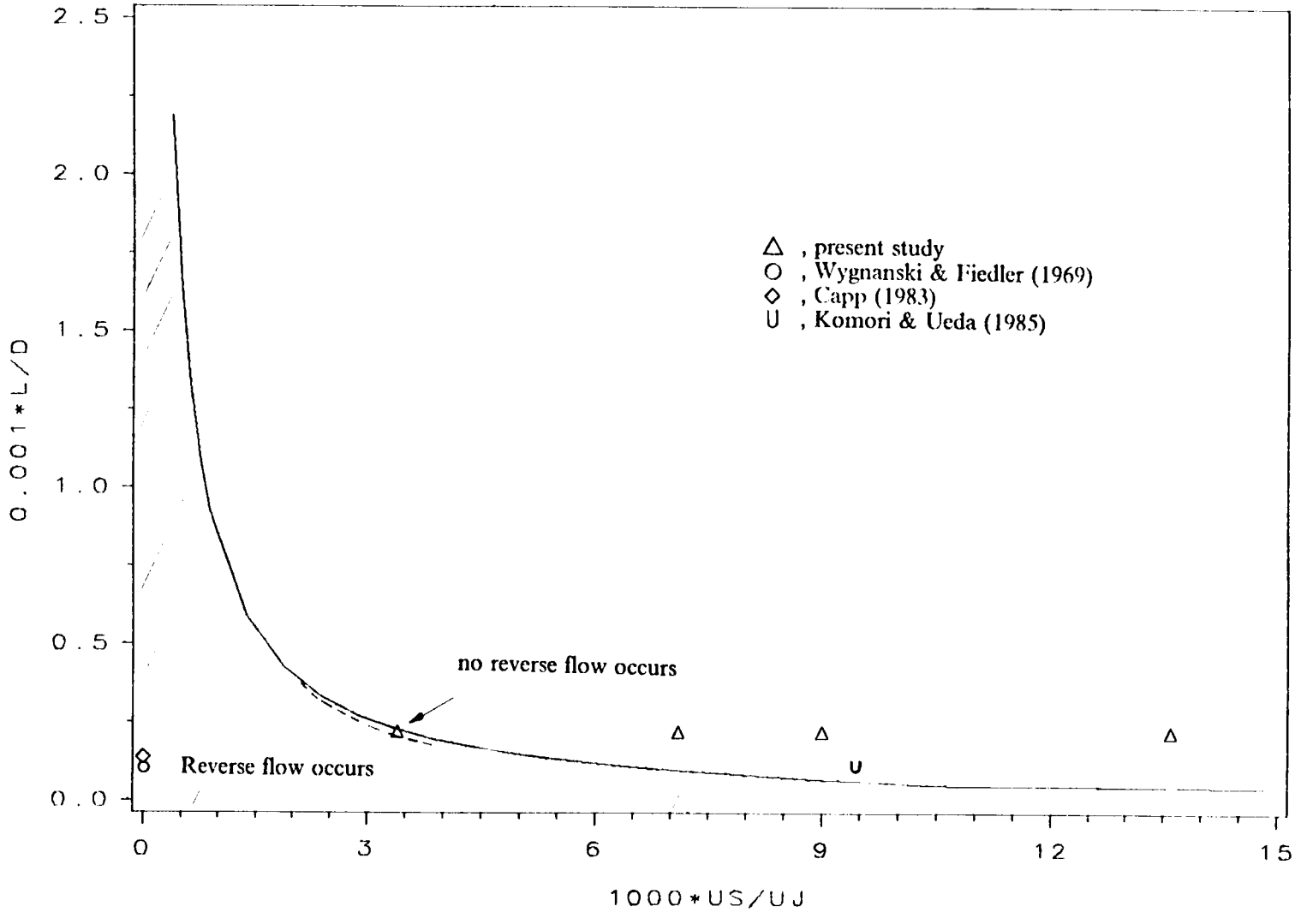

Figure 40 Duct Size Versus Velocity Ratio.

Chapter 6 Conclusion

A confined water jet with several very slow coflowing stream was examined using a laser Doppler anemometer with the following observations:

1. For experiments a free jet can be approximated by a confined jet with a coflow. The problem of the reverse flow which occurs in the usual "free jet" experiment is eliminated by the coflow. As long as the Craya-Curtet number of the coflow is above the critical value no recirculation zone occurs. Without recirculation the jet does not oscillate (flap). With a very slow coflow the jet development is comparable to an ideal free jet, including decay of the centerline velocity, the spreading rate and the entrainment rate.

2. Jet measurements made by hot-wire anemometers and even by LDA in air exhibit difficulties due to the high turbulence intensity (sometimes including directional ambiguity) and seeding bias. A better way to make both mean and

turbulence measurements in jets is by frequency-shifted LDA in water. Seeding bias and directional ambiguity can be avoided because the Doppler signals are nearly continuous and frequency shifted. Accurate mean measurements (and even rms measurements to a lesser extent) are obtained clear to the edge of the jet, producing complete distributions.

3. Momentum flux measurements require accurate data to the edge of the jet. Previous measurements have not included these. The contribution of the momentum flux in the region near the edge is significant. Reliable measurements show that momentum flux becomes constant but only beyond a distance of 40 exit diameters downstream. In the near field as described by Hussain and Clark (1977), the axial pressure variation becomes important.

4. These results, obtained in a test section of sixteen times the area, with a higher jet velocity and lower coflow velocity, measured with a different type of LDV tracker, agreed quite well with the earlier measurements of Walker (1984) except the half spreading angle is larger.

5. It is shown that it is not possible to reduce the velocity ratio U_s/U_j to an arbitrarily small value without backflow because the duct must become impractically large. The results indicate that the area of the duct needs to be increased four times if the velocity ratio is to be reduced to half its value at fixed Craya-Curtet number. The ratio of duct size to jet diameter (L / d) versus the velocity

ratio (U_s/U_j) was shown. The limitation of a jet experiment in a given flow facility can be estimated from these results.

6. By making measurements over a range of velocity ratios we extrapolated to zero coflow to obtain free jet results. This approach has not been used before and appears to be an appropriate way to obtain repeatable free jet results. Universal profiles were obtained for mean and rms velocity and linear variation of parameters along the axis were consistent with a self-preserved flow. Measurements of centerline velocity decay rate (B_u), spreading angle and entrainment rate fell within the range of results from previous experiments, but with reduced uncertainty.

Future study should include measurements of Reynolds stress and mean pressure distributions.

Bibliography

1. Abramovich, G. N., *The Theory of Turbulent Jets*, English Translation, Cambridge, MA : The MIT Press, 1963.

2. Albertson, M. L., Y. B. Dai, Jensen, R. A., and Rouse, H., "Diffusion of Submerged Jets," *Trans. ASCE, 115*, 1950, p 639-697.

3. Alexander, L. G., *et al*, "Transport of Momentum and Energy in a Ducted Jet," *American Institute of Chemical Engineering Journal, 1*, 1955, p 55-61.

4. Alpinieri, L. J., "Turbulent Mixing of Coaxial Jets," *American Institute of Aeronautics and Astronautics Journal, 2*, 9, 1964, p 1560-1567.

5. Antonia, R. A. and Chambers, A. J., "Errors in Simultaneous Measurements of Temperature and Velocity in the Outer Part of a Heated Jet," *Physics of Fluids, 23*, 5, 1980, p 871-874.

6. Antonia, R. A. and Bilger, R. W., "An Experimental Investigation of an Axisymmetric Jet in a Coflowing Air Stream," *Journal of Fluid Mechanics, 61*, 1973, p 805-828.

7. Antonia, R. A., Prabhu, A., and Stephenson, S. E., "Conditionally sampled measurements in a heated turbulent jet," *Journal of Fluid Mechanics, 72*, 1975, p 445-480.

8. Armstrong, K. K., Michalke, A. and Fuchs, H. V., "Coherent Structures in Jet Turbulence and Noise," *American Institute of Aeronautics and Astronautics Journal, 15*, 7, 1977, 1011-1017.

9. Baker, R. J., "The Application of a Filter Bank to Measurements of Tubulence in a Fully Developed Jet Flow," *Proceedings of the second International Workshop on Laser Velocimetry*, March 27 - 29, Purdue University, 1974, p 355-397.

10. Baker, C. B., "An Analysis of the Turbulent Buoyant Jet," Ph.D. Dissertation, 1980, Pennsylvania State University.

11. Barchilon, M. and Curtet, R., "Some Details of the Structure of an Axisymmetric Confined Jet With Backflow," *Transactions of the American Society of Mechanical Engineers : Journal of Basic Engineering*, 1964, p 777-787.

12. Barnett, D. O. and Giel, T. V., Jr., "Application of a Two-Component, Bragg-Diffracted Laser Velocimeter to Turbulence Parameter Determination in an Isothermal, Subsonic Jet," *Minnesota Symposium on Laser Anemometry Proceedings*, 1975, p146-183.

13. Bendat, J. S. and Pierson A. G., *Engineering Applications of Correlation and Spectral Analysis*, 1980, John Wiley & Sons, Inc.

14. Beavers, G. S. and Wilson, T. A., "Vortex Growth in Jets," *Journal of Fluid Mechanics, 44*, 1970, p 97-112.

15. Becker, H. A., Hottel, H. C. and Williams, G. C., "Mixing and Flow in Ducted Turbulent Jets," *Proc. 9th Int. Symp. on Combustion,*, 1962, p 7-20.

16. Becker, H. A., Hottel, H. C. and Williams, G. C., "The Nozzle-Fluid Concentration Field of the Round, Turbulent, Free Jet," *Journal of Fluid Mechanics, 30*, 1967, p 285-303.

17. Becker, H. A., and Massaro, T. A., "Vortex Evolution in a Round Jet," *Journal of Fluid Mechanics, 31*, 1968, p 435-448.

18. Birch, A. D., D. K. Brown, M. G. Dodson, and J. R. Thomas, "The Turbulent Concentration Field of a Methane Jet," *Journal of Fluid Mechanics, 88*, 1978, p 431-449.

19. Boguslawski, L. and Popiel, C. O., "Flow Structure of the Free Round Turbulent Jet in the Initial Region," *Journal of Fluid Mechanics, 90*, 3, 1979, p 531-539.

20. Bradbury, L. J. S., "The Structure of a Self-Preserving Turbulent Jet," *Journal of Fluid Mechanics, 23*, 1965, p 31-64.

21. Brighton, J. A., Razinsky, E., and Bowlus, D. A., "Turbulent Mixing of a Confined Axisymmetric Jet," *Proc. Fluidics Internal Flows, 2*, 1969, p57-90.

22. Capp, S. P. "Experimental Investigation of the Turbulent Axisymmetric Jet," Ph.D. Dissertation, 1983, State University of New York at Buffalo.

23. Carnahan, B., Luther, H. A., and Wilkers, J. O., *Applied Numerical Methods*, 1969, John Wiley & Sons, Inc.

24. Champagne, F. H., and Wygnanski, I. J., "Coaxial Turbulent Jets," Boeing Sci. Res. Lab D1-82-095.

25. Champagne, F. H., "The Fine-Scale Structure of the Turbulent Velocity Field," *Journal of Fluid Mechanics, 86*, 1978, p 67-108.

26. Chambers, A. J., Antonia, R. A., and Browne, L. W. B., "Effect of Symmetry and Asymmetry of Turbulent Structures on the Interaction Region of a Plane Jet," *Experiments in Fluids, 3*, 1985, p343-348.

27. Chevray, R. and Tutu, N. K., "Intermittency and Preferential Transport of Heat in a Round Jet," *Journal of Fluid Mechanics, 88*, 1978, p 133-160.

28. Corrsin, S., "Investigation of Flow in an Axially Symmetrical Heated Jet of Air," NACA Wartime Report Acr 3L23, 1943.

29. Corrsin, S. and Uberoi, M. S., *Natl. Advisory Comm. Aeronaut. Tech. Notes, No. 1865*, 1949.

30. Corrsin, S. and Uberoi, M. S., "Further Experiments on the Flow and Heat Transfer in a Heated Turbulent Air Jet," NACA Report 998, 1950.

31. Corrsin, S. and Uberoi, M. S., "Spectra and Diffusion in a Round Turbulent Jet," NACA Report 1040, 1951.

32. Craya, A. and Curtet, R., "On the Spreading of a Confined Jet," *Comptes-rendus, 241*, 1955, p 621-622.

33. Crow, S. C., and Champagne, F. H., "Orderly Structure in Jet Turbulence," *Journal of Fluid Mechanics, 48*, 1971, p 547-591

34. Curtet, R., "Confined Jets and Recirculation Phenomena with Cold Air," *Combustion and Flame, 2*, 4, 1958, p 383-411.

35. Curtet, R., "On the Flow of an Enclosed Jet," *Publications Scientifiques et Techniques du Ministere de l'Air, 359*, 1960, Paris.

36. Curtet, R. and Ricou, F. P., "On the Tendency to Self-Preservation in Axisymmetric Ducted Jets," *Transactions of the American Society of Mechanical Engineers : Journal of Basic Engineering, 86*, 4, 1964, p 765-776.

37. Davies, P. O. A. L., Fisher, M. J., and Barratt, M. J., "The Characteristics of the Turbulence in the Mixing Region of a Round Jet," *Journal of Fluid Mechanics, 15*, 1962, p 337-367.

38. Draper and Smith, *Applied Regression Analysis*, John Wiley and Sons, 1966.

39. Durst, F., Melling, A., and Whitelaw, J. H., *Principles and Practice of Laser-Doppler Anemometry*, 1976, N. Y. : Academic Press.

40. Elghobashi, S. E., Samuelsen, G. S., Wuerer, J. E., and LaRue, J. C., "Prediction and Measurement of Mass, heat, and Momentum Transport in a Nonreacting Turbulent Flow of a Jet in an Opposing Stream," *Journal of Fluids Engineering, 103*, 1981, p 127-132.

41. Elghobashi, S. E., Pun, W. M., and Spalding, D. B., "Concentration Fluctuations in Isothermal Turbulent Confined Coaxil Jets," *Chemical Engineering Science*, 32, 1977, p 161-166.

42. Fink, L. E., "Influence of External Turbulence on Mixing of Axisymmetric Coaxial Jets," *Symposium on Turbulent Shear Flows*, Pennsylvania State University, April 18-20, 1977, p 2.11-2.21.

43. Flora, Jr., J. J. and Goldschmidt, V. W., "Virtual Origins of a Free Plane Turbulent Jet," *J. AIAA, 7*, 1969, p 2344-2346.

44. Forstall, W. and Gaylord, E. W., "Momentum and Mass Transfer in a Submerged Water Jet," *Journal of Applied Mechanics, 22*, 1955, p 161-164.

45. Forstall, W. and Shapiro, A. H., "Momentum and Mass Transfer in Coaxial Gas Jets," *Journal of Applied Mechanics*, 1950, p 399-408.

46. Freeman, R. W. and Tavlarides, L. L., "Observations of the Instabilities of a Round Jet and the Effect of Cocurrent Flow," *Physics of Fluids, 22*, 4, 1979, p 782-783.

47. George, W. K., Seif, A. A. and Baker, C. B., "Momentum Balance Considerations in Axisymmetric Turbulent Jets," *Report No. TRL-119*, 1982, Turbulence Research Laboratory, SUNY/Buffalo.

48. Gerald, C. F., *Applied Numerical Analysis*, 2nd edition, 1978, Addison-Wesley.

49. Gortari, J. Cervantes de, and Goldschmidt, V. W., "The Apparent Flapping Motion of a Turbulent Plane Jet-Further Experimental Results," *Journal of Fluids Engineering, 103*, 1981, p 119-126.

50. Gutmark, E., and C. M. Ho., "Preferred Modes and the Spreading Rates of Jets," *Physics of Fluids, 26*, 4, 1983, p 2932-2938.

51. Heskestad, G. "Measurements in a Two-Dimensional Turbulent Jet," *J. Appl. Mech., 32*, 1962, p721.

52. Hill, B. J., "Measurement of Local Entrainment Rate in the Initial Region of Axisymmetric Turbulent Air Jets," *Journal of Fluid Mechanics, 51*, 1972, p 773-779.

53. Hill, P. G., "Turbulent Jets in Ducted Streams," *Journal of Fluid Mechanics, 22*, 1965, p 161-186.

54. Hinze, J. O., *Turbulence*, 1975, McGraw-Hill.

55. Hinze, J. O. and van der Hegge Zijnen, B. G., "Transfer of Heat and Matter in the Turbulent Mixing Zone of an Axially Symmetrical Jet," *Applied Scientific Research, A1*, 1949, p 435-461.

56. Holman, J. P., *Experimental Methods for Engineers*, 4th edition, 1984, McGraw-Hill, Inc.

57. Horowitz, P. and Hill, W. *The art of Electronics*, 1981, Cambridge University Press.

58. Hussain, A. K. M. F., and Clark, A. R., "Upstream Influence on the Near Field of a Plane Turbulent Jet," *Physics of Fluids, 20*, 1977, p 1416-1426.

59. Hussain, A. K. M. F. "Coherent Structures - Reality and Myth," *Physics of Fluids, 26*, (10), 1983, p 2816-2850.

60. Johnson, B. V. and Bennett, J. C., "Statistical Characteristics of Velocity, Concentration, Mass Transport forCoaxial Jet Mixing in a Confined

Duct," *Journal of Engineering for Gas Turbines and Power*, 106, 1984, p 121-127.

61. Keagy, W. R., and A. E. Weller, "A Study of Freely Expanding Inhomogeneous Jets," *2nd Heat Transfer & Fluid Mechanics Inst.*, Berkeley, California, 1949, p 89-98.

62. Khwaja, N. S. S., "Investigation of the Turbulent Axisymmetric Jet Mixing Layer," M.S. Thesis, 1980, SUNY at Buffalo.

63. Kizer, K. M., "Material and Momentum Transport in Axisymmetric Turburlent Jets of Water," *AIChe Journal, 9*, 1963, p 386-390.

64. Kobashi, Y, "Experimental Studies on Compound Jets," *Proceedings of the second Japan National Congress for Applied Mechanics*, 1952, p 223-226.

65. Komori, S. and Ueda, H. I., "Turbulent Effects on the Chemical Reaction for a Jet in a Nonturbulent Stream and for a Plume in a Grid-Generated Turbulence," *Physics of Fluids, 27*, 1, 1984, p 77-86.

66. Komori, S. and Ueda, H. I., "The Large-Scale Coherent Structure in the Intermittent Region of the Self-Preserving Round Free Jet," *Journal of Fluid Mechanics, 152*, 1985, p 337-359.

67. Kotsovinos, N. E., "A Note on the Spreading Rate and Virtual Origin of a Plane Turbulent Jet," *Journal of Fluid Mechanics, 77*, 1976, p 305-311.

68. Kotsovinos, N. E., "A Note on the Conservation of the Axial Momentus of a Turbulent Jet," *Journal of Fluid Mechanics, 87*, 1978, p 55-63.

69. Kovasznay, L. S. G., Kibens, V. and Blackwelder, R. F., "Large-Scale Motion in the Intermittent Region of a Turbulent Boundary Layer," *Journal of Fluid Mechanics, 41*, 1970, p 283-326.

70. Labus, T. L. and Symons, E. P., "Experimental Investigation of an Axisymmetric Free Jet with an Initially Uniform Velocity Profile," *NASA TND-6783*, 22.

71. Lau, J. C., Morris, P. J. and Fisher, M. J., "Measurements in Subsonic and Supersonic Free Jets Using a Laser Velocimeter," *Journal of Fluid Mechanics, 93*, 1979, p 1-27.

72. Lee, M. and W. C. Reynolds, "Bifurcating and Blooming Jets," *Fifth Symposium on Turbulent Shear Flows*, 1985, p 1.7-1.12.

73. List, E. J. "Turbulent Jets and Plumes," *Ann. Rev. Fluid Mech., 14*, 1982, p 189-212.

74. Maczynski, J. F. J., "A Round Jet in an Ambient Co-axial Stream," *Journal of Fluid Mechanics, 13*, 1978, p 597-608.

75. McLaughlin, D. K. and Tiederman, W. G., "Biasing Correction for Individual Realization of Laser Anemometer Measurements in Turbulent Flows," *Physics of Fluids, 16*, 12, 1973, p 2082-2088.

76. Morris, P. J., "Turbulent Measurements in Subsonic and Supersonic Axisymmetric Jets in a Parallel Stream," *American Institute of Aeronautics and Astronautics Journal, 14*, 10, 1976, p 1468-1475.

77. Mikhail, S., "Mixing of Coaxial Streams Inside a Closed Conduit," *Journal of Mechanical Engineering Science, 2*,1960, p 59-68.

78. Miller, D. R. and Comings, E. W., "Static Pressure Distribution in the Free Turbulent Jet," *Journal of Fluid Mechanics, 3*, 1957, p 1-16.

79. Mobbs, F. R., "Spreading and Contraction at the Boundaries of Free Turbulent Flows," *Journal of Fluid Mechanics, 33*, 1968, p 227-239.

80. Morris, P. J., "Turbulence Measurements in Subsonic and Supersonic Axisymmetric Jets in a Parallel Stream," *AIAA Journal*, 14, 1976, p 1468-1475.

81. Nee, N., "Turbulence Measurements in an Axisymmetric Jet Using a LDA," M. S. Thesis, 1983, SUNY at Buffalo.

82. Oler, J. W., and Goldschmidt V. W., "Coherent Structures in the Similarity Region of Two-Dimensional Turbulent Jets," *Journal of Fluids Engineering, 106*, 1984, p187-192.

83. Paizis, S. T. and Schwarz, W. H., "Entrainment Rates in Turbulent Shear Flows," *Journal of Fluid Mechanics, 68*, 1975, p 297-308.

84. Pande, B. B. L. and Rajaratnam, N., "Turbulent Jets in Coflowing Streams," *J. Eng. Mech. Div., ASCE, 105*, 1979, p 1025-1038.

85. Papanicolaou, P. N. and List, E. J., "Investigations of Round Vertical Turbulent Buoyant Jets," *Journal of Fluid Mechanics, 195*, 1988, p 341-391.

86. Pikes, E. R., et al., "Measurement of Turbulent Velocities from the Doppler Shift in Scattered Laser Light," *Journal of Physics, E, 1*, 1968.

87. Pitts, W. M. and Kashiwagi, T., "The Application of Laser-Induced Rayleigh Light Scattering to the Study of Turbulent Mixing," *Journal of Fluid Mechanics, 141*, 1984, p 391-429.

88. Rajaratnam, N., *Turbulent Jets*, Amsterdam, The Netherlands: Elsevier Scientific Publishing Co., 1976.

89. Rajaratnam, N., "Theory of Turbulent Jets," published in *Handbook of Fluids in Motion*, ed. Cheremisinoff, N. P. and Gupta, R., Ann Arbor, Michigan : Ann Arbor Science, 1983, p 251-278.

90. Ramaprian, B. R., and Chandrasekhara, M. S., "LDA Measurements in Plane Turbulent Jets" *Journal of Fluids Engineering, 107*, 1985, p 264-271.

91. Rankin, G. W., Sridhar, K., Arulraja, M., and Kumar, K. R., "An Experimental Investigation of Laminar Axisymmetric Submerged Jets," *Journal of Fluid Mechanics, 133*, 1983, p 217-231.

92. Razinsky, E. and Brighton, J. A., "Confined Jet Mixing for Nonseparating Conditions," *Transactions of the American Society of Mechanical Engineers : Journal of Basic Engineering*, 1971, p 333-349.

93. Reed, X. B., Spiegel, L., and Hartland, S., "Some Measurements of Spatial Correlations in an Axisymmetric Turbulent jet," *Proc. Symp. on Turbulent Shear Flows, Penna. State Univ.*, 1977,p 223-232.

94. Ricou, F. P. and Spalding, D. B., "Measurements of Entrainment by Axisymmetrical Turbulent Jets," *Journal of Fluid Mechanics, 11*, 1961, p 21-32.

95. Rodi, W., "A New Method of Analyzing Hot-Wire Signals in Highly Turbulent Flow, and Its Evaluation in a Round Jet," *DISA Info., 17*, 1975, p 9-18.

96. Rodi, W., "A Review of Experimental Data of Uniform Density Free Turbulent Bounday Layers," published in *Studies in Convection : Theory, Measurement and Applications, Volume 1*, ed. Launder, B. E., N.Y. : Academic Press, 1975, p 79-165.

97. Rodi, W., *Turbulent Buoyant Jets and Plume*, Pergamon Press, NY, 1982.

98. Rosensweig, R. E., H. C. Hottel, and G. C. Williams "Smoke Scattered Light Measurement of Turbulent Concentration Fluctuations," *Chem. Eng. Sci., 15*, 1961, p 111-129.

99. Rosler, R. S. and Bankoff, S. G., "Large Scale Turbulence Characteristics of a Submersed Water Jet," *AIChe Journal, 9*, 5, 1963, p 672-676.

100. Ruden, P., "Turbulente Ausbereitvorgange im Freistahl," *Naturwissen-Schaften, 21*, 1933, p375-378.

101. Schlichting, H., *Boundary Layer Theory*, 6th ed., 1968, N.Y.: McGraw-Hill Book Co..

102. Schneider, W., "Flow Induced by Jets and Plumes," *Journal of Fluid Mechanics, 108*, 1981, p 55-65.

103. Shaughnessy, E. J. and Morton, J. B., "Laser Light-Scattering Measurements of Particle Concentration in a Turbulent Jet," *Journal of Fluid Mechanics, 80*, 1977, p 129-148.

104. Seif, A. A., "Higher Order Closure Model for Turbulent Jets," Ph. D. Dissertation, 1981, SUNY at Buffalo.

105. So, R. M. C., Ahmed, S. A. and Yu, M. H., "The Near Field Behavior of Turbulent Gas Jets in a Long Confinement," *Experiments in Fluids, 5*, 1987, p 2-10.

106. Sreenivasan, K. R., Antonia, R. A. and Britz, K, "Local Isotropy and Large Structures in a Heated Turbulent Jet," *Journal of Fluid Mechanics, 94*, 1979, p 745-775.

107. Sunavala, P. D., C. Hulse, and M. W. Turing, "Mixing and Combustion in Free and Enclosed Turbulent Jet Diffusion Flumes", *Combust. Flame, 1*, 1957, p 79-193.

108. Tani, I. and Kobashi, Y., "Experimental Studies on Compound Jets", *Proceedings of the First National Congress for Applied Mechanics*, 1951, p 465-468.

109. Taylor, G. I., "Flow Induced by Jets", *Journal of the Aero/Space Sciences, 25*, 1958, p 464-465.

110. Tennekes, H. and Lumley, J. L., *A First Course in Turbulence*, 1972, The MIT Press.

111. Townsend, A. A., *Structure of turbulent Shear Flow*, Second Edition, 1976, Cambridge : Cambridge University Press.

112. Trentacoste, N., and P. M. Sforza "An Experimental Investigation of Three Dimensional Free Mixing in Incompressible Turbulent Free Jets", *Report 81, Department of Aerospace Engineering, Polytechnic Institute of Brooklyn*, NY, 1966.

113. Uberoi, M., and L. C. Garby, "Effect of Density Gradient on an Air Jet", *Physics of Fluids, 10*, 1967, p 200-202.

114. Walker, D. A., "Measurements on an Axisymmetric Jet in a Slow Coflowing Stream", Ph.D. Dissertation, 1984, Johns Hopkins University.

115. Walker, M. D., "Laser Doppler Measurements of Grid Turbulence in a Box", Ph.D. Dissertation, 1986, Johns Hopkins University.

116. Walker, M. D., "Signal Validation in Laser-Doppler-Velocimetry," *Proc. of 11th Symp. on Turbulence*, 1988, Rolla, Missouri.

117. Way, J. and Libby, P. A., "Application of Hot-Wire Anemometry and Digital Techniques to Measurements in a Turbulent Helium Jet", *AIAA Journal, 9*, 8, 1971, p 1567-1573.

118. Wilson, R. A. M., and P. V. Danckwerts, "Studies in Turbulent Mixing II: A Hot Air Jet", *Chem. Eng. Sci., 19*, 1964, p85-895.

119. Wygnanski, I. and Fiedler, H., "Some Measurements in the Self-Preserving Jet", *Journal of Fluid Mechanics, 38*, 1969, p 577-612.

120. Wygnanski, I. and Fiedler, H., "The Two Dimensional Mixing Region", *Journal of Fluid Mechanics, 41*, 1970, p 327-361.

121. Yeh, Y. and Cummins, H. Z., "Localized Fluid Flow Measurements with an He-Ne Laser Spectrometer", *Applied Physics Letter, 4, 10*, 1964, p 176-178.

122. Yule, A. J., "Spreading of Turbulent Mixing Layer", *J. AIAA, 10*, 1972, p 686-687.

123. Yule, A. J., "Large Scale Structures in the Mixing Layer of a Round Jet", *Journal of Fluid Mechanics, 89*, 1978, p 413-432.

Appendix A. Schematic Diagram

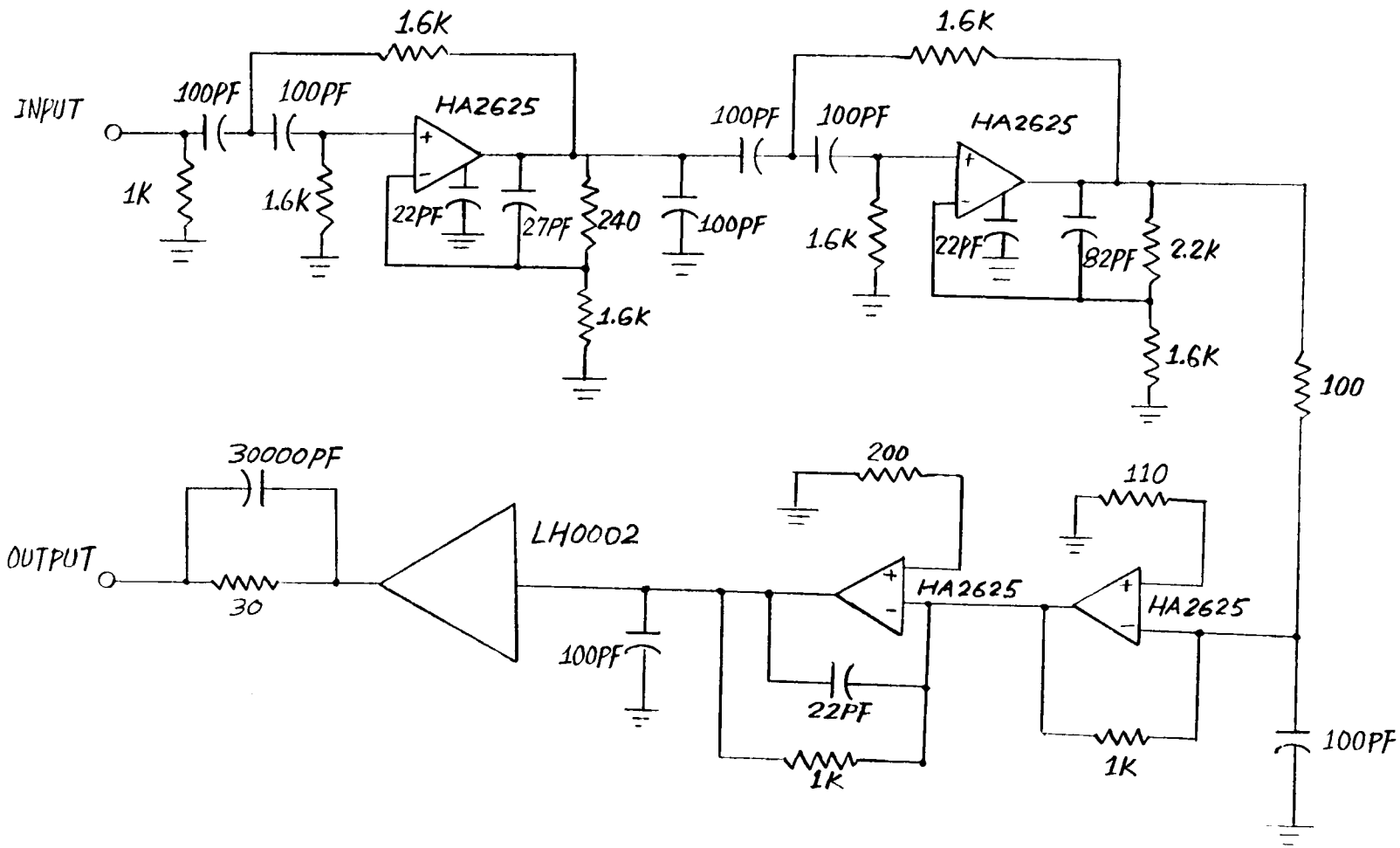

Figure 41 Amplifier and Filter for Frequency Tracker.

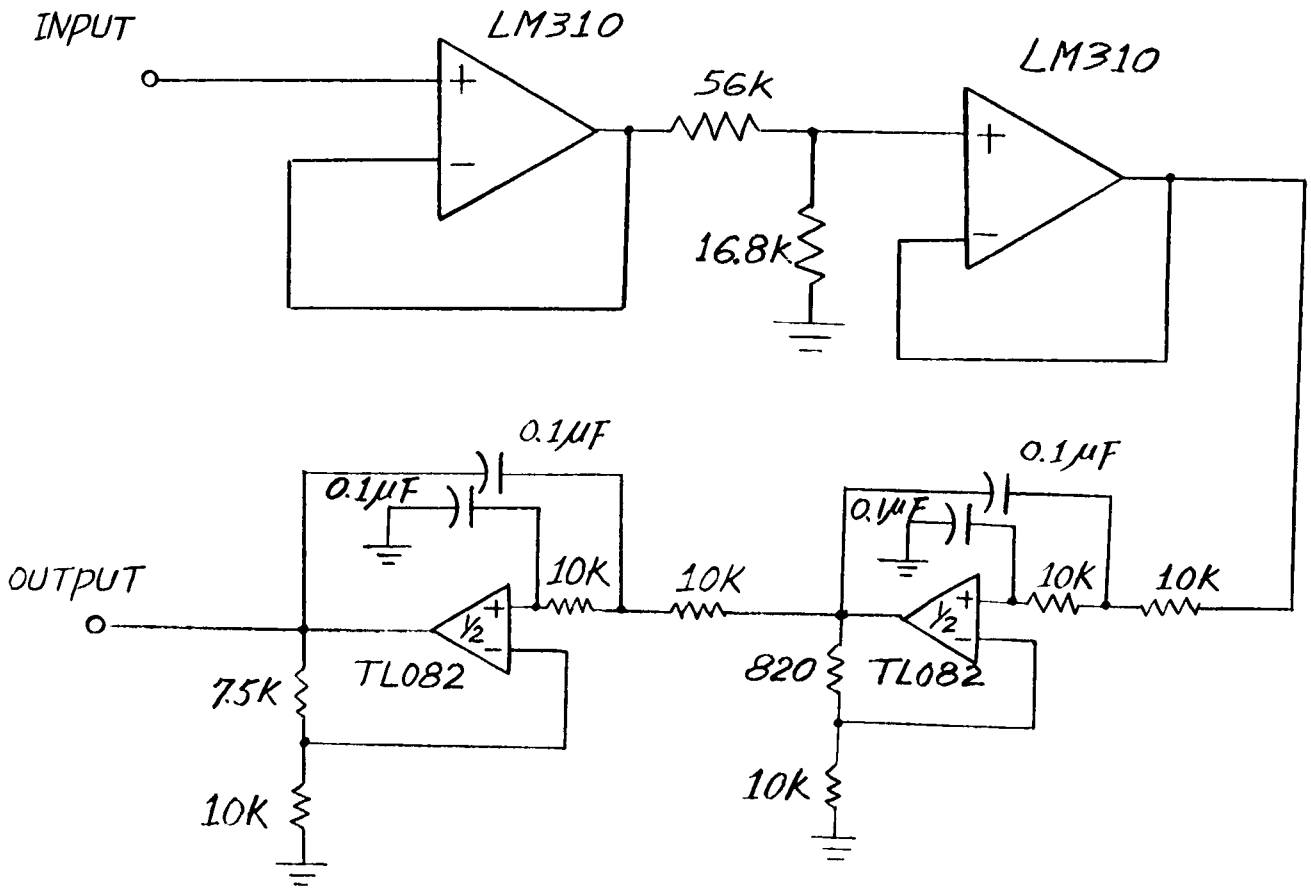

Figure 42 Filter for LVDT.

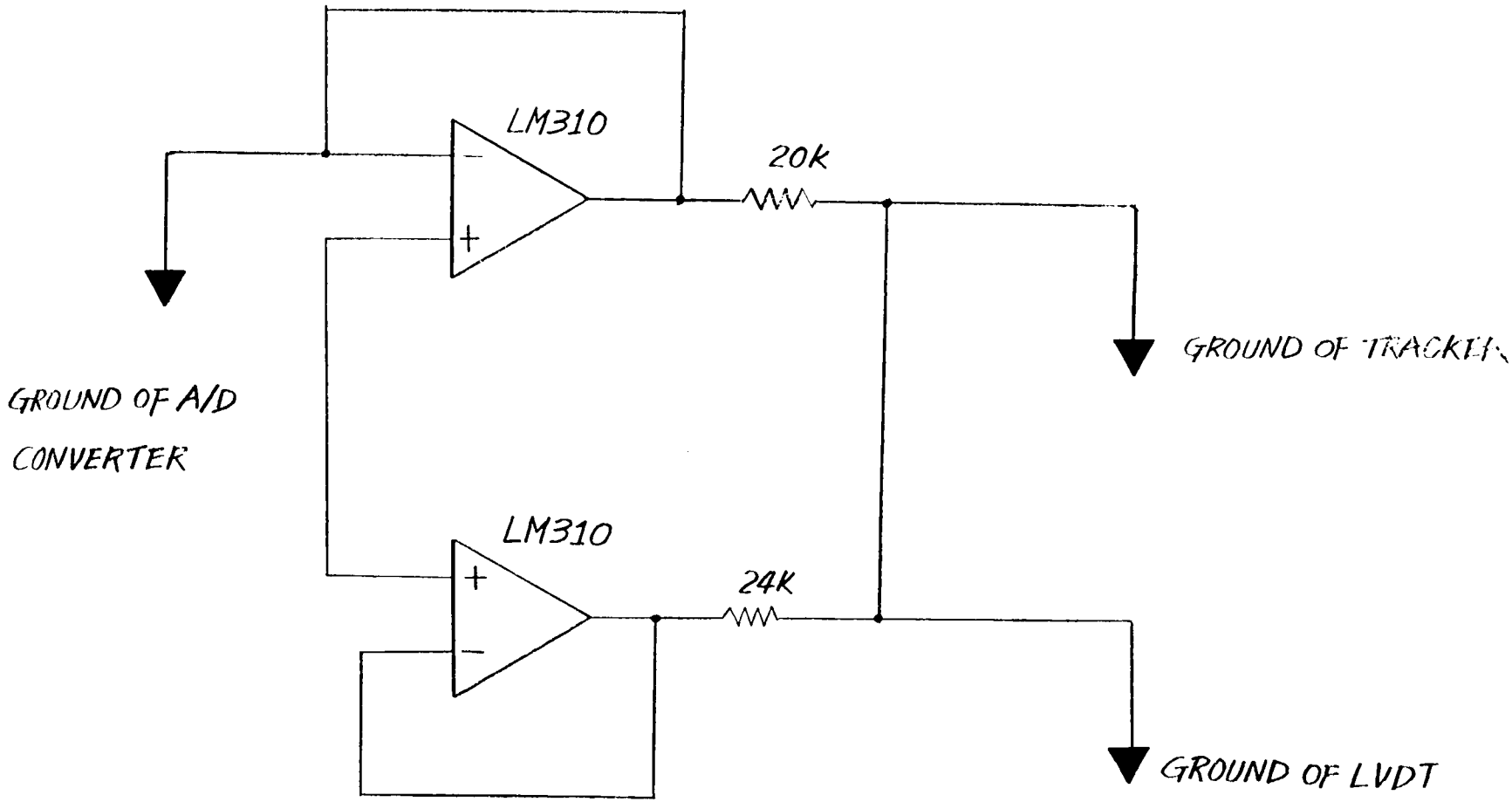

Figure 43 Protection Circuit for A/D Converter.

The vita has been removed from the scanned document